THEORETICAL AND EXPERIMENTAL STUDY OF

THE ANOMALOUS HALL PROPERTIES OF (Hg,Cd)Te

BY

Theodore Tin Sek Wong

SUBMITTED IN PARTIAL FULFILLMENT OF THE

REQUIREMENTS FOR THE DEGREES OF

BACHELOR OF SCIENCE

AND

MASTER OF SCIENCE

AT THE

MASSACHUSETTS INSTITUTE OF TECHNOLOGY

MAY 1974

Signature of Author _____
          Department of Electrical Engineering, May 10, 1974

Certified by _____
                              Thesis Supervisor (Academic)

Certified by _____
              Thesis Supervisor (VI-A Cooperating Company)

Accepted by _____
          Chairman Departmental Committee on Graduate Students

1

THEORETICAL AND EXPERIMENTAL STUDY OF

THE ANOMALOUS HALL PROPERTIES OF (Hg,Cd)Te

by

Theodore Tin Sek Wong

Submitted to the Department of Electrical Engineering on May
10, 1974 in partial fulfillment of the requirements for the
Degrees of Bachelor of Science and Master of Science.

ABSTRACT

A theoretical and experimental study of the anomalous Hall
effect in (Hg,Cd)Te is reported and a model successfully
explaining these anomalies is presented. It is shown that the
anomalous Hall coefficient, which is characterized by either a
"peak' or a "double reversal of sign" in its temperature
dependence, is not attributable to classical transport theory
for electrically homogeneous semiconduction of holes or
electrons in a crystal lattice.

The results of the surveys on anomalous Hall properties
observed in five other semiconductors and the possible models
for their anomalies show that the conducting-surface model --
the existence of an n-type surface on a p-type sample -- is
more favorable for (Hg,Cd)Te. A theory is developed on the
basis of this model to include the effects of the magnetic
field and the bulk and the surface properties on the apparent
Hall quantities that one measures. A method for deducing the
bulk carrier density directly from the anomalous data is
derived.

The model accounts for the previously unexplained phenomena,
such as the effects of the impurity density, the sample thickness,
and the magnetic field strength on the anomalous Hall coefficient,
and the results of the electron irradiation experiments. A
good qualitative agreement between data and calculations is
obtained.

With a different fabrication technique p-type Hall characteristics
are obtained from several previously measured peak-type samples.
The bulk hole densities for several peak-type samples are calculated
to be less than 2×10^{15} cm^{-3}. Finally, a more general model is
developed to give more flexibility in the physical interpretations
of the anomalies.

THESIS SUPERVISOR: C. G. Fonstad

TITLE: Assistant Professor of Electrical Engineering

TABLE OF CONTENTS

5

LIST OF FIGURES

7

LIST OF TABLES

9

LIST OF SYMBOLS

SYMBOL	MEANING	UNITS
A_i	The fraction of the total crossection of the sample passed by the current i	- - -
B	Magnetic Field	Gauss
b	Bulk electron to hole mobility ratio	- - -
d	Sample thickness	cm
d_s	Inversion layer thickness	cm
E	Electric field	v/cm
E_H	Hall electric field	V/cm
Eg	Energy of the bandgap	eV
E_A	Acceptor activation energy	eV
I	Current	Amperes
$J_{n,p}$	Current densities of electrons and holes respectively	Amp/cm^2
k	Boltzmann's constant	eV/°K
L	Effective Debye length	cm
Ln,p	Diffusion lengths for electrons and holes respectively	cm
$N_{A,D}$	Acceptor and donor densities respectively	cm^{-3}
N_A^-, N_D^+	Ionized acceptor and donor densities respectively	cm^{-3}
N_V	Effective dnesity of states in the valence band	cm^{-3}
ΔN_s	Surface excess electron density	cm^{-2}
n_i	Intrinsic carrier density	cm^{-3}
$n_{b,}$	Electron densities in the bulk and the surface respectively	cm^{-3}

ΔP_S	Surface Excess hole density	cm^{-2}
$P_{b,s}$	Hole densities in the bulk and at the surface respectively	cm^{-3}
q	Electronic charge	coulomb
R	Apparant Hall coefficient	$cm^3/coul$
R_M	Apparant Hall coefficient at maximum	$cm^3/coul$
$R_{n,p}$	Hall coefficient of n and p-type semiconductors respectively	$cm^3/coul$
T	Temperature	$^\circ K$
T_M	Temperature at which R is maximum	$^\circ K$
T_o	Temperature at which R is zero	$^\circ K$
T_L	Low Temperature	$^\circ K$
u_b	nromalized bulk potential	- - -
V_M	Madelung floating potential	Vdts
$v_{n,p}$	Drift velocities for electron and hole respectively	cm/sec
x	Mole fraction	- - -
$\gamma_{n,p}$	Hall coefficient factors for electrons and holes respectively	- - -
ϵ_s	Permittivity of the semiconductor	F/cm
λ	Mean free path of electrons	cm
$\mu_{Hn,Hp}$	Hall mobilities for electrons and holes respectively	$cm^2/v-sec$
$\mu_{nb,ns}$	Electron mobilities in the bulk and at the surface respectively	$cm^2/v-sec$

11

$\mu_{pb,ps}$	Hole mobilities in the bulk and at the surface respectively	$cm^2/v\text{-}sec$
ν	Normalized potential near the surface	- - -
ρ	Apparant resistivity	$\Omega\text{-}cm$
σ	Apparant conductivity	$(\Omega\text{-}cm)^{-1}$
$\sigma_{nb,ns}$	Electron conductivities in the bulk and at the surface respectively	$(\Omega\text{-}cm)^{-1}$
$\sigma_{pb,ps}$	Hole conductivities in the bulk and at the surface respectively	$(\Omega\text{-}cm)^{-1}$
ψ	Potential	volts
ψ_s	Surface potential	volts

ACKNOWLEDGEMENTS

The author expresses his most grateful appreciation to J. D.
Beck, M. B. Reine of Honeywell Radiation Center and Professor
C. G. Fonstad of M.I.T. for their constant guidance, encourage-
ment, and criticism throughout the present work. Thanks espe-
cially are due to J. D. Beck for his initial formulation of
the thesis topic and to M. B. Reine for his informing the
author of the results of the recent electron radiation experi-
ments. The author is also indebted to P. F. Tumelty who has
supplied a rich collection of Hall data which makes this
research possible.

Further thanks go to B. Goddard for his assistance in the
taking of the Hall measurements, to B. A. Paul for her help in
fabricating the Hall samples, and especially to D. Butler for
her efforts in improving the fabrication techniques which have
been most helpful in the preliminary stages of this work.

Finally, the assistance of N. Boucher, D. Dabose, and R. Knapp
for the typing, C. Wright for the illustrations and the Printing
Department is gratefully acknowledged.

CHAPTER I
INTRODUCTION

1.1   INTRODUCTION

The alloy system $Hg_{1-x}Cd_xTe$ has been of great interest in the field of infrared detection in recent years because the energy gap of this alloy can be varied continuously from -0.3 eV in semimetal HgTe to 1.6 eV in wide gap semiconductor CdTe by adjusting the composition x [1]. As a result, the alloy is suitable as an intrinsic photon detector covering the major atmospheric windows of the infrared spectrum at short (around 2 microns), middle (3 to 5 microns) and long (8 to 14 microns) wavelengths. To understand the basic electrical properties is a critical step in the development of (Hg,Cd)Te.

The two most important parameters in the study of the electrical properties of materials are the carrier concentration and the mobility. The experimental technique employed to measure these quantities is the Hall effect which is usually measured as a function of temperature between 4° and 300°K.

The electrical properties of n-type (Hg,Cd)Te have been reported by a number of authors and were reviewed in reference (1). However, the behavior of the Hall coefficient R and the resistivity ρ as functions of temperature in some (Hg,Cd)Te samples is much more complex and difficult to interpret by classical semiconductor physics.

14

The primary goal of this thesis research is to verify the hypothesis that an n-type layer on p-type bulk is responsible for the anomalous Hall effect in (HgCd)Te. The ultimate value of this research is that it offers the possibility that heretofor uninterpretable Hall data on (Hg,Cd)Te may finally be understood.

1.2   CLASSIFICATION OF (Hg,Cd)Te ELECTRICAL PROPERTIES

In general, there are four types of (Hg,Cd)Te samples as depicted by their measured Hall properties. Plotting the absolute Hall coefficient $|R|$ as a function of temperature T, one finds that all plots can be classified into the following four groups:

a) n-type: the Hall coefficient is negative at all temperatures and is temperature independent from 4.2°K up to the on set of the intrinsic region;

b) p-type: the Hall coefficient is positive at low temperatures and negative at high temperatures and has a single crossover next to the intrinsic region;

c) Peak-type*: the Hall coefficient is negative at all temperatures and is temperature independent at low temperatures, reaching a "maximum" next to the intrinsic region;

* A "peak" in the $|R|$ vs T plot is actually when R reaches a minimum if R is negative.
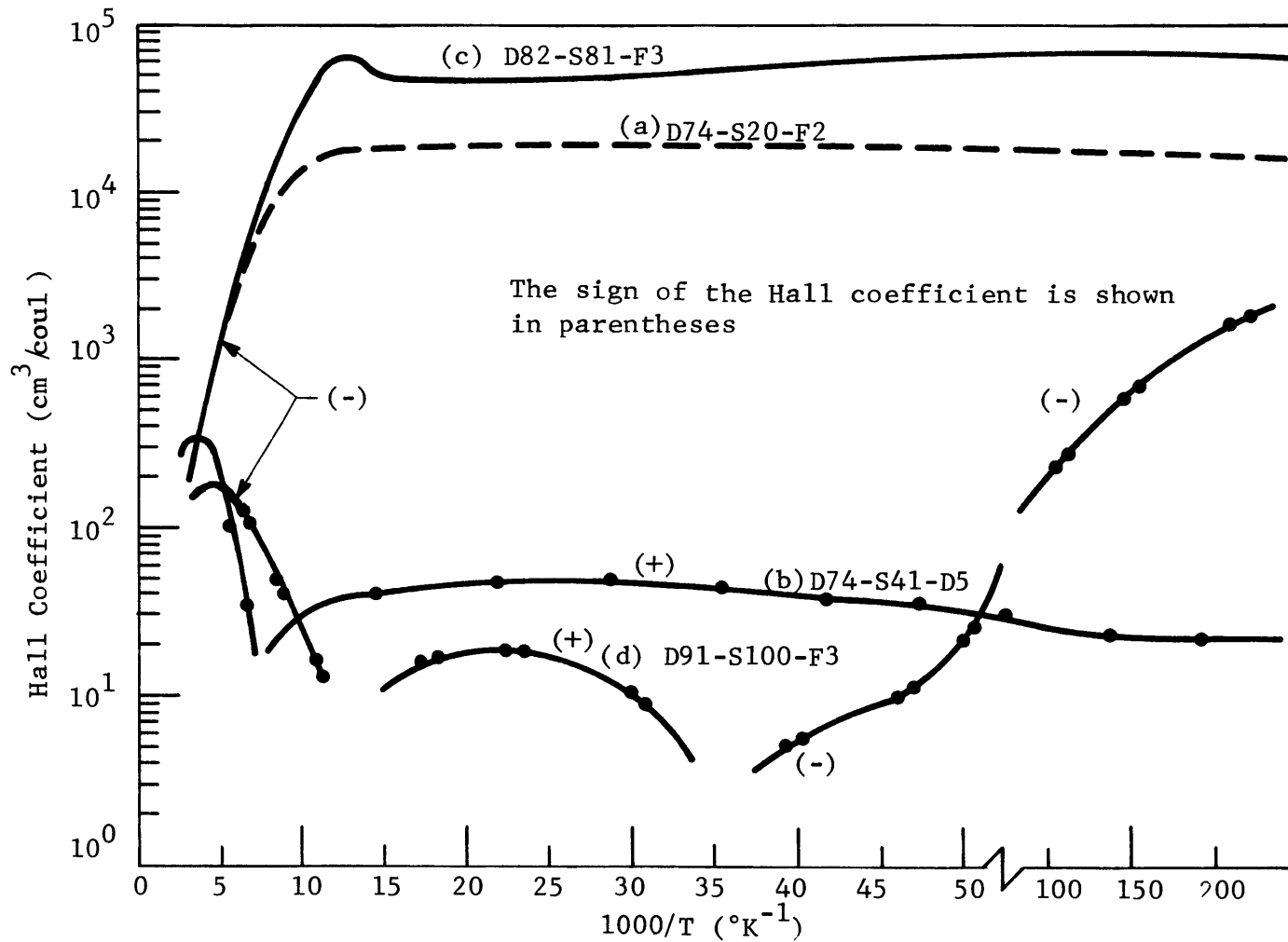
Figure 1.2.1   THE MEASURED TEMPERATURE DEPENDENT HALL COEFFICIENTS FOR
(a) n-TYPE (b) p-TYPE (c) PEAK-TYPE and (d) DCO-TYPE $(Hg_{0.8}Cd_{0.2})Te$
The sign of the Hall coefficient is shown in parentheses.
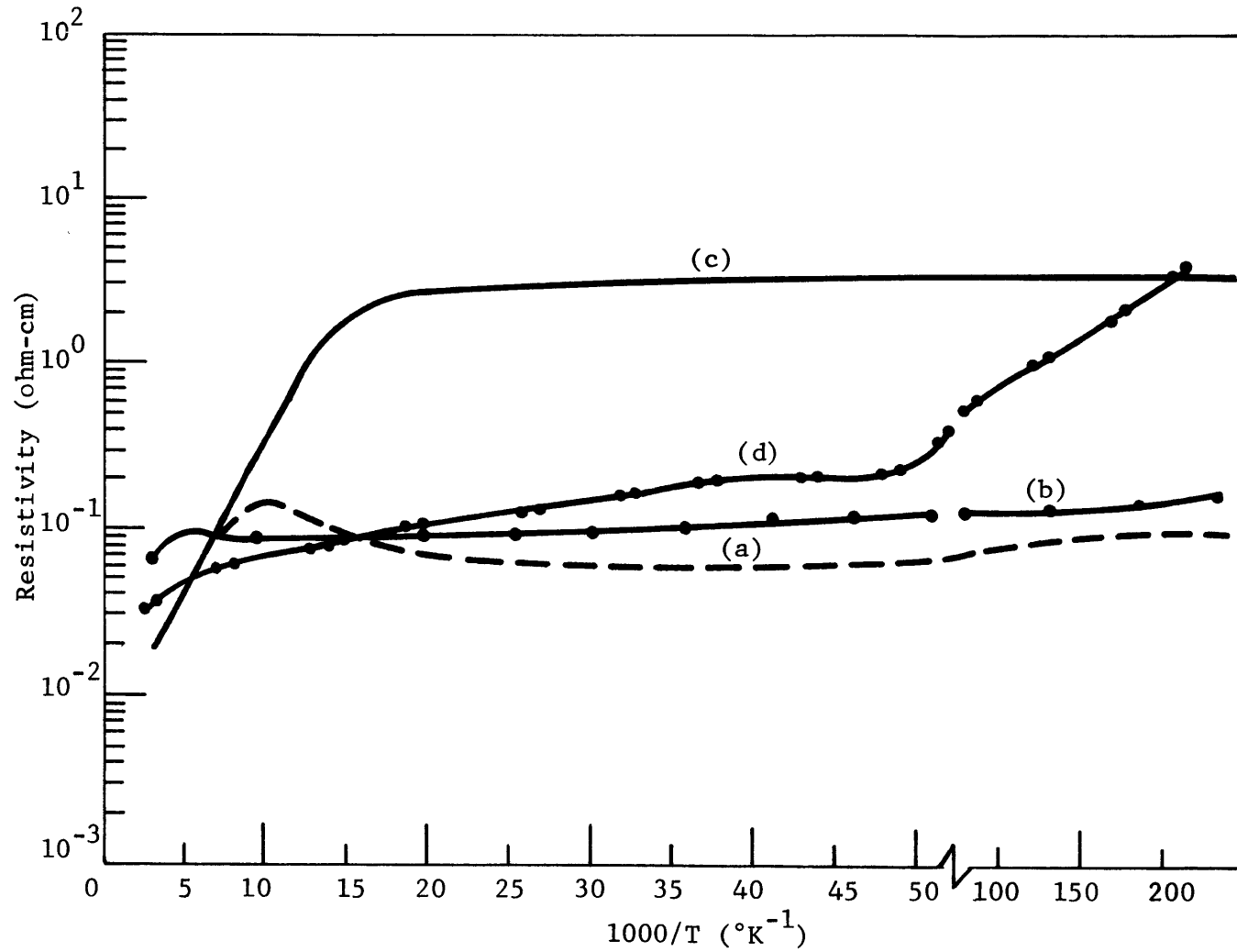
Figure 1.2.2   THE MEASURED TEMPERATURE DEPENDENT RESISTIVITIES FOR
(a) n-TYPE (b) p-TYPE (c) Peak-TYPE (d) DCO-TYPE $(Hg_{0.8}Cd_{0.2})Te$

17
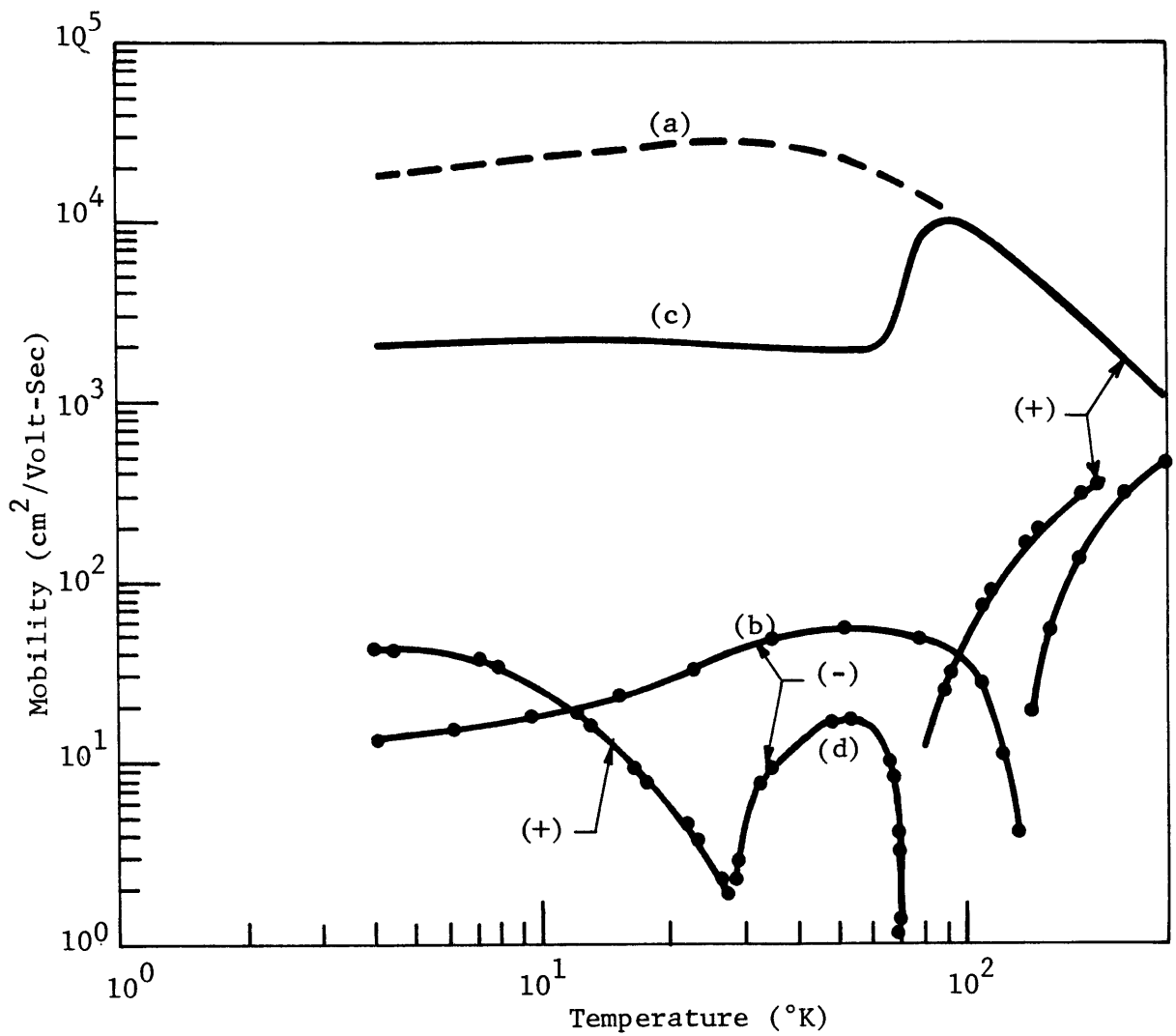
Figure 1.2.3   THE TEMPERATURE DEPENDENT HALL MOBILITIES FOR
(a) n-TYPE (b) p-TYPE (c) Peak-TYPE (d) DCO-TYPE
$(Hg_{0.8}Cd_{0.2})Te$

d) DCO-type (double crossover): the Hall coefficient
   is negative at low temperatures, positive at
   medium temperatures and becomes negative again at
   high temperatures and has two crossover (sign
   reversal) points.

Typical examples of these four types of temperature dependent
Hall coefficients are shown in Figure 1.2.1 and their corres-
ponding temperature dependent resistivities and mobilities are
shown in Figures 1.2.2 and 1.2.3, respectively. Previously,
(Hg,Cd)Te samples characterized as Peak- or DCO-type by their
Hall measurements were not fully understood in terms of clas-
sical semiconductor physics. This means that these anomalous
electrical properties, unlike those of n- and p-type material,
were not interpreted by means of conductions of electrons and/
or holes in the conducting bands. Therefore, the Peak- and
DCO-type samples were classified as material having anomalous
electrical properties. This research will be dealing with
these anomalous (Hg,Cd)Te materials.

1.3   SCOPE OF THIS THESIS

To achieve clarity of presentation, the Hall effect in classical
materials (n-type or p-type with mixed conduction), will be pre-
sented first.

In Chapter II, expressions for the Hall coefficient, conductivity and mobility for classical materials will be derived from the transport equations; numerical calculations will be made for p-type $Hg_{0.8}Cd_{0.2}Te$. The calculations serve two purposes: first, they prove that anomalies cannot be realized by the classical conduction processes involving the effects of mixed conduction, compensation and freeze-out; second, they provide the mathematical groundwork for the later analysis of the anomalies.

In Chapter III, reviews on the anomalies observed in five other semiconductors and on a number of models proposed to explain such anomalies will be given. A particular model will be selected to explain anomalies in (Hg,Cd)Te.

In Chapter IV, a theoretical analysis of this model, the conducting-surface model, will be presented. In Chapter V, this model will be applied to explain various experimental results.

The concluding chapter, Chapter VI, will be a discussion of the results, of the areas for further investigation, and of the conclusions that can be drawn from this study.

CHAPTER II

BULK CONDUCTIONS IN SEMICONDUCTORS

In this chapter we present and discuss the bulk conduction mecha-
nisms in semiconductors, that is, carrier transport in the con-
ductive band and the valence band. This is to lay down a ground
work which is essential both for the study of classical n- and
p-type semiconductors and for the treatment of anomalous pheno-
mena in the chapters to come.

We begin by deriving the Hall coefficient, the conductivity and
the Hall mobility from the transport equations for the case
where both electrons and holes are present. Then we discuss
qualatatively the temperature dependence of these parameters
under the influence of compensation and freezout of impurities.
Next, we make some numerical calculations for the case of p-type
$(Hg_{0.8}Cd_{0.2})Te$ material. Finally, we do some quantitative ana-
lysis on the magnetic field dependence of the Hall coefficient
on the basis of the equations we have derived.

2.1   THE BULK TRANSPORT FORMALISM

In 1879 the American physicist E. C. Hall (1855-1929) discovered
the so called "Hall Effect" which is a direct manifestation of
the Lorentz force on moving charges under the presence of a

magnetic field B and an electric field E. Suppose first that the moving charges are electrons, having a negative charge $-|q|$. When the electric field $\vec{E}$ is applied in the positive x direction, the actual motion is in the negative x direction with the velocity v_n (see Figure 2.1.1). When the magnetic field B is applied along the positive z direction (into the paper), the electrons are subjected to an additional force $-|q|(\vec{v}_n \times \vec{B})$ which results in the negative y direction. Therefore the electrons drift to one side of the sample which consequently become negatively charged. The other side, being deficient in the usual number of electrons, becomes positively charged.

As a result an electric field $\vec{E}_{Hn}$ in the negative y direction is produced. When the force $-|q|\vec{E}_{Hn}$ on the electrons, which is directed in the positive y direction, equilibrium results. A similar analysis can be made to hole transport, only now both the charge q and the drift velocity $\vec{v}_p$ are positive. It is interesting to note that both electrons and holes deflect toward the same side of the sample, therefore this corresponding Hall field will have opposite polarities. By measuring the polarity of the resulting field, one is able to tell whether the dominant carriers are electrons or holes.
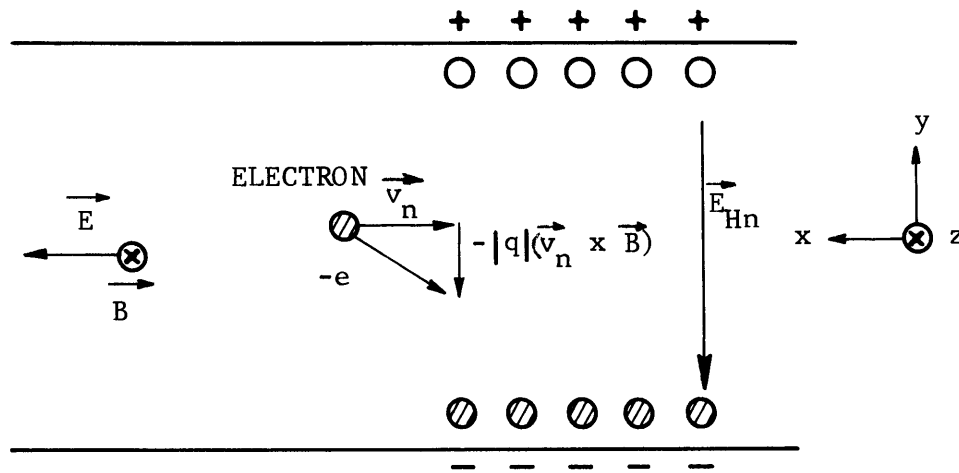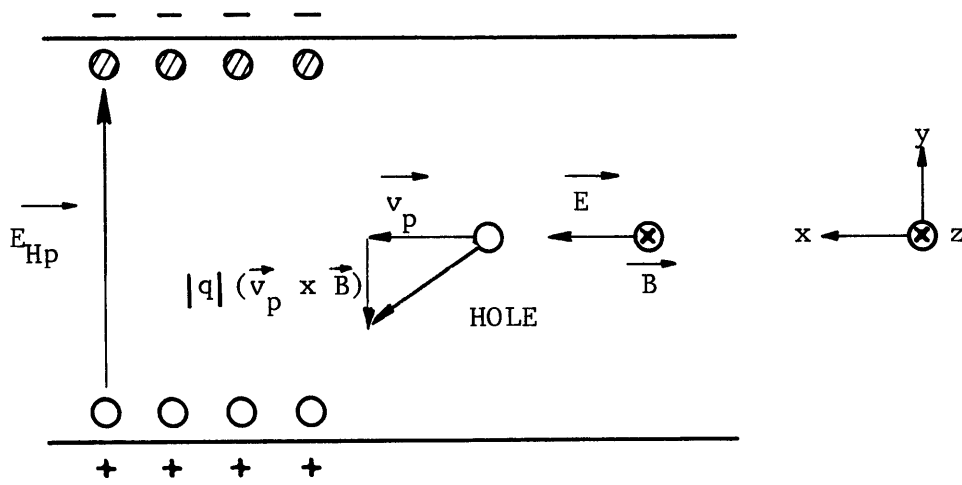
Figure 2.1.1 THE HALL EFFECT FOR (a) ELECTRONS AND (b) HOLES.

Now we are ready to examine the dynamics of charged carriers in a crystal. The total current density for each type of carriers is the sum of the current densities due to the electric field, to the magnetic deflection, and to the concentration gradients. The drift velocities $\vec{v}_E$ due to the electric field for electrons and holes are given by

$$\vec{v}_{En} = \mu_n \vec{E};$$

$$\vec{v}_{Ep} = \mu_p \vec{E},$$

where the subscripts "n" and "p" refer to electrons and holes respectively; and μ_n and μ_p are the drift mobilities for the corresponding carriers; the negative sign indicates that electrons drift against the direction of the electric field. The drift current densities are

$$\vec{J}_{En} = -|q| n \vec{v}_{En} = |q| n \mu_n \vec{E};$$

$$\vec{J}_{Ep} = |q| n \vec{v}_{Ep} = |q| p \mu_p \vec{E}.$$

The Hall velocities, $\vec{v}_H$, due to the magnetic deflection are given by

$$\vec{v}_{Hn} = \mu_{Hn} (\vec{v}_{En} \times \vec{B}) = \mu_{Hn} \mu_n (\vec{E} \times \vec{B});$$

$$\vec{v}_{Hp} = \mu_{Hp} (\vec{v}_{Ep} \times \vec{B}) = \mu_{Hp} \mu_p (\vec{E} \times \vec{B}),$$

where μ_{Hn} and μ_{Hp} are the Hall mobilities of electrons and holes, respectively. Their associated current densities are

$$\vec{J}_{Hn} = -|q|n\,\vec{v}_{Hn} = -|q|n\,\mu_{Hn}\,\mu_n\,(\vec{E} \times \vec{B});$$

$$\vec{J}_{Hp} = |q|p\,\vec{v}_{Hp} = |q|p\,\mu_{Hp}\,\mu_p\,(\vec{E} \times \vec{B}).$$

The current densities due to the concentration gradients are given by

$$\vec{J}_{Dn} = -|q|(-D_n)\vec{\nabla}n;$$

$$\vec{J}_{Dp} = |q|(-D_p)\vec{\nabla}p,$$

where D_n and D_p are the diffusion coefficients of the corresponding carriers.

The total current densities are the sum of all these three components, and hence

$$\vec{J}_n = |q|n\,\mu_n\vec{E} - |q|n\,\mu_{Hn}\,\mu_n\,(\vec{E} \times \vec{B}) + |q|D_n\vec{\nabla}n; \qquad (2.1.1)$$

$$\vec{J}_p = |q|p\,\mu_p\vec{E} + |q|p\,\mu_{Hp}\,\mu_p\,(\vec{E} \times \vec{B}) - |q|D_p\vec{\nabla}p. \qquad (2.1.2)$$

Now let the longitudinal electric field E_x, the Hall field E_H, and the magnetic field B_z be in the x, y and z directions respectively as shown in Figure 2.1.1. Further, if we assume that the electrons and holes are in equilibrium, we can ignore the diffusion currents since the gradients are zero. The vector equations (2.1.1) and (2.1.2) can be reduced to their scalar forms in the y direction:

$$J_{ny} = |q|n\,\mu_n\,E_y + |q|n\,\mu_{Hn}\,\mu_n\,E_x\,B_z; \qquad (2.1.3)$$

$$J_{py} = |q|p\,\mu_p\,E_y - |q|p\,\mu_{Hp}\,\mu_p\,E_x\,B_z. \qquad (2.1.4)$$

The sign changes in these equations compared with their vector forms are due to the property of the determinant associated with

25

the cross products.

Under steady state conditions the sum of the electron and hole current densities must be zero. It follows that

$$J_y = J_{ny} + J_{py} = 0 \;.$$

(2.1.5)

The steady state condition, together with (2.1.3) and (2.1.4), serve to determine E_y,

$$E_y = - \frac{\mu_{Hn} \mu_n n - \mu_{Hp} \mu_p p}{\mu_n n + \mu_p p} E_x B_x \;,$$

(2.1.6)

Now we must pause for a moment and note the difference between the drift mobilities, μ_n and μ_p, and the Hall mobilities, μ_{Hn} and μ_{Hp}. In general, one can relate them by a proportionality constant γ, namely,

$$\left. \begin{array}{l} \mu_{Hn} = \gamma_n \mu_n; \\[1mm] \mu_{Hp} = \gamma_p \mu_p, \end{array} \right\}$$

(2.1.7)

where γ_n and γ_p depend on the nature of the scattering, the band structure, the magnetic field strength, and on the statistics characterizing the distribution of velocities of the carriers. Their functional dependence on these variables is usually small, and in most cases their values differ from unity by less than ± 50 per unit. Since our main concern in this research is not in scattering mechanisms, we will let $\gamma_n = \gamma_p = 1$ throughout this paper for convenience.

Equation (2.1.6) may become more transparent by using the following definition:

$$\mu = \frac{\mu_n^2 n - \mu_p^2 p}{\mu_n n + \mu_p p} \;,$$

(2.1.8)

26

where μ is the effective Hall mobility for the mixed conduction of both electrons and holes. By means of (2.1.7) and (2.1.8), we may rewrite (2.1.6) as follows:

$$E_y = -\mu E_x B_z. \tag{2.1.9}$$

The electric field E_x and the current density J_x can be related by manipulating the scalar forms of equations (2.1.1) and (2.1.2) in the x direction:

$$J_{nx} = |q| n \mu_n E_x - |q| n \mu_{Hn} \mu_n E_y B_z;$$

$$J_{px} = |q| p \mu_p E_x + |q| p \mu_{Hp} \mu_p E_y B_z.$$

The total current density J_x is the sum of the two. Using equation (2.1.6), we have,

$$J_x = \left[|q| n \mu_n (1 + \mu_{Hn}^2 B_z^2) + |q| p \mu_p (1 + \mu_{Hp}^2 B_z^2) \right] E_x .$$
$$\tag{2.1.10}$$

If we consider the case where $B_z = 0$, the conductivity σ can be defined as follows

$$\sigma = \left. \frac{J_x}{E_x} \right|_{B_z = 0} = |q| n \mu_n + |q| p \mu_p . \tag{2.1.11}$$

Substituting (2.1.10) into (2.1.9), we have

$$E_y = \frac{-\mu}{\sigma} J_x B_z . \tag{2.1.12}$$

27

Now we are ready to make the following definition:

$$R = \frac{E_y}{J_x B_z} \quad , \tag{2.1.13}$$

where R is called the Hall coefficient. From (2.1.12) and 2.1.13), we obtain the following relationship

$$R = \frac{-\mu}{\sigma} \quad , \tag{2.1.14}$$

or

$$R = - \frac{\mu_n^2 n - \mu_p^2 p}{|q| (\mu_n n + \mu_p p)^2} \quad . \tag{2.1.15}$$

For extrinsic semiconductors, (2.1.8), (2.1.11) and (2.1.15) can be simplified as follows:

$$\mu = \begin{cases} \mu_n & \text{for n-type} \quad , \\ -\mu_p & \text{for p-type} \quad ; \end{cases} \tag{2.1.16}$$

$$\sigma = \begin{cases} |q| \mu_n n & \equiv \sigma_n \text{ for n-type,} \\ |q| \mu_p p & \equiv \sigma_p \text{ for p-type;} \end{cases} \tag{2.1.17}$$

and

$$R = \begin{cases} -1/|q| n & \equiv R_n \text{ for n-type,} \\ 1/|q| p & \equiv R_p \text{ for p-type.} \end{cases} \tag{2.1.18}$$

From (2.1.13) we know that R is a measurable parameter. It is very important quantity in solid state physics because, together with the conductivity, it enables us to know both the carrier concentration from (2.1.18) and the mobility from

(2.1.14). The sign of R (or μ), reveals the type of majority

carriers. In other words, a negative R (or positive μ) indica-

tes that the sample being measured is n-type.

Equations (2.1.2) applies only to the Hall effect in the limit

of small magnetic field. If we want to express the Hall coef-

ficient in terms of a magnetic field with arbitary strength,

quantities which are of second order in the magnetic field must

be considered. According to Chamber[20], the magnetic field de-

pendent Hall coefficient can be expressed as follows

$$R = \frac{\sigma_n^2 R_n + \sigma_p^2 R_p + \sigma_n^2 \sigma_p^2 B^2 R_n R_p (R_n + R_p)}{(\sigma_n + \sigma_p)^2 + \sigma_n^2 \sigma_p^2 B^2 (R_n + R_p)^2} \qquad (2.1.19)$$

Clearly when B = 0, these equations becomes its original form .

2.2 TEMPERATURE DEPENDENT BULK ELECTRICAL PROPERTIES OF CLASSICAL n- AND p-TYPE MATERIALS

In the preceeding sections, we derived expressions for the con-

ductivity, the Hall coefficient and the Hall mobility for the

mixed conduction of electrons and holes in semiconductors. We

now summarize our results as follows:

$$\sigma = |q| \mu_n n + |q| \mu_p p; \qquad (2.2.1)$$

$$R = - \frac{\mu_n^2 n - \mu_p^2 p}{|q| (\mu_n n + \mu_p p)^2} \; ; \tag{2.2.2}$$

$$\mu = \frac{\mu_n^2 n - \mu_p^2 p}{\mu_n n + \mu_p p} \; . \tag{2.2.3}$$

Also we have the following expressions for the extrinsic case:

$$\sigma_n = |q| \mu_n n \; ; \tag{2.2.4}$$

$$\sigma_p = |q| \mu_p p \; ; \tag{2.2.5}$$

$$R_n = \frac{-1}{|q| n} \; ; \tag{2.2.6}$$

$$R_p = \frac{1}{|q| p} \; ; \tag{2.2.7}$$

$$\mu_n = - \frac{R_n}{\sigma_n} \; ; \tag{2.2.8}$$

and

$$\mu_p = \frac{-R_p}{\sigma_p} \; , \tag{2.2.9}$$

where the subscripts "n" and "p" represent the extrinsic carrier types.

By means of the separation of carrier types, (2.2.1) to (2.2.3) can be rewritten in a more concise form:

$$\sigma = \sigma_n + \sigma_p \; ; \tag{2.2.10}$$

$$R = R_n \left(\frac{\sigma_n}{\sigma} \right)^2 + R_p \left(\frac{\sigma_p}{\sigma} \right)^2 \; ; \tag{2.2.11}$$

30

and

$$\mu = \mu_n \frac{\sigma_n}{\sigma} + \mu_p \frac{\sigma_p}{\sigma} \; ; \qquad\qquad (2.2.12)$$

For simplicity, we first assume that the donor level and the acceptor levels are merged with the conduction band and the valence band respectively. Thus, even at very low temperatures the carriers are fully ionized having the same densities as their corresponding impurity densities, and they remain constant as the temperature is raised, since intrinsic excitation will be small compared to the free carriers from the impurities. The mobilities in this temperature range will be constant if impurity scattering is small. However, at some higher temperature, the mobilities decrease due to thermal scattering while the free carrier densities remain constant. This gives rise to a fall in the $\sigma(T)$ curve as depicted in Figure 2.2.1. As the temperature is further increased, the mobilities will continue to fall while the free carriers increase exponentially due to intrinsic excitation and eventually will prevail and the conductivity will rise rapidly.

The $R(T)$ curves differ drastically from n- to p-type semiconductors as contrary to the $\sigma(T)$ curves. In an n-type semiconductor, in which R is always negative, the temperature dependance of R is similar to the temperature dependence of the in-

31
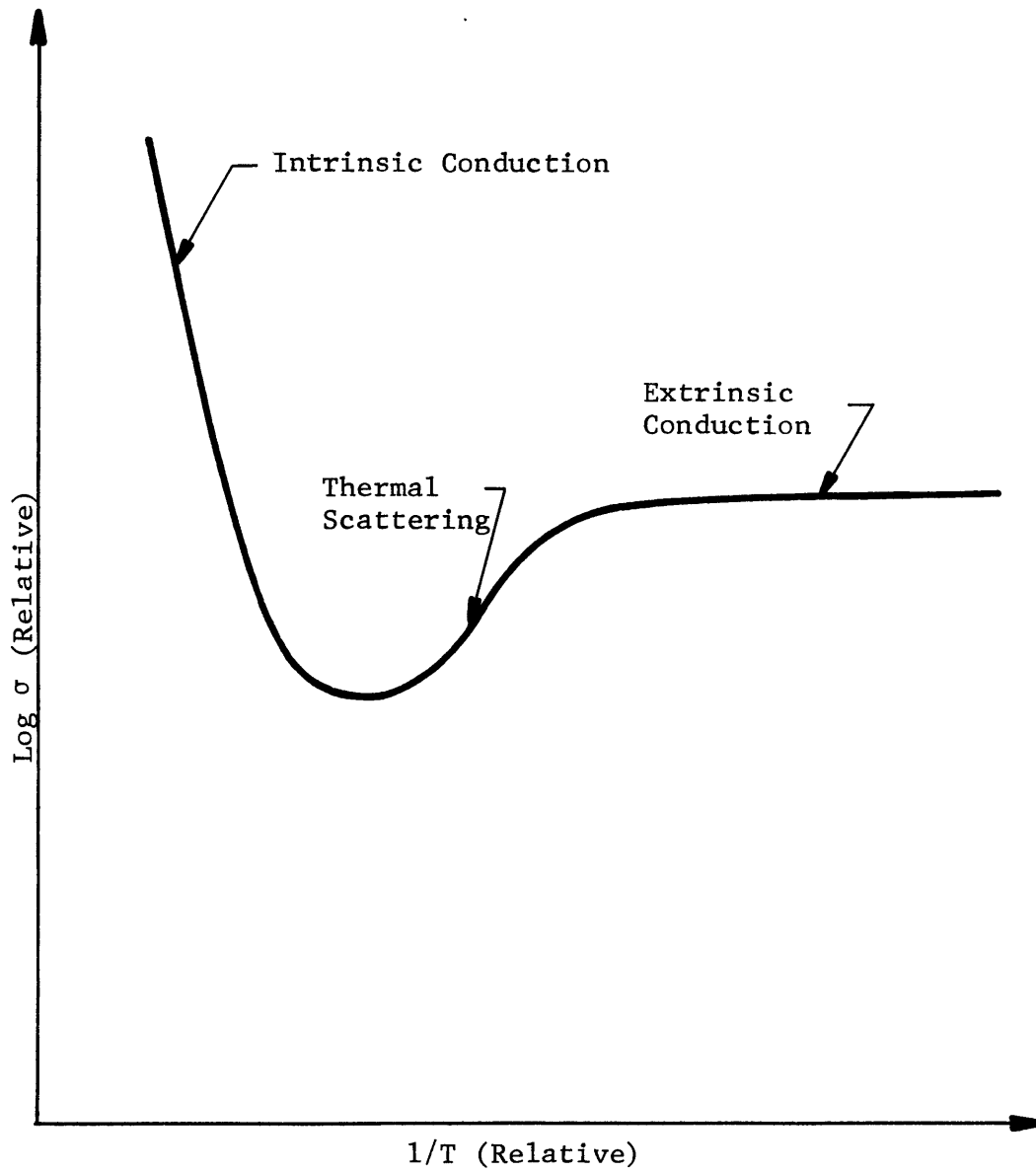
Figure 2.2.1   THE TEMPERATURE DEPENDENT CONDUCTIVITY FOR
BOTH n- and p-TYPE SEMICONDUCTORS.

32
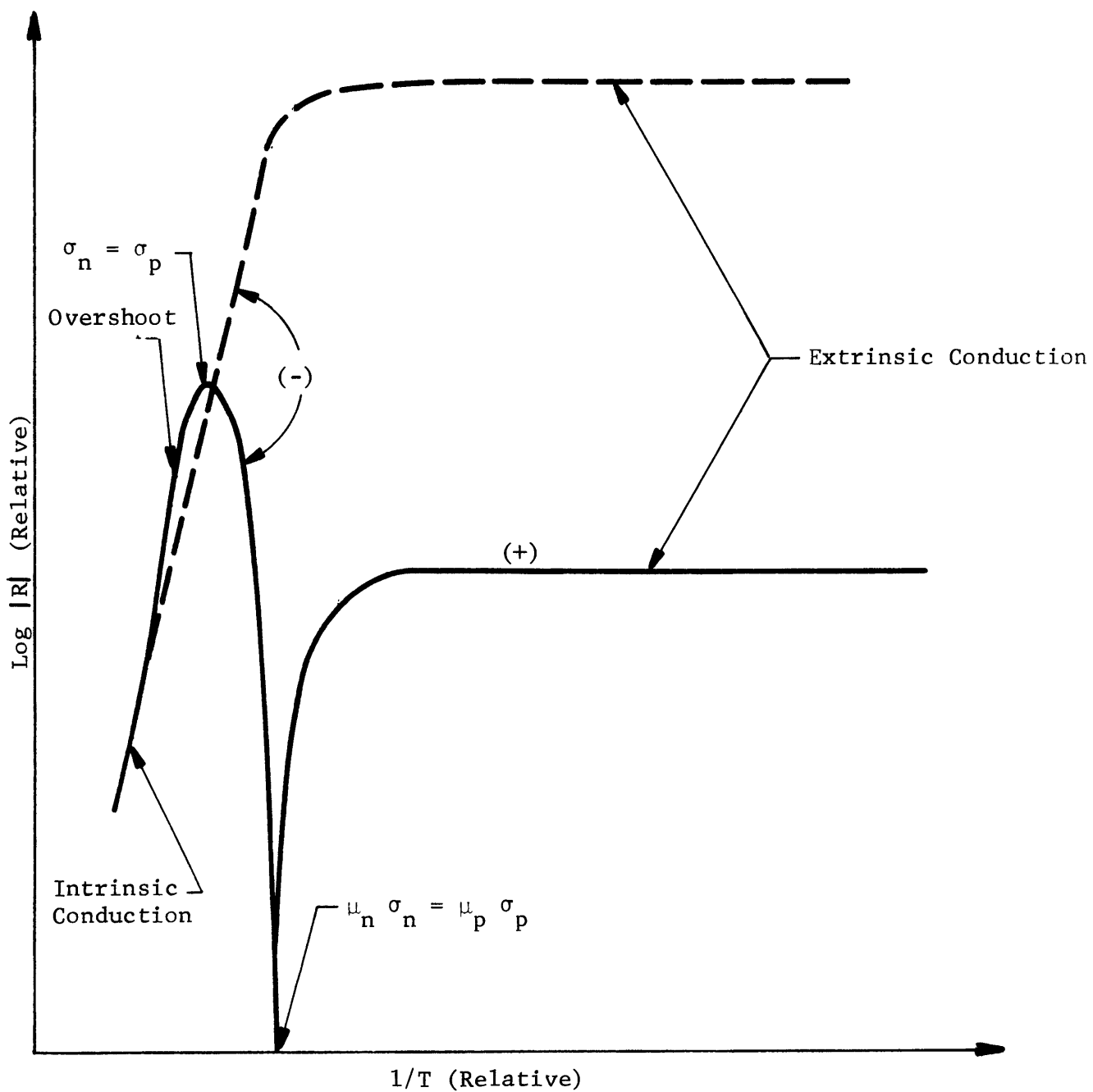
Figure 2.2.2   THE TEMPERATURE DEPENDENT HALL COEFFICIENTS FOR
              BOTH n-(— —) and p-type (——) SEMICONDUCTORS.

33

verse of n and is represented by the dotted curve in Figure 2.2.2. The donor density N_d can be obtained from the value of R_n at low temperatures (2.2.6).

On the other hand, a p-type semiconductor will have positive R at low temperatures. Since μ_n is in general larger than μ_p, as the temperature rises, eventually the term $\mu_n^2 n$ in (2.2.2) will dominate and the sign of R will change to negative. The crossover point of R is where $\mu_n \sigma_n = \mu_p \sigma_p$. After R changes to negative, its absolute value rises rapidly with increasing temperature, reaches a maximum at $\sigma_n = \sigma_p$, then falls and matches up with the n-type curve in the intrinsic region. The maximum of $|R|$ can be determined by setting the derivative of $|R|$ with respect to the temperature to zero, and is given by [26]

$$|R_M| = \frac{(1 - b)^2}{4 \, q \, b \, p} \; , \qquad (2.2.13)$$

where b is the electron to hole mobility ratio,

$$b = \frac{\mu_n}{\mu_p} \; . \qquad (2.2.14)$$

Using the conditions that R reaches a maximum at $\sigma_n = \sigma_p$, with large b value, and $p \simeq N_A$ at such high temperature, at equilibrium, we obtain the following from (2.2.13):

$$N_A \simeq p = 4 \, q \, |R_M| \, \left[n_i(T_M) \right]^2 \; , \qquad (2.2.15)$$

34

and

$$b (T_M) = \left[4 q \left| R_M \right| n_i (T_M) \right]^2 \quad , \qquad\qquad (2.2.16)$$

where T_M is the temperature at which $R = R_M$. Provided that $n_i(T)$ is known, $R(T)$ enables us to calculate simultaneously the doping density and the mobility ratio. The plateau region of $R(T)$ may be used to calculate N_A according to (2.2.7). But for many p-type simiconductors, such as (Hg,Cd)Te, the freeze-out effect which will be discussed in the next section together with the reversal of sign will obscure the plateau region of $R(T)$

As a result, the accuracy of calculating the acceptor density using the plateau is reduced. This is the reason why (2.2.15) is widely used in doping determination for p-type materials. As indicated in Figure 2.2.2, an overshout in the p-type $R(T)$ curve appears which, according to Putley [26], is always the case when b >3.7.

The situation considered so far is rather ideal. In reality, semiconductors are generally compensated - the presence of both donors and acceptors, and the donor levels and the acceptor levels are separated from the conduction band and the valance band respectively. Hence, the Hall effect is only the measurement of the conduction by the "excess"

35

carriers which is proportional to the degree of compensation, and by the "ionized" carriers which is governed by the activation energy.

Let us now consider a compensated semiconductor. At absolute zero all carriers are tied to their impurity centers. As the temperature rises a few degrees, electrons gain enough energy to be free from donors and likewise holes are liberated from acceptors. Electrons will then recombine with holes until the exhaustion of one type of carriers. Then the excess carriers can either be electrons or holes depending on the density of the donor compared to that of the acceptors. Some of these excess carriers will be ionized to the conductor band or the valence band and will contribute to the conduction. At low temperatures, the ionized excess carriers are of small quantity, corresponds to a large value of $|R|$. As the temperature rises, more excess carriers are ionized and $|R|$ decreases according to (2.2.6) or (2.2.7), flattening out when the impurity centers are exhausted. The plateau region now can only be used to calculate the compensated impurity density, i.e. $|N_A| - |N_D|$. As intrinsic excitation becomes appreciable, $|R_p|$ shows a crossover and both $|R_p|$ and $|R_n|$ will decrease exponentically when intrinsic conduction predominates (Figure 2.2.3).

36
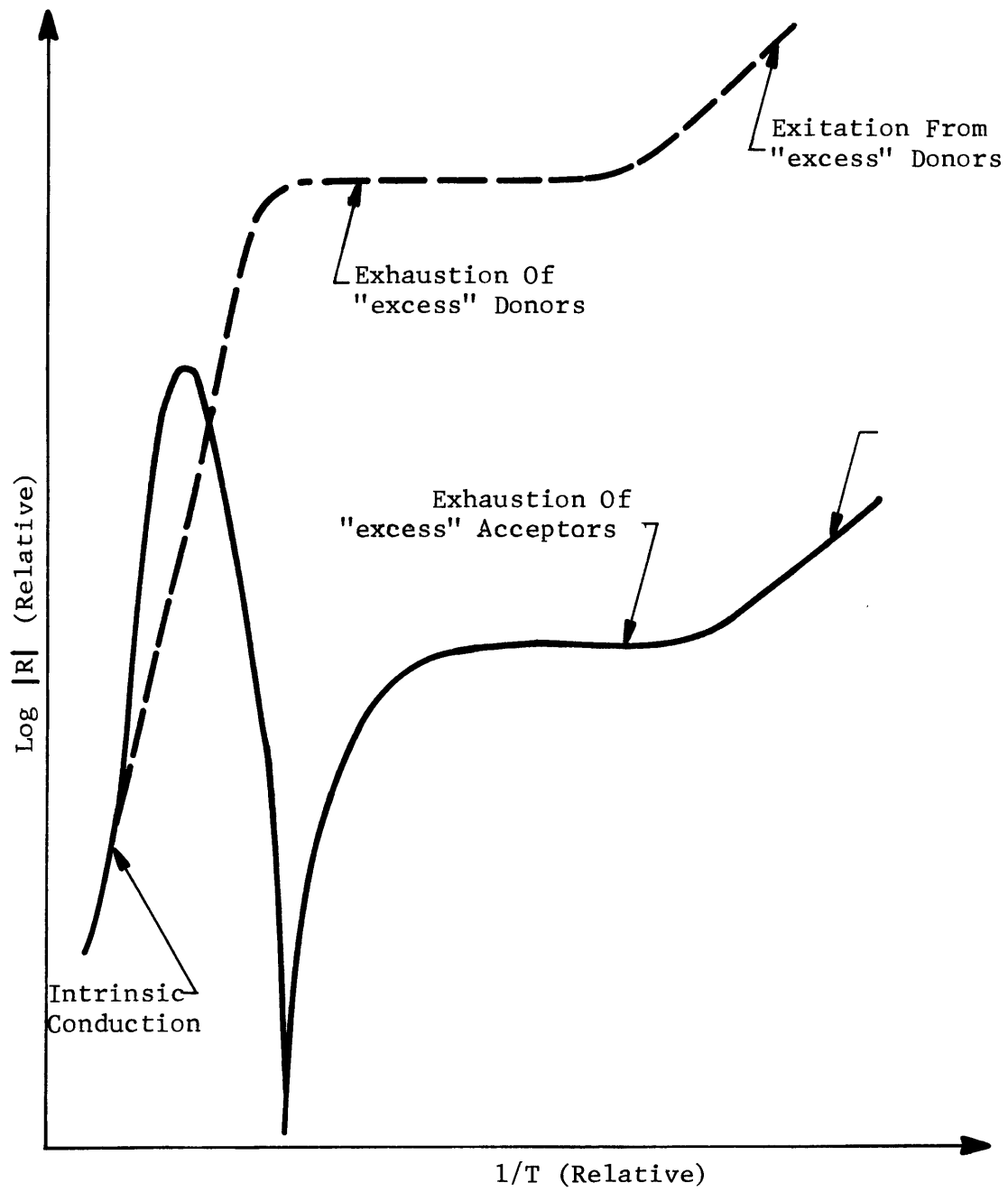
Figure 2.2.3   EFFECTS OF COMPENSATION AND FREEZE-OUT OF IMPURITIES
ON R = |R (T)|.

2.3   NUMERICAL CALCULATIONS ON p-TYPE $(Hg_{0.8}Cd_{0.2})Te$

In this section, we will use the model developed in the pre-
ceding sections to calculate R as a function of temperature
using x = .2 p-type $(Hg_{1-x}Cd_x)Te$ as a representative material.
The effects of compensation and freeze-out of acceptors will
be taken into account so that the mathematical model presented
here can describe realistically the Hall behaviors of any clas-
sical p-type $(Hg_{0.8}Cd_{0.2})Te$ sample and serves as an illustra-
tion in the understanding of the complicated conduction in p-
type semiconductors in general. The calculations will therefore
lay down a mathematical groundwork for future material evalua-
tions and will demonstrate the fact that the observed anomalous
Hall behavior is not attributable to the effects of mixed con-
duction, compensation or freeze-out.

In order to calculate the temperature dependence of the Hall
coefficient, we need to know the temperature dependence of the
intrinsic carrier density $n_i(T)$, the hole density p(T) and the
electron and hole mobilities, $\mu_n(T)$ and $\mu_p(T)$, respectively.

n_i vs absolute temperature for (Hg,Cd)Te has been calculated
and conformed to experimental results by curve fitting. The
following expression was written to give n_i in closed form:[27]

$$n_i(T) = (8.445 - 2.2875 \ x + 0.00342) \ 10^{14}$$

$$\cdot \ E_g(T)^{3/4} \cdot T^{3/2} \cdot \exp \ (-E_g/2KT), \qquad (2.3.1)$$

where x is the mole fraction, T is the temperature in °K, and E_g is the band gap in eV which is given by[28]

$$E_g(T) = 1.59x - 0.25 + 5.233 \cdot 10^{-4} \cdot (1-2.08\,x)$$

$$\cdot T + 0.327x^3. \qquad (2.3.2)$$

With both compensation and freeze-out of acceptors taken into account, the temperature dependence of p is no longer simple. Fortunately, in the temperature range considered here (4.2 - 300 °K), the Fermi energy for the p-type (Hg,Cd)Te is always a few KT above the valence band.[28] This enables us to use the result given by Blakemore[50] that the net ionized acceptor density is

$$N_a^-(T) - N_d^+(T) = \frac{2(N_a-N_d)}{[1+(N_d/\beta N_v)\exp(\epsilon_a)]+ \Big([1+(N_d/\beta N_v)\exp(\epsilon_a)]^2}$$

$$+ \ (4/\beta N_v)(N_a-N_d)\exp(\epsilon_a)\Big)^{1/2} \qquad (2.3.3)$$

where N_a^- and N_d^+ are ionized acceptor and donor densities respectively; N_a and N_d are total acceptor and donor densities respectively; $\beta = 1/2$ is the degenacy factor; $\epsilon_a = E_a/K_T$ is the reduced acceptor energy level;

$$N_v = 2\left(\frac{2\pi m_h \ KT}{h^2}\right)^{3/2}$$

is the effective density of states in the valence band. At

39

equilibrium, the charge neutrality implies the following:

$$p(T) = \frac{1}{2} \left[(N_a^- - N_d^+) + \sqrt{(N_a^- - N_d^+)^2 + 4n_i^2} \right] ; \quad (2.3.4a)$$

$$n(T) = n_i^2(T)/p(T). \quad\quad\quad (2.3.4b)$$

Thus we obtain a complete description of the temperature dependence of p and n.

The next parameter to be considered is the electron mobility $\mu_n(T)$ which has been discussed by various authors[29]. But, no theoretical calculation has yet been developed which can satisfactorily describe experimental results for all temperatures. Furthermore, the calculated expression for μ_n involves integration which is difficult to evaluate. Therefore we adopt the empirical approach. The temperature dependence of μ_n for all n-type $(Hg_{0.8}Cd_{0.2})Te$ shows similar fashion: μ_n increases slightly from 4.2°K to approximately 40°K, then it decreases rapidly with increasing temperatures. The scalings with temperature are a 0.125 power at low temperatures and a (-2.27) power at high temperatures. But the magnitude of μ_n at 4.2°K varies with doping and compensation, hence a constant scaling factor has been added to modify the empirical equation. Assuming that at 300°K, μ_n is doping independent and has a value of 10^4 cm^2/v-s, we obtain, by curve fitting, the following expression from Figure 2.3.1:
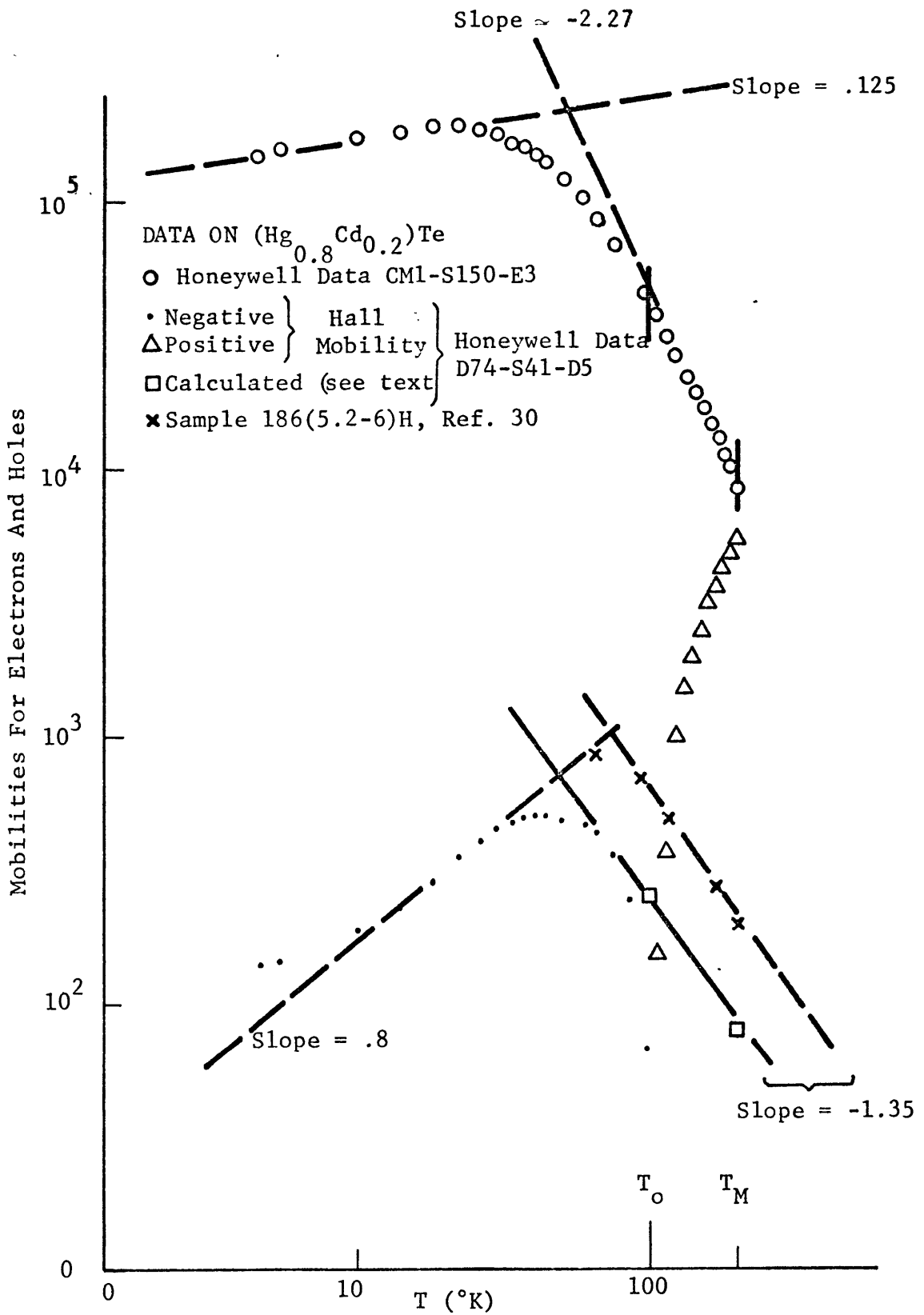
Figure 2.3.1 ELECTRON AND HOLE MOBILITIES VS TEMPERATURE.

41

$$\frac{1}{\mu_n(T)} = \frac{1}{\mu_{n\ell}(T)} + \frac{1}{\mu_{nh}(T)}, \tag{2.3.5}$$

where the low temperature mobility $\mu_{n\ell}$ is given by

$$\mu_{n\ell}(T) = \frac{\mu_n(4.2°K)}{1.2} T^{0.125}, \tag{2.3.6}$$

and the high temperature mobility μ_{nh} is given by

$$\mu_{nh}(T) = 4.2 \times 10^9 \times T^{-2.27}. \tag{2.3.7}$$

In (2.3.6), $\mu_n(4.2°K)$ is the scaling factor which can be found from Figure 8 of Reference 29 if the free carrier concentration at 4.2°K is known, otherwise it is assumed to be 1.5×10^5 cm^2/v-sec.

The hole mobility μ_p is a much less known quantity. No theoretical consideration has yet been given. Its low temperature values $\mu_{p\ell}(T)$ are found directly from Hall measurements when the sample is p-type; its high temperature values $\mu_{ph}(T)$ can be calculated after the intrinsic region is reached.

From equations (2.2.1) and (2.2.1), with the condition that $n=p=n_i$, $\mu_{ph}(T)$ can be written as

$$\mu_{ph}(T) = \mu_{nh}(T) + R \tag{2.3.8}$$

when μ_{nh} is given empirically by (2.3.7), R and σ are measured quantities at the corresponding temperatures. Equation (2.3.8) has rather low accuracy because it determines μ_{ph} from

subtracting two large quantities μ_{nh} and $R\sigma$ (R is negative).

But these values of μ_{ph} can be checked by the two calculated

values of μ_p. Assuming intrinsic conduction, $\nu_p(To)$, where To

is the temperature at which R = 0, is given by

$$\mu_p(To) = \frac{\nu_n(To)\ n_i(To)}{p} \quad \text{at } R = 0, \tag{2.3.9}$$

where $\mu_n(To)$ and $n_i(To)$ are to be evaluated at T = To and p

can be obtained from (2.2.15). The other value of ν_p can be

found at T = Tm which is the temperature when $|R|$ is a maximum,

that is

$$\mu_p(Tm) = \frac{\nu_n(T_m)}{b(T_m)} \quad \text{at } |R| = |R_m| , \tag{2.3.10}$$

where $b(T_m)$ is given by (2.2.16) and $\nu(T_m)$ by (2.3.7).

A typical p-type $(Hg_{0.8}Cd_{0.2})Te$ Hall mobility for holes is

shown in Figure 2.3.1. The low and high temperature slopes

found in the log-log plot are .8 and -1.35, respectively. The

Hall coefficient and the resistivity of this sample are shown

in Figure 2.3.2 for reference. The acceptor density calculated

from Figure 2.3.2 is about 4×10^{17} cm^3. A point to be noted

is the absence of freeze-out even at the lowest temperature

which enables us to check the doping calculated from R_{max}. The

two calculations are within a factor of 1.5. For comparison, we

also plot in Figure 2.3.1 the hole mobility for a p-type

$(Hg_{0.8}Cd_{0.2})Te$ with 1.6×10^{16} cm^{-3} acceptor density[30]. The
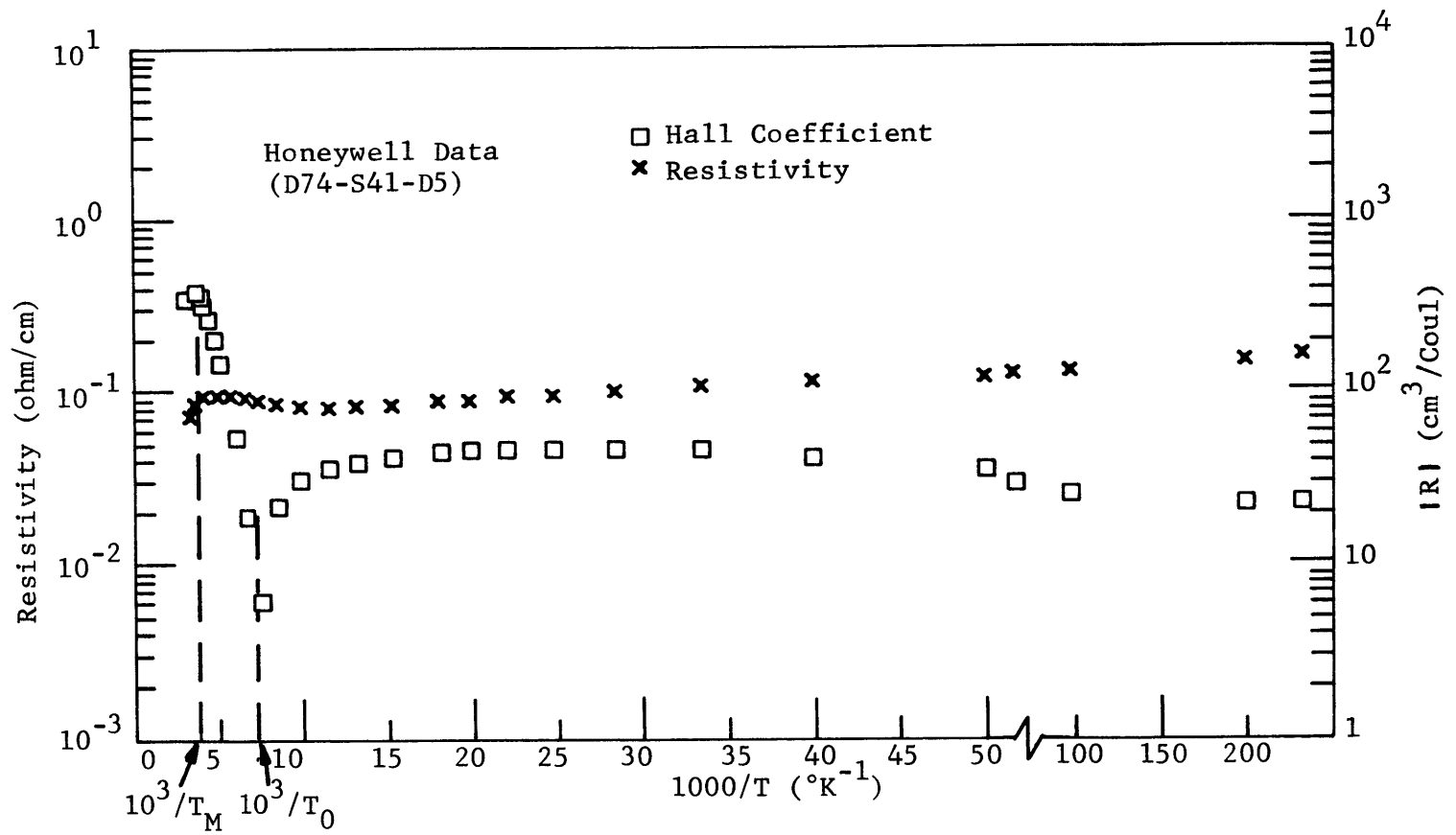
Figure 2.3.2   THE TEMPERATURE DEPENDENT HALL COEFFICIENT AND RESISTIVITY OF A p-TYPE $(Hg_{0.2}Cd_{0.8})Te$.

low doping sample apparently has a higher hole mobility at the temperature slope calculated from this sample is consistent with the one we obtain. We will use the average values of the two curves in our calculations,

$$u_{p\ell}(T) = \frac{500}{20^{0.8}} \times T^{0.8} \quad ; \tag{2.3.11}$$

$$u_{ph}(T) = 150 \times 300^{1.35} \times T^{-1.35}. \tag{2.3.12}$$

And the complete hole mobility expression is again

$$\frac{1}{u_p(T)} = \frac{1}{u_{p\ell}} + \frac{1}{u_{ph}} . \tag{2.3.13}$$

Now an explicit expression for the temperature dependence of the Hall coefficient can be obtained by substituting $p(T)$, $n(T)$, $u_p(T)$, and $\mu_n(T)$ into (2.2.2). $R(T)$ vs $10^3/T$ is then plotted in Figure 2.3.3, Figure 2.3.4 and Figure 2.3.5 as functions of various parameters.

Figure 2.3.3 illustrates the freeze-out effect on the uncompensated 10^{17} cm^{-3} p-type (Hg,Cd)Te. We can see that the value of the slope at low temperatures is proportional to the acceptor activation energy E_A, while the high temperature region is almost unaffected.

Figure 2.3.4 illustrates the effect of compensation on p-type materials having $N_A = 10^{17}$ cm^{-3} and $E_A = 0.004$ eV. Increasing compensation would increase the relative magnitude and shift both the maximum and the crossover positions toward lower
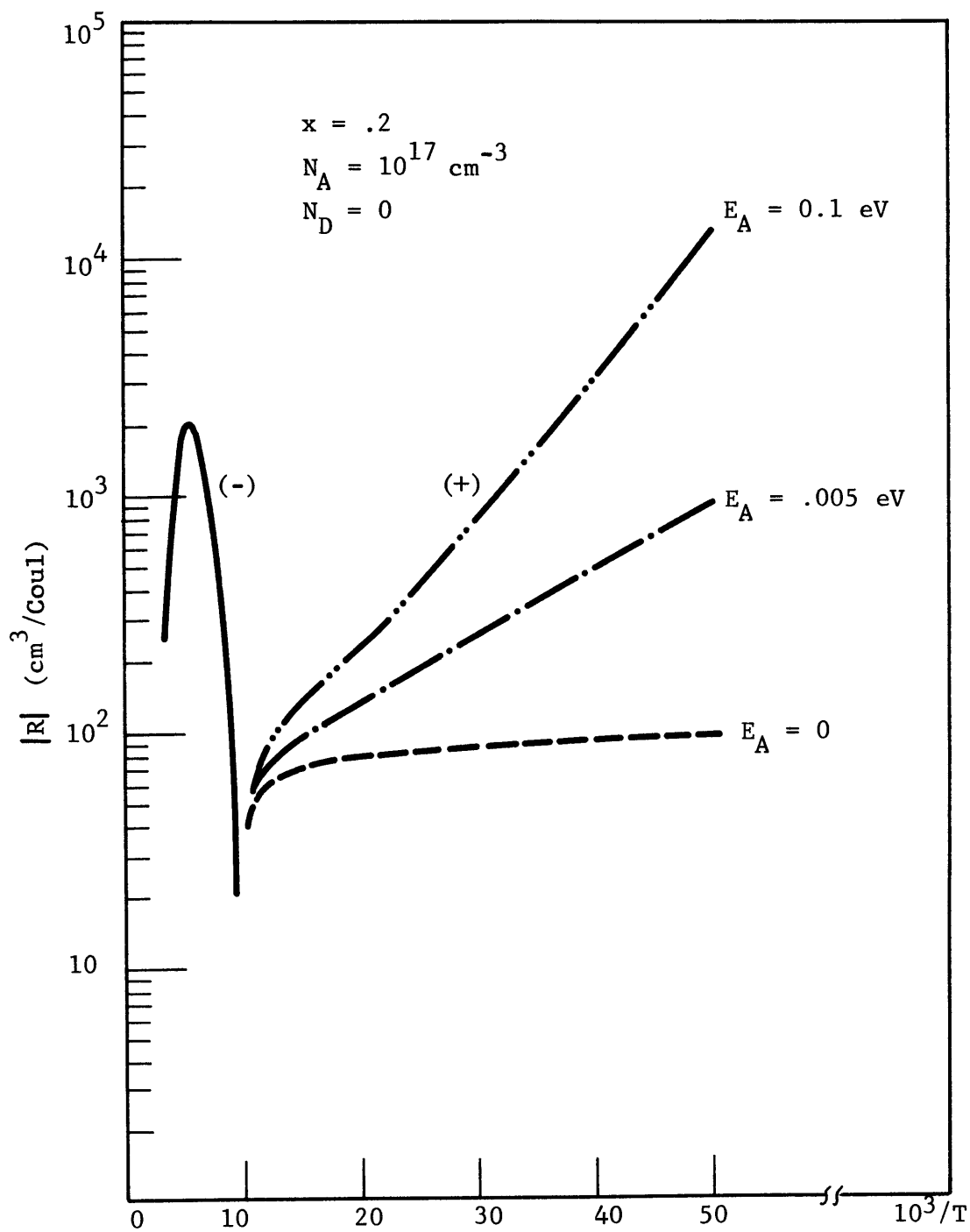
Figure 2.3.3 THE CALCULATED R(T) AS A FUNCTION OF E_A
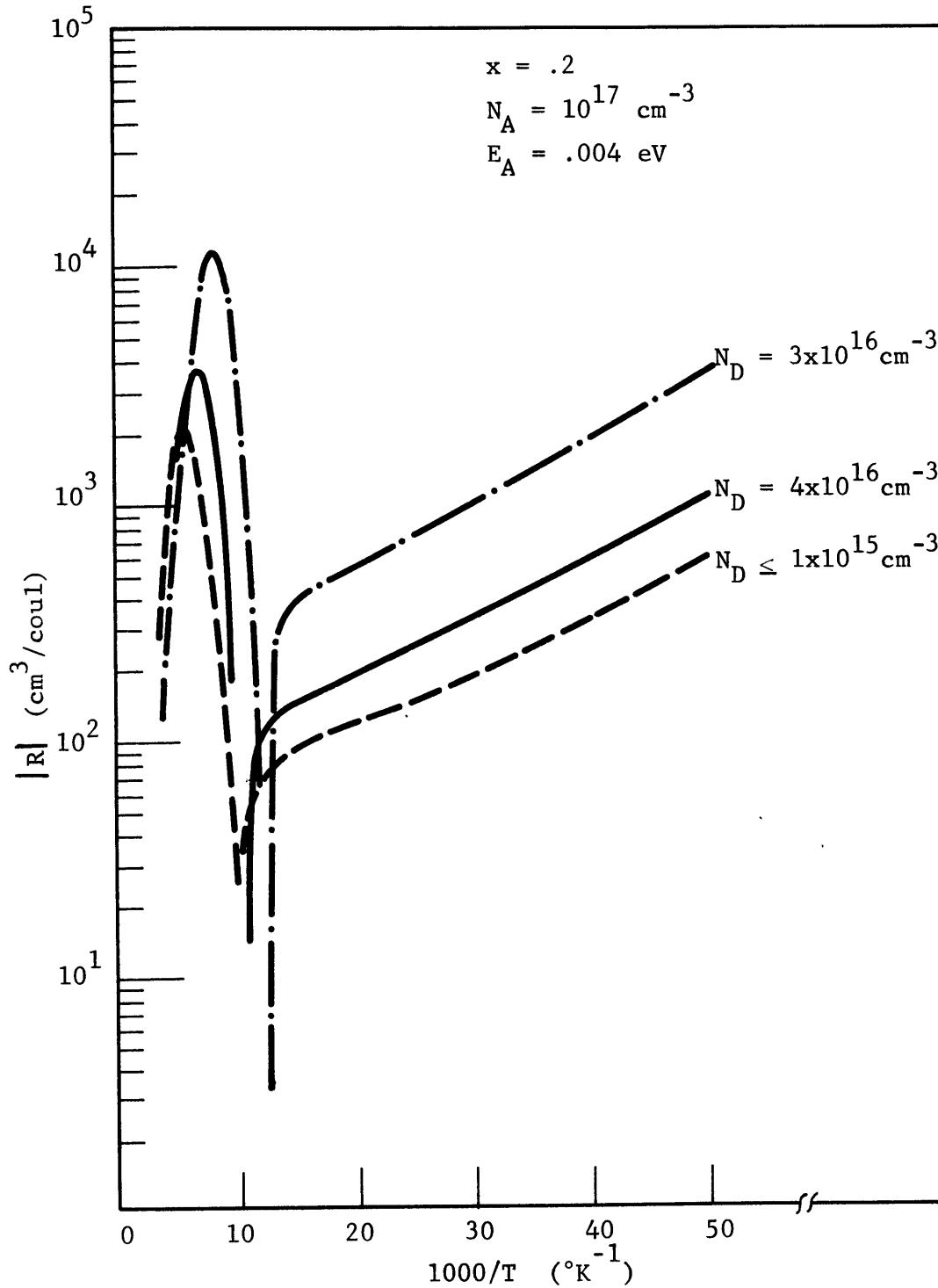
FIG. 2.3.4 THE CALCULATED R(T) AS A FUNCTION OF N_A.

47
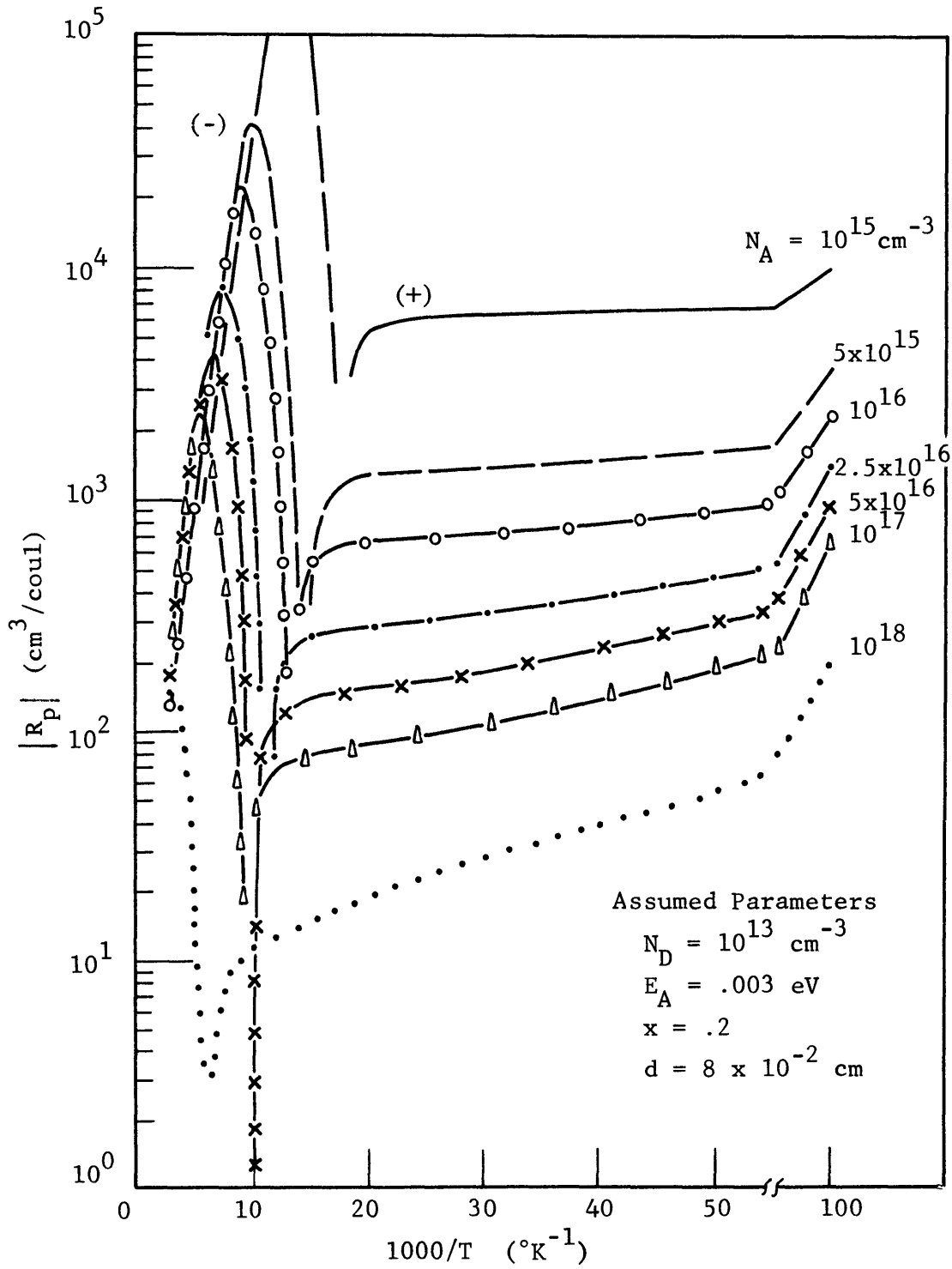
Figure 2.3.5 THE CALCULATED R(T) AS A FUNCTION OF N_A.

temperatures. For $N_D < 10^{15}$ cm^3, the compensation effects are negligible on the R(T) curves.

Figure 2.3.5 shows a family of R(T) for various acceptor concentrations with $E_A = .003$ eV and $N_D = 0$. Note that N_A has a similar effect on R(T) as N_D, that is increasing N_A would increase the relative magnitude and shift both the maximum and the crossover positions toward lower temperatures. But unlike the effects of compensation, increasing N_A tends to move the onset of freeze-out to a higher temperature. For $N_A = 10^{18}$ cm^3, the freezing out of holes starts almost at the crossover temperature which is 16.7°K.

2.4   QUANTITATIVE ANALYSIS ON THE MAGNETIC FIELD DEPENDENT HALL COEFFICIENT

Our concern in this section is to examine equation (2.1.19) for (Hg,Cd)Te as a function of temperature and magnetic field. Before going into numerical details, we first simplify (2.1.19) based on the fact that the mobility ratio for (Hg,Cd)Te is large. Then we consider the case for n-type material in which (2.1.19) can be further simplified by ignoring contribution from holes. Finally, numerical computation will be made to show the magnetic field dependence of the variable temperature Hall coefficient for p-type (Hg,Cd)Te.

For convenience, let us rewrite (2.1.19) below in a different form:

$$R(B) = \frac{\sigma_n^2 R_n C_n + \sigma_p^2 R_p C_p}{(\sigma_n C_n + \sigma_p C_p)^2 + B^2 (\sigma_n^2 R_n C_n + \sigma_p^2 R_p C_p)^2} , \qquad (2.4.1)$$

where

$$C_n = (\mu_n B)^{-2} ;$$

$$C_p = (\mu_p B)^{-2} . \qquad (2.4.2)$$

It can be shown that (2.4.1) is identical to (2.1.19). We know that $\mu_n \gg \mu_p$ for (Hg,Cd)Te. For n-type materials, we have $n\mu_n^i \gg p\mu_p^i$ for $i = 1$ or 2. Equation (2.4.2) thus reduces to

$$R_n(B) \simeq - (|q| n_b)^{-1} \text{ for } 0 \leq B \leq 10^5 \text{ G,}$$

which is independent of B. For p-type material, however, $n\mu_n^i$ may be comparable to $p\mu_p^i$ ($i = 1,2$) at the crossover temperature region, and $R_p(B)$ is clearly B dependent when mixed conduction prevails. Figure 2.4.1 shows that the p-type Hall coefficient, which is calculated on the basis of quantities obtained in the previous section, varies as a function of the magnetic field. Note that the effects of increasing B-field are to lower the value $|R_{max}|$ and shift the crossover to a higher temperature. These calculations are consistent with measurements done on p-type InSb[8].

50

The y-axis is labeled $|R|$ (cm^3/coul) with values 10^5, 10^4, 10^3, 10^2, 10, 1.

The x-axis is labeled $1000/T$ ($^\circ$K^{-1}) with values 0, 5, 10, 15, 20, 25, 30, 35, 40, 45, 50, 100, 150, 200.

Legend:
- B = 0
- B = 20 KG
- B = 40 KG

Assumed Parameters

$x = .2$

$N_A = 5 \times 10^{15}$ cm^{-3}

$N_D = 10^{13}$ cm^{-3}

$E_A = .003$ eV

$d = 8 \times 10^{-2}$ cm
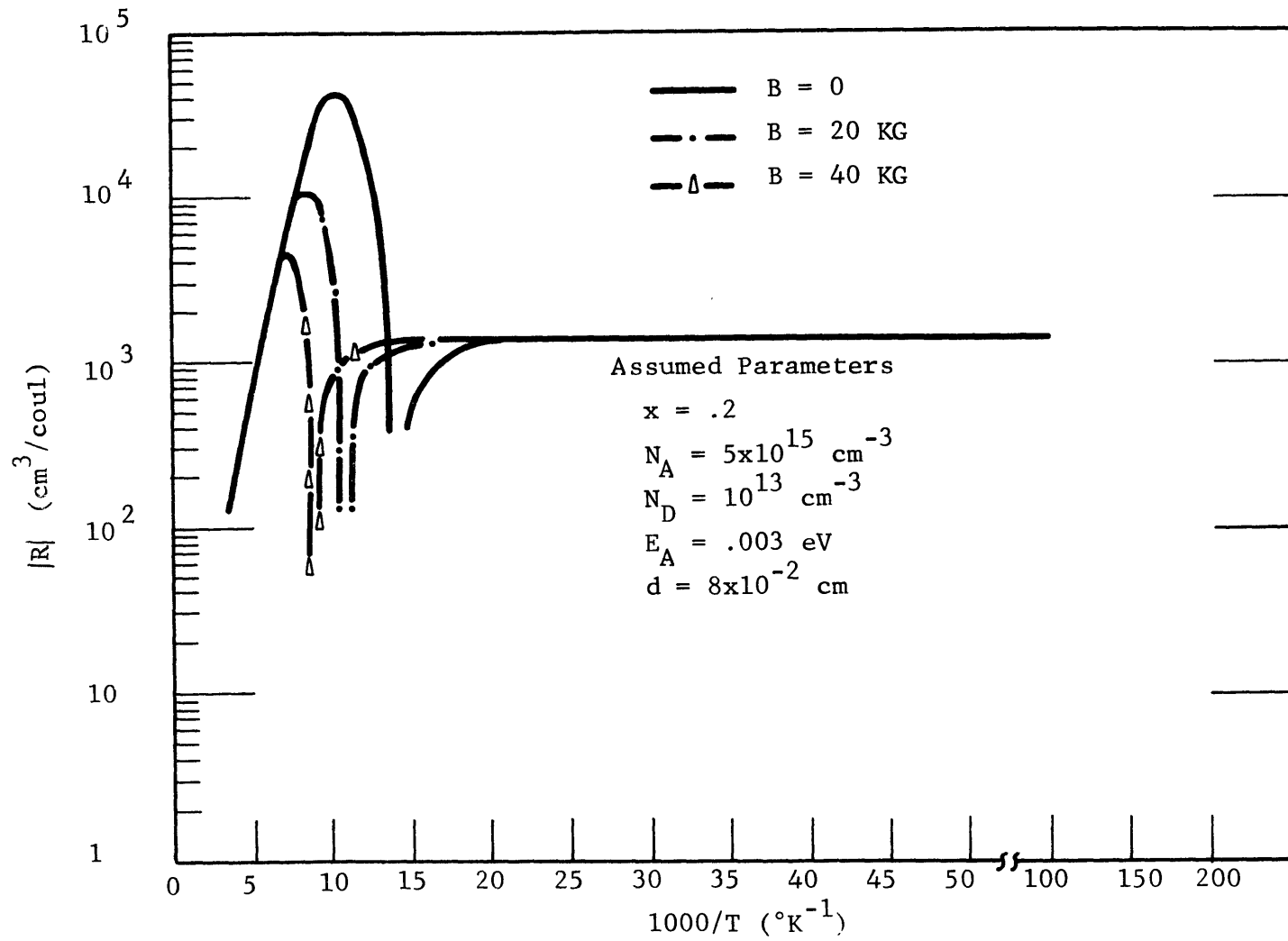
Figure 2.4.1   THE CALCULATED R(T) AS A FUNCTION OF THE MAGNETIC FIELD B.

Although transport properties for p-type semiconductors are complicated by mixed conduction at high temperatures and effects of freeze-out and compensation at low temperatures, the temperature dependence of the Hall coefficient cannot account for the anomalous behaviors as characterized by the peak and DCO mentioned in Chapter I. Therefore, we conclude that the anomalies are not due to either single or mixed conduction via the conduction band or/and the valence band which will be referred to as "bulk conductions" hereafter. Various models have been proposed to account for the anomalous conduction and they will be discussed in detail in Chapter III.

CHAPTER III
ANOMALOUS CONDUCTION IN SEMICONDUCTORS

Since the discovery of the Hall effect, Hall measurements have been made in almost every semiconductor in the study of the electrical properties. It was soon discovered that certain anomalies associated with the variable temperature Hall quantities were reproducible and they were found in many semiconductors. They are called anomalies because they cannot be interpreted on the basis of "bulk" conduction which has been discussed in the previous chapter. Being able to identify the origins of these anomalous conductions will be extremely valuable from the standpoints of fundamental physics as well as device applications.

This chapter is concerned with the present-day understanding variable temperature Hall properties of these anomalies. We begin by reviewing the anomalous temperature dependent Hall coefficients found in five representative semiconductors. Similarities and major differences among them will be summarized. We then present six models proposed to account for the anomalies in various semiconductors. Finally, we recommend the most favorable model for (Hg,Cd)Te.

3.1   REVIEW OF ANOMALOUS ELECTRICAL PROPERTIES IN SEMI-
        CONDUCTORS

Anomalous Hall coefficient temperature relationships have been

observed in many other semiconductors as well as in (Hg,Cd)Te.

The terminology used in Section 1.2 for (Hg,Cd)Te can also be

applied to classify anomalies observed in other semiconductors

if the corresponding temperature regions are modified. In

other words, all anomalous Hall coefficients either show a peak

or DCO. However, this does not mean that anomalies of all

materials are due to a single origin. Anomalies of various

materials may appear in a similar fashion even if they are

caused by different mechanisms. In fact, as we will discuss in

Section 3.2, there are quite a few models proposed to explain

the anomalies in different materials. In this section, we

briefly review anomalous Hall measurements done on a group of

semiconductors: Ge, InSb, GaAs, Mg_2Sn and InSb.

    (a) Ge (n- and p-types): The observations of Hung[2,3,4]

         and Fritzsche on Ge showed that at temperatures between

         80°K and 900°K the Hall coefficients behaved classi-

         cally, that is, n- or p-type. But as the temperature

         was reduced from 80°K to 4.2°K, the Hall coefficients

         showed peaks at temperatures where the resistivities

         seemed to saturate. With increasing impurities, the

         onsets of the anomalies shifted to higher temperatures.

Yonemitsu et al[7] further observed DCO's of the Hall
coefficients in the heavily compensated samples.

(b) InSb(p-type): Anomalies identical to those discovered
in Ge had been found in p-type InSb at low temperatures[8].
Putley[9] pointed out that the anomalies depended on the
nature of the surface. Etching reduced the value of
the peak in the Hall coefficient by about an order of
magnitude and produced a corresponding decrease in the
resistivity. The mobility, however, was not very
dependent upon the surface treatment. Vinogradova et
al[10] later found DCO's when high biased current was
applied. As the current was reduced, the second cross-
overs disappeared and the Hall coefficients were left
with peaks only which were no longer sensitive to the
current.

(c) GaAs (n-type): The temperature dependent Hall coeffi-
cient showed two peaks. The lower temperature peak
might occur over a wide range of temperatures[11] (from
15°K to 100°K), while the high temperature peak only
occurred at the onset of the intrinsic region[12,13].
Both the magnitude and the position of the low temper-
ature peak were impurity density dependent while those
of the high temperature peak were not.

(d) Mg_2Sn (n- and p-types): At low temperatures, n-type Mg_2Sn samples showed DCO's and p-type samples showed only peaks[14]. Ground surfaces seemed to show a lower second crossover temperature than cleaved surfaces.

(e) InAs (p-type): DCO's and peaks very similar to those observed in (Hg,Cd)Te were found in heavily compensated ($N_A < 10^{17}$ cm^{-3}) p-type InAs[15,16]. Later, it was found that anomalies could be removed by etching the surface[17,18] or by heat treatment[15]. The second sign reversal laid at lower temperatures for samples having higher doping[15,18]. Peaks at low temperatures similar to those in Ge and InSb had also been reported[19].

Anomalous Hall coefficients for all the semiconductors discussed above are plotted in Figures 3.1.1 to 3.1.5 for comparison
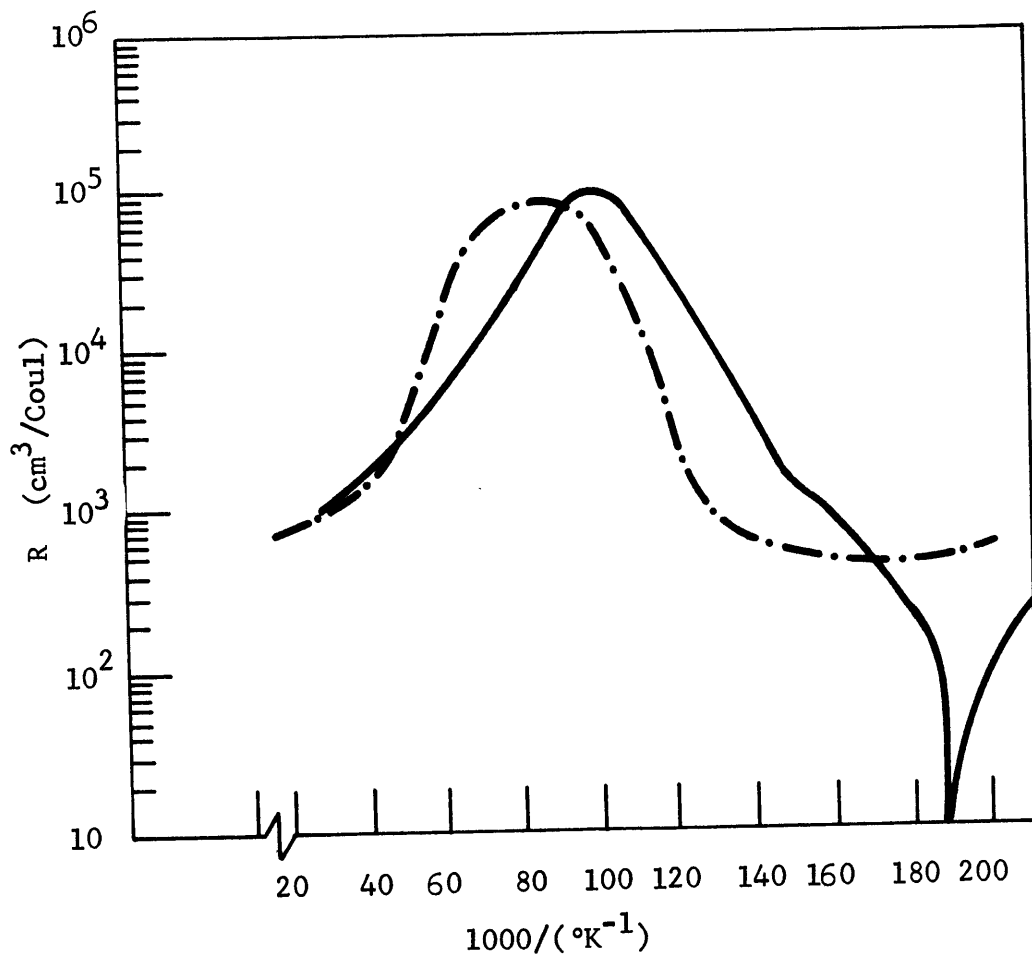
FIG. 3.1.1   R VS 10^3/T IN Ge(——),REF. 7;(—··—),REF.4.

57
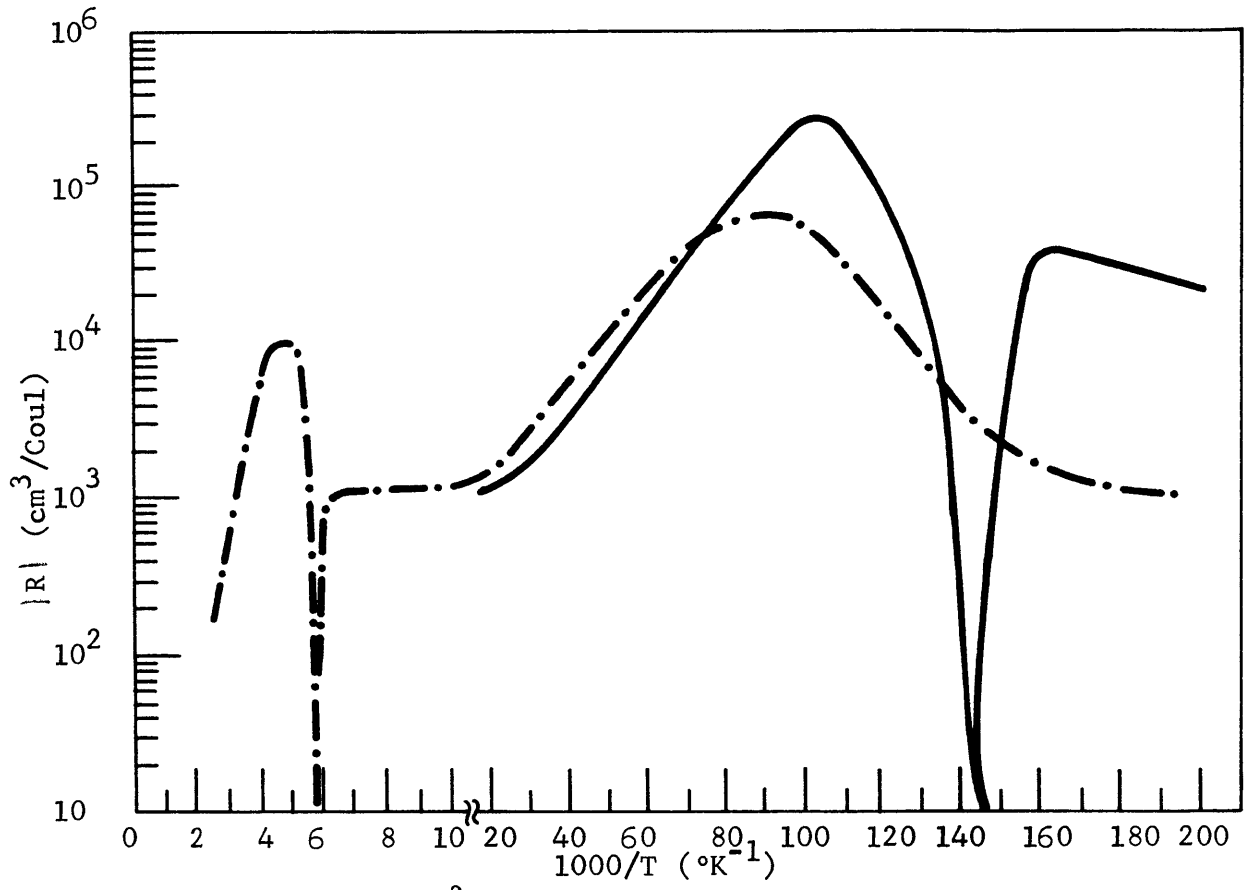
FIG. 3.1.2   R VS 1o³/T IN InSb: (——),REF. 10; (–·–),REF. 8.

58
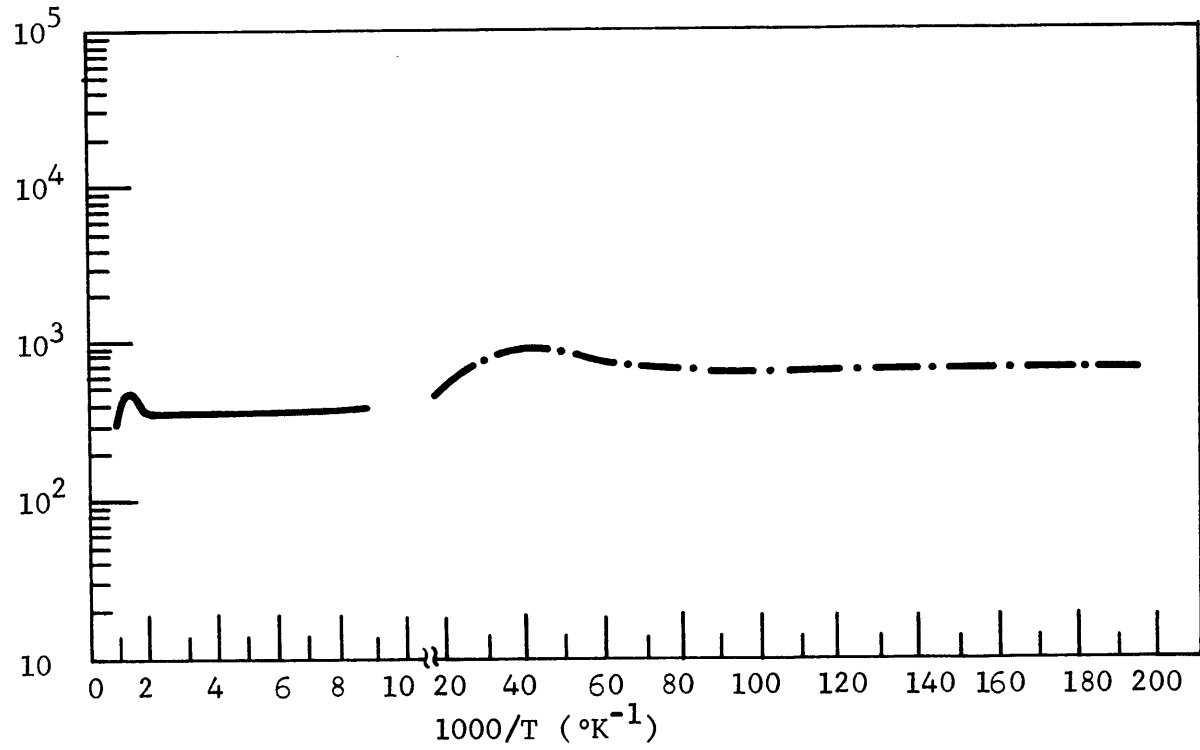
FIG. 3.1.3   R VS 10^3/T IN GaAs: (——), ref.13; (←·→),REF. 11.
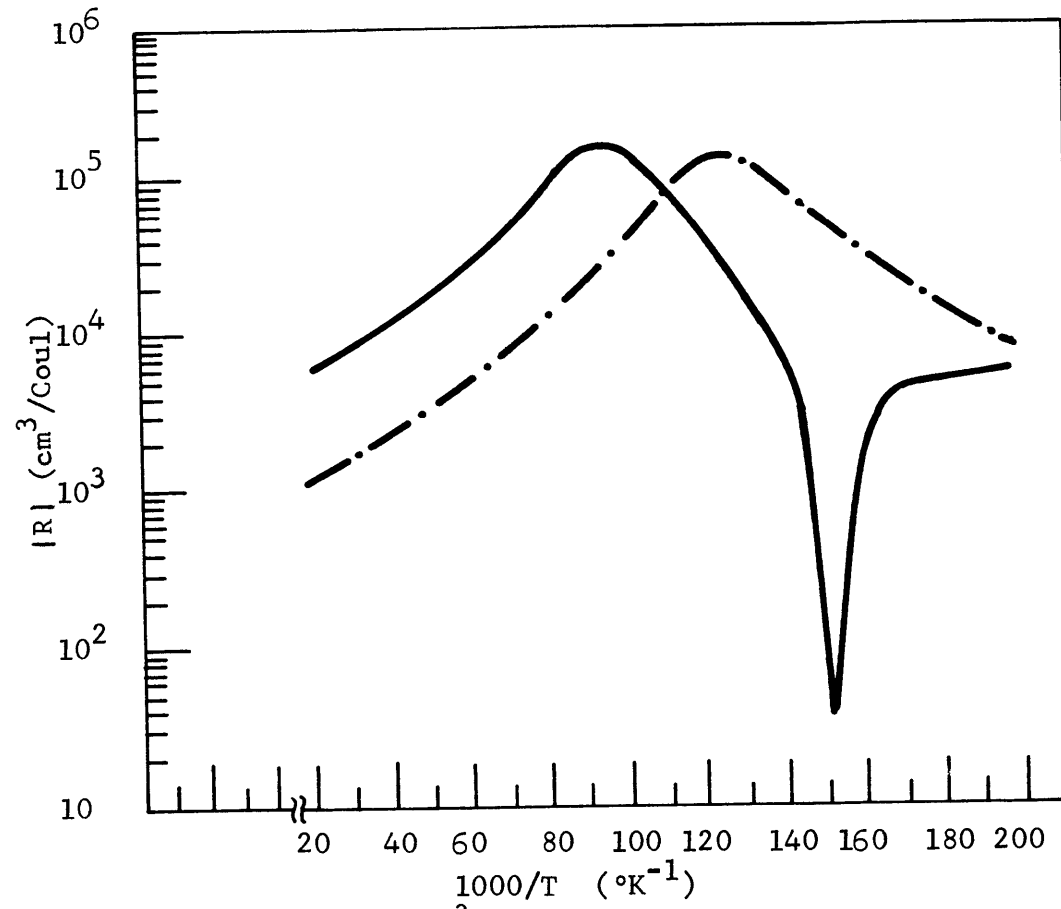
FIG.3.1.4   R VS 10^3/T IN Mg_2Sn, REF. 14.
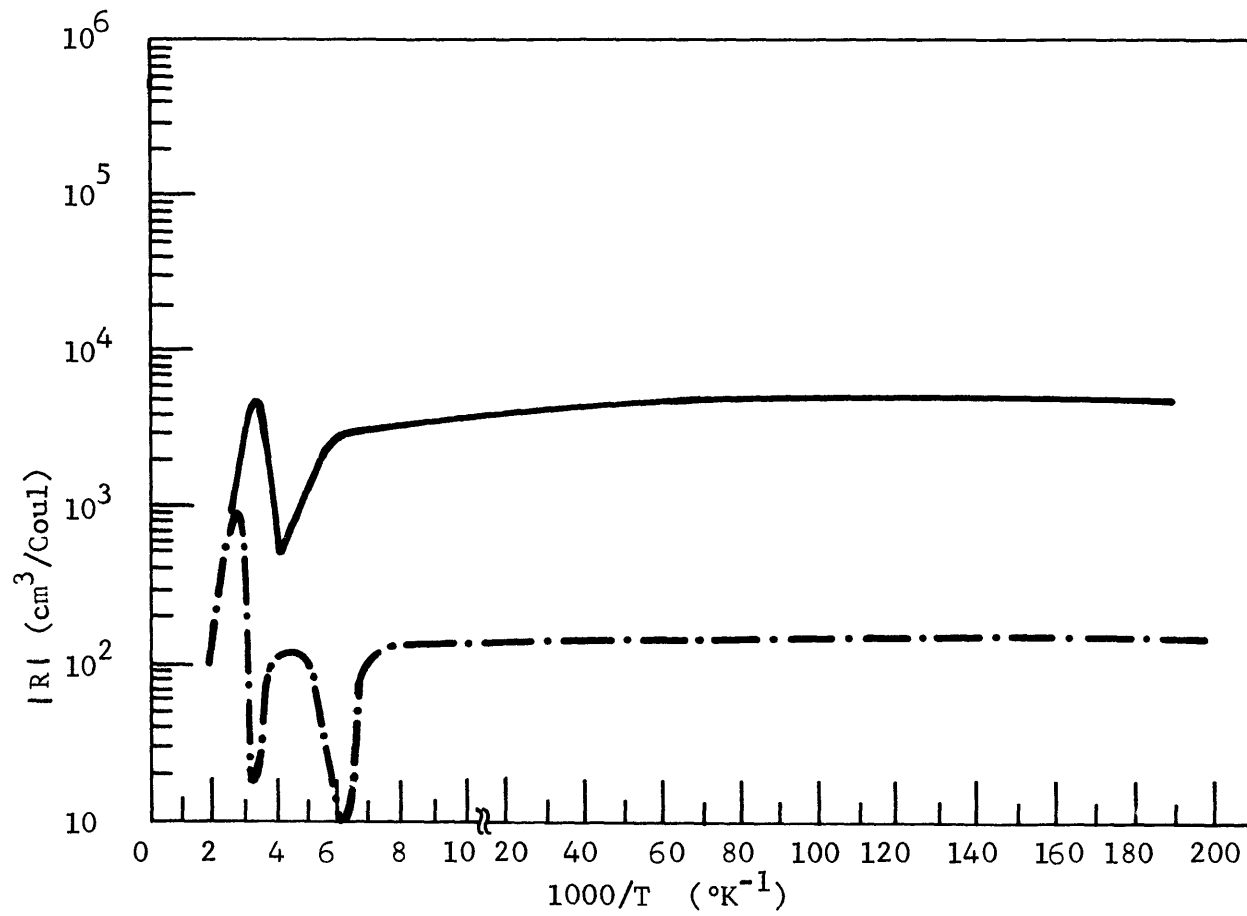
FIG. 3.1.5 R VS $10^3/T$ IN InAs,REF. 16.

By studying the anomolous in these materials, one can summarize their general features as follows:

a. The second crossovers in most of these simiconductors generally occur at the very low temperatures, unlike those associated with (Hg,Cd)Te, which appear in the medium temperatures and over a much wider range.

b. The second crossovers always appear at lower temperatures than the peaks for all semiconductors mentioned.

c. The Hall coefficient is alwasy negative at the intrinsic region. The sign for the peaks is determined by the number of crossovers.

d. For the materials having more than one peak, the low temperature peaks are larger both in magnitude and in covered temperature range than the near-intrinsic peaks.

e. All peaks increase in magnitude and shift to lower temperatures as the impurity doping is reduced.

f. Most anomalous are sensitive to sample surface treatments.

Examples of the wide variety of anomalous Hall coefficients observed in (Hg,Cd)Te are shown in Figure 3.1.6-7. These data are all for $Hg_{1-x}Cd_xTe$ ingots of nominal composition $x \simeq 0.2$. The major differences between the anomalies of (Hg,Cd)Te and those of other semiconductors are:
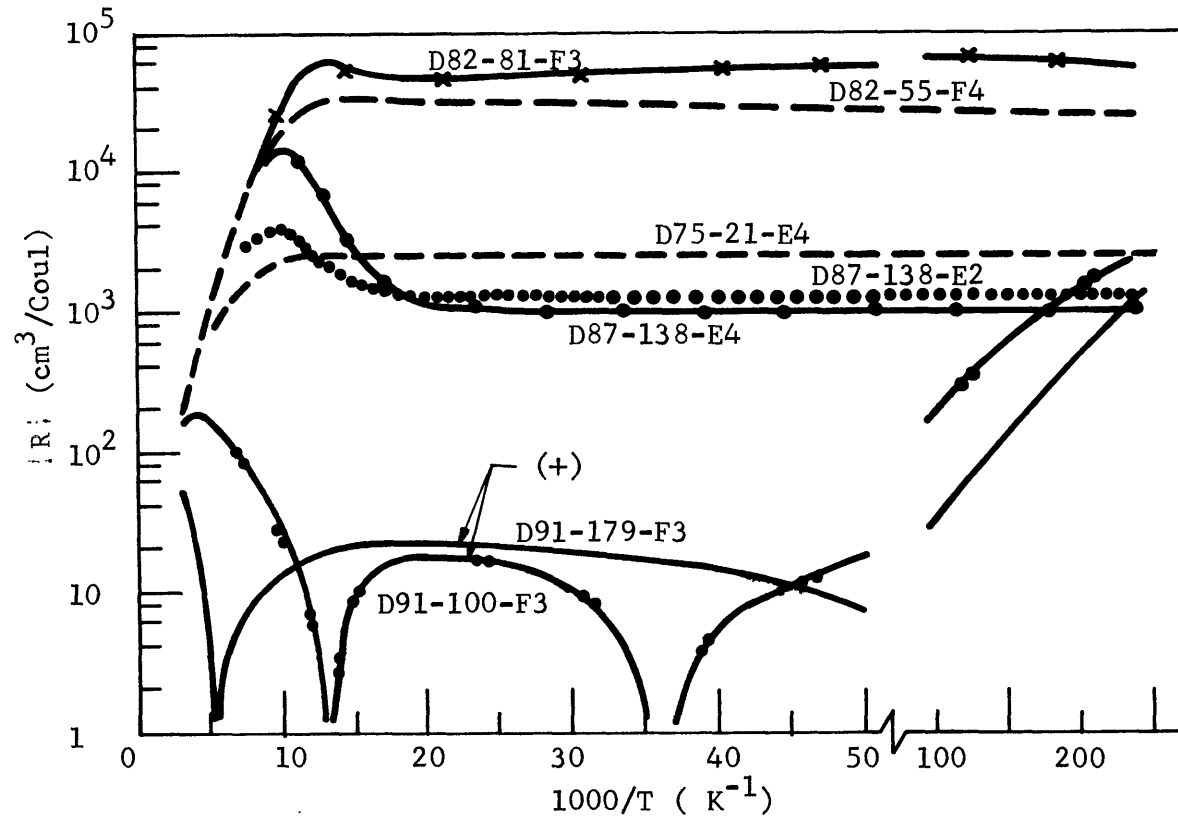
Fig. 3.1.6 R Vs 10^3/T FOR SEVERAL $(Hg_{0.8}Cd_{0.2})$Te SAMPLES.
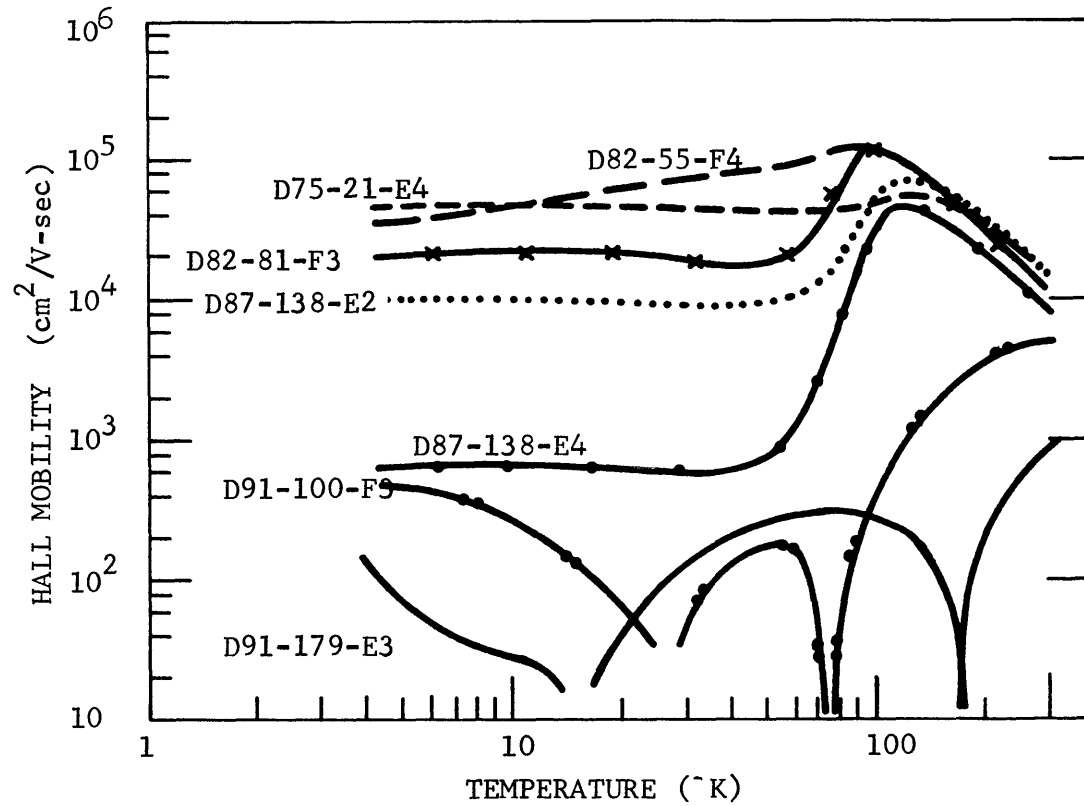
FIG. 3.1.7 HALL MOBILITIES VS TEMPERATURE FOR SEVERAL $(Hg_{0.8}Cd_{0.2})Te$ SAMPLES.

a. The peaks of R(T) always occur at the onset of the intrinsic temperatures, unlike those of Ge, InSb and Mg_2Sn which occur at low temperatures, or those of GaAs which occur at either high or low temperatures.

b. The second crossovers of R(T) occur over a wide range of temperatures, unlike those of InAs which always occur at high temperatures(greater than 100°K), or those of Ge, InSb, and Mg_2Sn which always occur at low temperatures (less than 10°K).

3.2   REVIEW OF VARIOUS MODELS

Various models have been put forward, most of which have in common that the current is carried by at least two parallel conduction mechanisms, while the degree to which the various mechanisms participate varies with temperature. The total conductivity σ is the sum of the conductivity in the "bulk", which is conduction via the conduction band and/or the valence band (indicated by the subscript b) and the conductivity in the "anomalous origins" (subscript a), each mechanism has its own mobility and carrier density*,

$$\sigma = A_a\sigma_a + A_b\sigma_b = A_a \left| q \right| n_a \mu_a + A_b \left| q \right| n_b \mu_b \; , \qquad (3.2.1)$$

and the Hall coefficient is *

$$R = - \frac{\gamma_a A_a \mu_a \sigma_a + \gamma_b A_b \mu_b \sigma_b}{(\sigma_a + \sigma_b)^2} \; , \qquad (3.2.2)$$

where A_a and A_b are the fractions of the total cross section of the sample passed by the two currents, and γ_a and γ_b are the Hall coefficient factors depending on the nature of the scattering. Equation 3.2.2 leads to a maximum in $R = \left| R(T) \right|$ if n_a/n_b varies with temperature while $\mu_a \neq \mu_b$[19]. It may also give rise to

---

* In general, one may write

$$\sigma = \sum_k A_k \sigma_k \; ,$$

and

$$R = - \frac{\sum_k \gamma_k A_k \mu_k \sigma_k}{(\sum_k A_k \sigma_k)^2} \; .$$

66

DCO if n_a and n_b are of different types of carriers. The bulk components have been treated in detail already . In this section, our main concern is the origin of the anomalous components. Models proposed to account for the anomalies are reviewed in the following.

a) Surface Conduction

Most of the anomalies in various semiconductors depend on surface treatment as mentioned in the last section. This is a good indication of the importance of the conduction at the surface. The surface conduction arises from the space charge layer at the surface due to the existence of surface states which trap holes or electrons at the surface of the sample. The carrier densities at the surface are different from that in the bulk. The carrier densities and the carrier types at the surface are determined by the density and charge of the surface states. Thus, it is not uncommon to have an n-type layer coated on a p-type bulk or vice versa. The surface component together with the bulk make the overall conductivity and Hall coefficient fairly complex and can possibly give rise to anomalies if the prescribed conditions (3.2.1) and (3.2.2) are satisfied.)

This model has been suggested to explain anomalies in InAs[20] and Mg_2Sn[14].

b) Inhomogeneity Conduction

Anomalous phenomenon may also be due to macroscopic or
microscopic inhomogeneities within the crystal. Macro-
scopic inhomogeneities can be detected by electrical,
thermal and optical probings. However, a crystal could
be highly inhomogeneous microscopically even if it is
proved by such methods to be macroscopically homogeneous.
Microscopic inhomogeneities could result from segrega-
tion of impurities around dislocations or crystalline
imperfections which are not easy to detect.

Owing to such inhomogeneities, the crystals may consist
of sections having a different concentration of carriers
and therefore both a different conductivity and a dif-
ferent temperature dependence of conductivity. The over-
all conductivity that one measures will be the sum of
each individual component. If the mobility variation
is large, such inhomogeneous conduction will have a
large effect on the measured Hall voltage and DCO or
peak may be expected if the required condition is satis-
fied.

This model was named to explain anomalies in InAs[15] and
InSb[10].

68

c) Impurity Band Conduction

An electron occupying a donor has a wave function local-
ized about the impurity and an energy slightly below the
conduction band minimum. Because there is a finite
overlap of the wave function of an electron on one donor
with neighboring donors, a conduction process is pos-
sible in certain circumstances in which the electron
moves between centers by tunneling without activation
into the conduction band. This is called impurity band
conduction. The circumstance in which impurity band
conduction is possible even though the overlap between
centers is very small in the presence of "compensation"
- the presence of charged minority dopants which recom-
bine some carriers from the majority dopants and thus
allows the movement of carriers from an occupied major-
ity center into an unoccupied one.

One feature of impurity band conduction, which distin-
guishes it from the normal semiconduction, is its
extreme sensitivity to impurity concentration. Another
feature is that, when the impurity concentration is low,
the semi-log plot of the resistivity versus $1/T$ exhibits
a finite slope in the temperature range where impurity
conduction predominates, suggesting that the charge
transfer between impurity centers must itself be

thermally activated. Above a critical doping level,
the resistivity becomes independent of temperature,
because the carrier can move freely without thermal
activation. The Hall coefficient expressed by (3.2.2)
thus shows a peak at the temperature where conductions
in both the impurity band and the conducting bands take
place. If the hole mobility is small, a heavily com-
pensated p-type material will exhibit DCO at the temper-
atures where electron movement among acceptors pre-
dominates.

Anomalies in $Ge^{2-5,7}$, $InSb^{8}$ and $GaAs^{11}$ are claimed to
be associated with this mechanism.

d) Higher Sub-band Conduction

In some semiconductors, there are higher-lying sub-bands
above the lowest conduction band minimum which may have
influence on the transport properties. An electron in
the conduction band can be excited into these higher
sub-bands by absorbing a photon or under the influence
of a high electric field. Usually these sub-bands lie
so high that electrons can hardly remain them in ther-
mal equilibrium. However, in some semiconductors the
sub-bands are only a few tenths of an eV above the
lowest conduction band that electrons can be evaporated

into these bands when temperature is increased. Thus, these sub-bands can play a role in the conduction.

Electrons in the higher sub-band are expected to have a higher mobility than those in the lowest conduction band if the effective mass at the sub-band is smaller. For a constant total number of electrons, (3.2.2) predicts an increase in the Hall coefficient with increasing occupation ratio n_a/n_b (n_a, n_b are electron concentrations at the sub-band and the lowest conduction band, respectively), i.e., with increasing temperature. A maximum is reached when the total number of electrons $(n_a + n_b)$ starts to increase at the onset of the intrinsic region, since then the Hall coefficient drops rapidly.

This mechanism predicts that a peak of the Hall coefficient can only occur at the onset of the intrinsic temperature. It fails to account for DCO since it involves only one type of carrier, hence, the Hall coefficient consists of components which are of the same sign. GaAs is believed to have higher sub-band conduction which causes the anomalous Hall properties[13].

e) Hall Contact p-n Junctions

If a crystal has a mixture of n-type and p-type regions, a "floating potential" will appear at the p-n junctions

71

in a magnetic field. By solving the transport equations, Madelung[24] showed that after application of a magnetic field, a floating potential must be set up to bias the p-n junction in such a way that the diffusion currents balance out the ambipolar currents. Thus, this floating potential can either enhance or even overcompensate for the Hall voltage drop in the p-region depending on the ambipolar current density of the p-region compared with that of the n-region. In general, according to Madelung, the floating potential is always directed opposite to the Hall voltage of the region in which the larger ambipolar current flows, i.e., essentially the Hall voltage of the more weakly doped region.

For the case where the n-region is doped much higher than the p-region, we have[24]

$$V_M = - (\mu_n + \mu_p) E_x B_z L_n;$$ (3.2.3)

similarly, when the p-region has much higher doping than the n-region, we have

$$V_M = - (\mu_n + \mu_p) E_x B_z L_p,$$ (3.2.4)

where V_M is the Madelung floating potential, L_n and L_p are diffusion lengths for the n- and p-regions, respectively.

Now consider the case where we have a p-type semi-
conductor in the magnetic field at which the Hall probe
is a contact with a p-n junction extending immediately
in front of it. The p-type bulk is bounded by two p-n
junctions and the net voltage appears at the Hall probes
will be the sum of the Hall voltage drop of the p-region
which is positive at low temperatures, and two Madelung
voltages which are always negative. The influence of
the Madelung potential can become so great that a second
sign reversal may occur in the Hall coefficient if the
following condition is satisfied:

$$\left| V_p \right| < \left| V_M \right| \tag{3.2.5}$$

where V_p is the Hall voltage drop across the p-region
and is given by equation (2.1.12), or

$$V_p = \mu_p E_x B_z d_p \tag{3.2.6}$$

where d_p is the thickness of the p-type bulk.

This effect was proposed to explain anomalies in InAs.

f) The Elliott - Spain Model

Elliott and Spain[25] proposed a simple model, involving
a deep acceptor level with an activation energy com-
parable to the band gap, to account for the anomalies.
They assumed that the acceptor density N_a was greater

73

than the donor density N_d, and that at very low temperatures, the acceptor activation energy, E_a, was greater than the band gap and was tied to the valence band. The donor levels were assumed to be merged with the conduction band. They further assumed that the band gap increased with temperature.

At zero degree Kelvin, there will be N_d free electrons and no free holes (Figure 3.2.1a). As the temperature is raised, the energy gap increases and the electron concentration will remain constant until E_a lies up with the bottom of the conduction band (Figure 3.2.1b). This would correspond to a negative Hall coefficient at low temperatures. Further increase in temperature results in a decrease in free electrons due to the presence of the acceptors. This would correspond to a rise in the Hall coefficient. As the temperature is further increased, the intrinsic region begins to occur and the Hall coefficient reaches a maximum before declines as $1/qn_i$.

The detailed behavior of the Hall coefficient, according to Elliott and Spain, depends on the degree of compensation. For a more lightly compensated material, $|R|$ may have a "dip" before reaches a maximum. A DCO
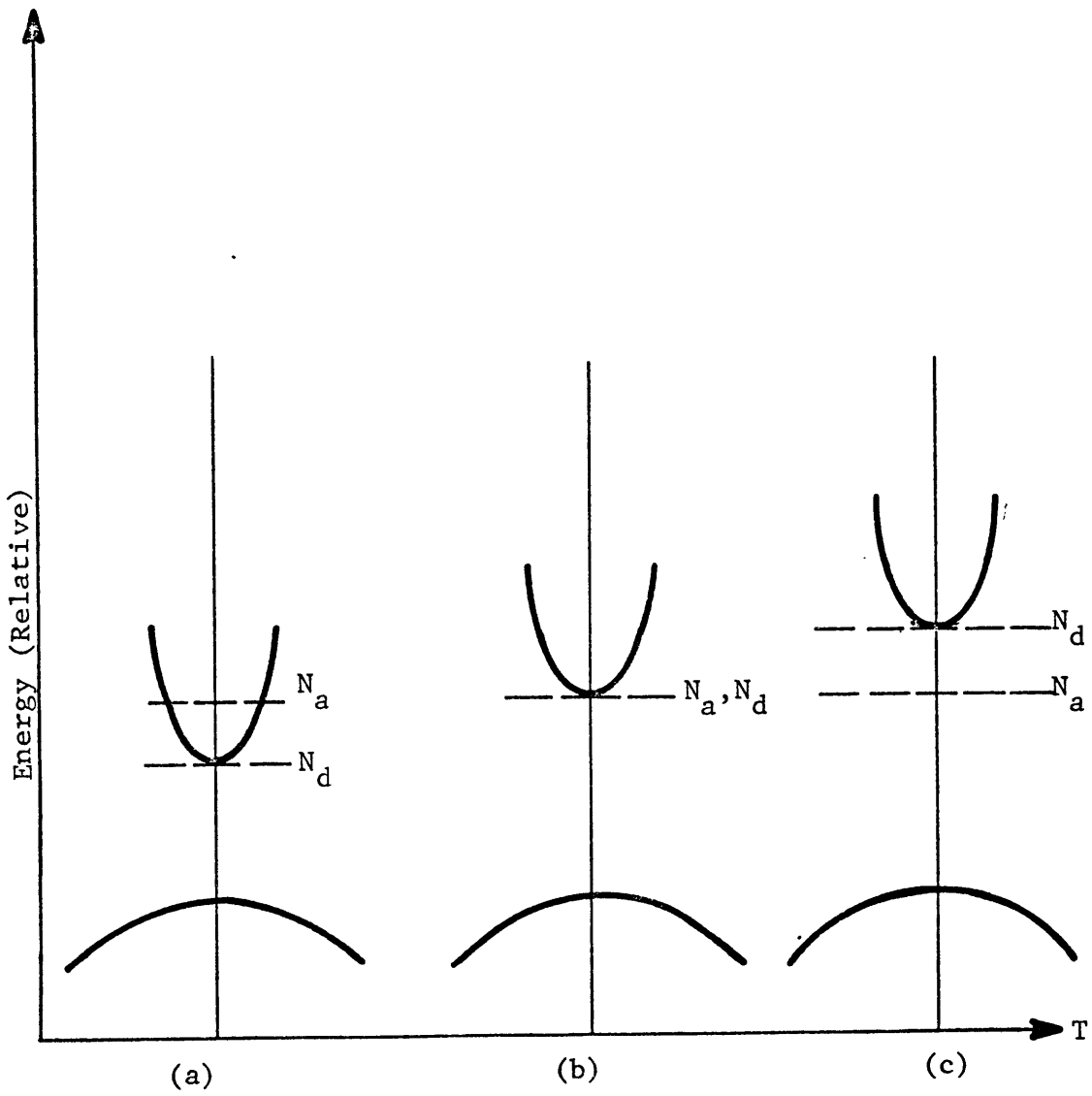
Figure 3.2.1   SCHEMATIC DIAGRAM SHOWING THE ELLIOTT-SPAIN MODEL
              (REF 25).

may occur if at some temperatures when $\sigma_p \mu_p > \sigma_n \mu_n$.

This model is suggested to account for the anomalies in (Hg,Cd)Te because the band gap for this material is rather sensitive to temperature.

3.3   A MODEL FOR (Hg,Cd)Te

The summary of possible models in the preceding section is by no means exhaustive. Any mechanism which can be expressed by (3.2.1) and (3.2.2) can also give rise to anomalous Hall behavior. Most of these models are phenomenological, and give us little in the way of a fundamental framework for the experimental findings in (Hg,Cd)Te. The reason, of course, is the great complexity of the problem when anything approaching a realistic model is employed.

Which model is more favorable for (Hg,Cd)Te? The impurity band conduction model fails to explain the presence of the high temperature peak. The higher sub-band model cannot account for the DCO. The inhomogeniety model predicts low reproducibility of the anomalies which is not the case. The Elliott-Spain model lacks substantial experimental support. The Hall contact model cannot explain the peak. The only model left is the conducting surface model.

Scott et al[23] first postulated that the anomalous properties observed in (Hg,Cd)Te were attributed to surface conduction.

They showed the effects of surface treatments and heat treatments on a DCO-type sample. The results showed that the influence of the surface on these anomalies was tremendous. Antcliffe[36] et al reported the existence of an inversion layer on p-type (Hg,Cd)Te by means of magnetoresistance measurements. Voronkov[22] et al took into consideration the effects of the Hall contact p-n junctions together with the conductivity layers on all lateral surfaces, and they were able to explain at least quantatively both the peak and DCO in the Hall coefficient of InAs.

In the early stage of this research, the author found the following fact deduced from the rich collection of Hall data supplied by Honeywell Radiation Center. That is the correlation between the sample thickness and the anomalous Hall coefficient and resistivity at low temperatures. These two quantities measured on thicker samples are in general larger than those on thinner ones. This effect has been observed in samples cut from the same ingot. From these observations, which will be discussed in more detail in Chapter V, we can rule out the possibilities of the impurity band model, the higher sub-band model, the Elliott-Spain model and the p-n junction model because they are clearly thickness independent. The inhomogeniety model was also rejected because it cannot explain the

direct proportionality between the measured quantities and the thickness.

Being motivated by the work of Scott[23], Antcliffe[36] and Voronkov[22], and by the observation of a thickness dependence in the data, we considered the conducting surface model to be preferable and concentrated our investigations mainly on this model. This does not mean that we excluded the possibility of any other models, but we directed our attention to the hypothesis that an inverted n-type surface was responsible for the anomalous Hall effect in (Hg,Cd) Te. The goal of this research was to verify or to reject this hypothesis on the basis of the theoretical study compared with experimental investigations.

CHAPTER IV
THE CONDUCTING-SURFACE MODEL

At the end of the preceding chapter, we made a comparative study of various models for the anomalous Hall properties in (Hg,Cd)Te. There are strong indications that the surface plays an important role in the anomalies. In order to investigate the conductivity and Hall properties of the surface, we need to understand the physics of semiconductor surfaces. Because of this, we will, in this chapter, develop the theoretical groundwork for the conducting-surface model with which we may quantitatively analyze existing anomalous Hall data of (Hg,Cd)Te and design specific experiments to verify the validity of this model.

We begin by considering the conditions at the sample surface. Then we study the characteristic properties of the surface such as the potential, the carrier concentration and the mobilities at the surface. Next, we derive the total conductivity and Hall coefficient by integrating the transport equations from the surface to the bulk and express the total as the sum of the surface and the bulk components by means of the effective mobility formalism. Next, we derive an expression for N_A which enables us to find N_A from the anomalous $R(T)$ data. Finally, we remove the constraint on the magnetic field B and express R as a function of B of arbitrary strength.

4.1 CONDITIONS OF SEMICONDUCTOR SURFACES

There are often states whose wave functions are concentrated in the vicinity of the surfaces of crystals. The energy levels of such "surface states" may either be discretely or continuously distributed and may be either within the band gap or within the allowed bands.

Surface states on clean semiconductor surfaces can be related to different causes. Tamm[31] assumed that the lattice potential terminated in an asymmetrical manner and predicted a band of energy states between the valence and conduction band edges and localized at the surface. Schockley[3], using a symmetric termination of the lattice potential, obtained the result that the bands of states should exist both between as well as overlapping the conduction and valence bands. Both Tamm and Schockley states depend on the nature of the perturbations and predict that the number of surface states available to trap electrons is approximately equal to the number of surface atoms that have unsaturated bands. The other type of surface state is more analogous to the bulk centers, arising from impurities or defects underneath or upon the surface. The third type of surface state does not originate in the semiconductor itself; it comes from layers of foreign materials coated on the semiconductor surface which are either an accidental or deliberate result of the preparation procedure.

80

All these types of surface states may, in principle, act as traps, recombination centers, or both. All surface states, regardless of their origins, can be characterized by their charge. The acceptor type states should make a clean surface become negatively charged and cause the surface of an n-type semiconductor to develop p-type surface conductance (depletion or inversion).

4.2   POTENTIAL WITHIN THE SEMICONDUCTOR SURFACE

Due to the existence of the surface states which introduce localized charges at the surface, the carrier concentrations may vary more or less rapidly as functions of position in the sample. The situation then becomes much more complicated, since any gradient in the free carrier concentrations will set up a diffusion current, and equilibrium can be obtained only if there is an electric field which would offset this current locally. Along with the field, there is necessarily a departure from electrical neutrality and this results in a space charge region. Thus, we must deal with the Poisson equation which relates the potential and the net charge density to the position.

Consider the energy band diagram of a p-type semiconductor shown in Figure 4.2.1 in which the surface potential ψ_s is measured from the intrinsic energy level. We shall calculate
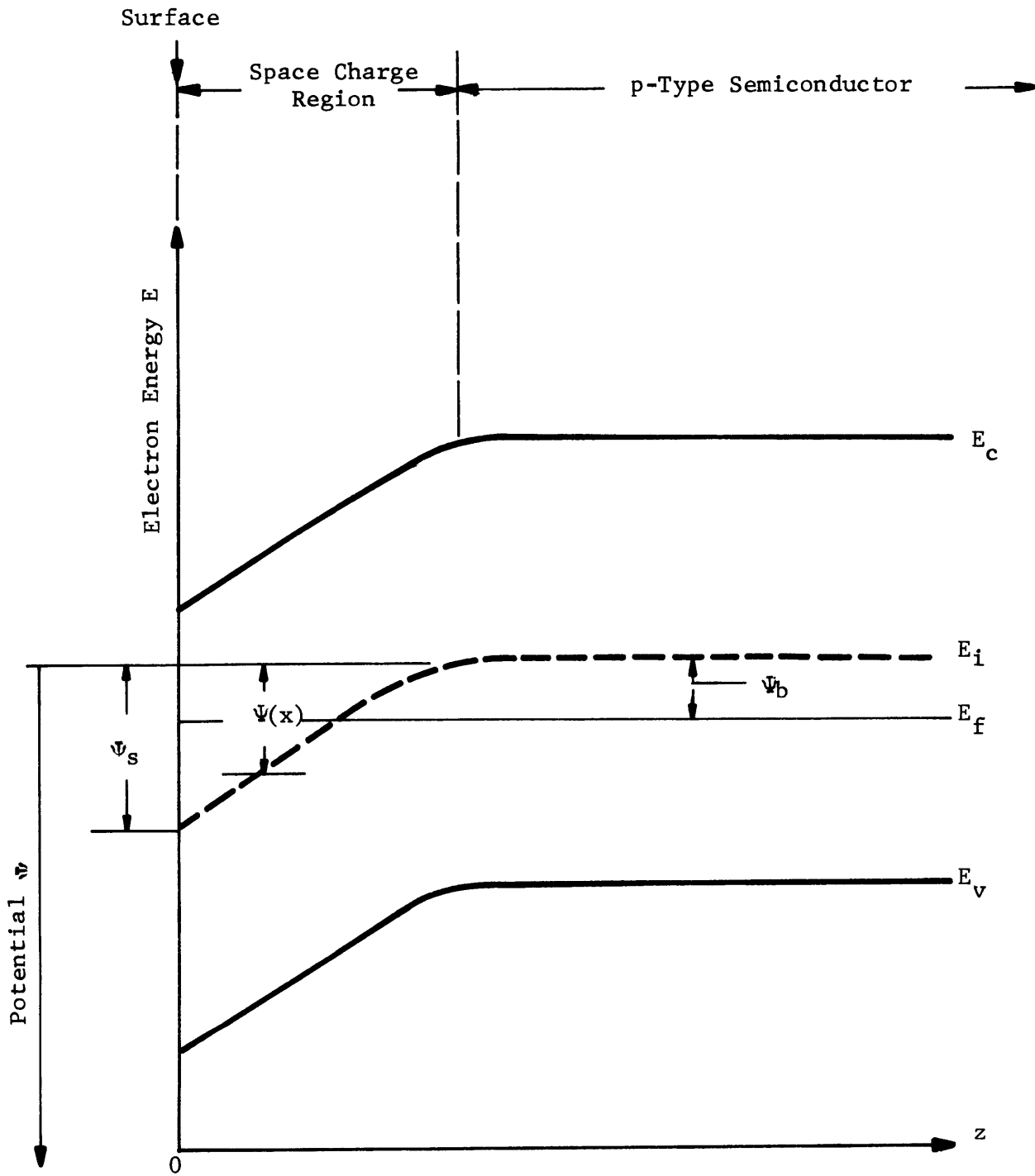
Figure 4.2.1   ENERGY BAND DIAGRAM NEAR THE SURFACE OF A
p-TYPE SEMICONDUCTOR

the potential and charge distribution within the semiconductor
as a function of ψ_s for a uniform doping $N_D^+ - N_A^-$ using the Pois-
son equation.

The charge density within the semiconductor $p(z)$ is the sum of
the charge due to holes, electrons and ionized impurities in
the bulk:

$$\psi(z) = q[p(z) - n(z) + N_D^+ - N_A^-] \qquad (4.2.1)$$

For a nondegenerate semiconductor, we have

$$\left.\begin{array}{l} n(z) = n_b e^{\beta\psi} = n_i e^{\beta(\psi_b + \psi)} \\[2mm] p(z) = p_b e^{-\beta\psi} = n_i e^{-\beta(\psi_b + \psi)} \end{array}\right\} \qquad (4.2.2)$$

where $\psi(z)$ is defined as zero in the bulk of the semiconductor
and equal to ψ_s at the surface, n_b and p_b are the equilibrium
densities of electrons and holes, respectively, in the bulk
of the semiconductor, and $\beta \equiv q/kT$.

The Poisson equation is given by

$$\frac{\partial^2 \psi}{\partial z^2} = -\frac{\rho(z)}{\epsilon_s} \qquad (4.2.3)$$

$$= \frac{-q}{\epsilon_s} [p_b(e^{-\beta\psi} - 1) - n_b(e^{\beta\psi} - 1)]$$

where ϵ_s is the permittivity of the semiconductor.

We shall introduce the following parameter:

$$d_s = 2 \sqrt{\frac{\epsilon_s}{q\beta(p_b + n_b)}} \qquad (4.2.4)$$

83

which is twice the effective Debye length (4.2.4). The effective Debye length $L = \frac{d_s}{2}$, characterizes the width of the inversion layer. More detailed calculations[33] show that, in accumulation and inversion layers, the characteristic length is a fraction of L, whereas in depletion layers, it is several times L.

With the help of (4.2.2) and (4.2.4), the Poisson equation becomes Equation (4.2.3), which can be more concisely expressed by using the following notations

$$\beta\psi = \nu$$

$$\beta\psi_b = u_b;$$

and the hyperbolic functions. (4.2.5) can thus be written as

$$\frac{\partial^2 \nu}{\partial z^2} = \frac{-4}{d_s^2} \left[\frac{\sinh (u_b + \nu)}{\cosh u_b} - \tanh u_b \right]. \qquad (4.2.5)$$

Multiplying both side by 2 $d\nu/dz$, we can integrate once and, using the conditions that $d\nu/dz = 0$ and $\nu = 0$ for $z = \infty$, we obtain

$$\frac{\partial \nu}{\partial z} = \mp \frac{2\sqrt{2}}{ds} \left[\frac{\cosh (u_b + \nu)}{\cosh u_b} - 1 - \nu \tanh u_b \right]^{1/2} \qquad (4.2.6)$$

The upper sign (minus) refers to $\upsilon > 0$, the lower sign (plus) to $\upsilon < 0$.

Equation (4.2.7) cannot be solved in closed form for the general case, but can be evaluated numerically[34].

84

For convenience, (4.2.7) can be rewritten by introducing the notation $F(u_b, \nu)$:

$$\frac{\partial \nu}{\partial z} = \mp \frac{2}{d_s} F(u_b, \nu), \qquad (4.2.7)$$

where

$$F(u_b, \nu) = 2 \left[\frac{\cosh(u_b + \nu)}{\cosh u_b} - 1 - \nu \tanh u_b \right]^{1/2} \qquad (4.2.8)$$

The important conclusion to be drawn from these equations is that the potential in the surface space charge region decreases approximately exponentially with distance from the surface. The characteristic length in which the potential drops to one-third of its value at the surface is the effective Debye length.

4.3   SURFACE EXCESS CARRIER DENSITY

The change in the number of holes or electrons per unit area which results from a finite surface potential can be described by the concept of surface excess carriers. The surface excess carrier densities are defined as the number   (per unit area) of mobile electrons ΔN_s, and holes ΔP_s, in the space-charge layer with respect to their numbers at flat band ($\psi_s = 0$). According to these definitions, the surface excesses are given by

$$\Delta N_s = \int_0^\infty (n(z) - n_b) \, dz;$$
$$\left. \right\} \qquad (4.3.1)$$
$$\Delta P_s = \int_0^\infty (p(z) - p_b) \, dz.$$

Substituting (4.2.2) and (4.2.8) into (4.3.1) and changing

the variable to ν, we obtain

$$\Delta N_s = n_b d_s \int_{\nu_s}^{o} \frac{e^{\nu}-1}{\mp F(u_b,\nu)} \, d\nu ,$$

$$\Delta P_s = P_b d_s \int_{\nu_s}^{o} \frac{e^{-\nu}-1}{\mp F(u_b,\nu)} \, d\nu . \qquad \qquad (4.3.2)$$

For the case of majority carriers in accumulation layers,

(4.3.2) can be written as

$$\Delta N_s = \frac{\Delta N_s}{ds} = n_b G^{+}(u_b,\nu_s) \text{ for } \nu_s \geq 0 \text{ in n-type}(u_b \geq 0);$$

$$\Delta P_s = \frac{\Delta P_s}{ds} = P_b G^{+}(u_b,\nu_s) \text{ for } \nu_s \leq 0 \text{ in p-type}(u_b \leq 0), \qquad (4.3.3)$$

where n_s and p_s are majority carrier concentrations (cm^{-3}) in

accumulation layers, and $G^{+}(u_b,\nu_s)$ is given by

$$G^{+}(u_b,\nu_s) = \int_{0}^{\nu_s} \frac{e^{\nu}-1}{F(|u_b|,\nu)} \, d\nu$$

which is always positive and has been numerically evaluated

in reference 34. Another case of interest is minority carriers

in inversion layers, where (4.3.3) can be written as

$$\Delta n_s = \frac{\Delta N_s}{d_s} = P_b g^{+}(u_b,\nu_s) \text{ for } \nu_s \geq 0 \text{ in n-type}(u_b \leq 0);$$

$$\Delta P_s = \frac{\Delta P_s}{d_s} = n_b g^{+}(u_b,N_s) \text{ for } \nu_s \leq 0 \text{ in p-type}(u_b \geq 0) \qquad (4.3.4)$$

where n_s and p_s are minority carrier concentration (cm^{-3}) in the inversion layers, and $g^+(u_b, \nu_s)$ is given by

$$g^+(u_b, \nu_s) = e^{-2|u_b|} \int_0^{|\nu_s|} \frac{e^\nu - 1}{F(-|u_b|, \nu)} d\nu$$

which is always positive and has been evaluated numerically in reference 34.

4.4   SURFACE EFFECTIVE MOBILITY

The surface excess carriers are expected to have mobilities different from those in the bulk. Their mobilities are usually called surface effective mobilities. When the surface is bombarded by carriers, it may behave as a completely diffuse (random) scatterer or, on the other extreme, as a specular (perfect) reflector. The former implies that carriers emerge from the surface with a Boltzmann distribution. This type of scattering clearly leads to a reduction in mobility. An increase in surface potential will also result in a decrease in surface mobility because the inversion layer width decreases with increasing surface potential and the narrower the layer, the more surface scattering. Specular reflection, on the other hand, requires that only a reversal of sign of the velocity normal to the surface, the velocities parallel to the surface remaining unchanged. There can obviously be no mobility reduction under these conditions. Specular reflection is the type of scattering one expects from an ideal surface.

Schreiffer[37] presented a classical approach to formulate sur-
face effective mobility due to diffuse scattering by solving
the Boltzmann transport equation. He predicted that the effec-
tive mobility was always less than the bulk mobility. He had
plotted the effective mobility as a function of surface poten-
tial (see Figure 4 of Reference 37). His calculations have
been refined to include the influence of the potential barrier
ν.

For the case of electrons in inversion layer of a p-type
sample, the surface effective mobility for electrons is given
by [34]

$$\mu_{ns} = \mu_{nb} \left[1 - \frac{\lambda n_b}{\Delta N_s} \Gamma (u_b, \nu_s, \lambda) \right], \qquad (4.4.1)$$

where the subscript "n" indicates electrons; "s" and "b" indi-
cate surface and bulk components respectively, ΔN_s is given by
(4.2.1), ν_s is the surface potential, $\lambda \equiv \frac{\mu_{nb}}{q} \sqrt{\frac{kTm_e^*}{2\pi}}$ is the
mean free path for electrons and Γ is defined as

$$\Gamma (u_b, \nu_s, \lambda) \equiv \int_{-\nu_s}^{o} e^{-\epsilon} \left[1 - \exp \left(- \frac{1}{r\sqrt{\pi}} \int_{-\epsilon}^{\nu_s} \frac{d\nu}{\sqrt{\nu+\epsilon} \ F(u_b,\nu)} \right) \right] d\epsilon,$$

$$(4.4.2)$$

where $F(u_b, \nu)$ is given by (3.2.9) and $r = \frac{2\lambda}{d_s}$ which can be
shown to be

$$r = \frac{2\lambda}{d_s} = \mu_{nb} \sqrt{\frac{m_e^* (n_b + p_b)}{2\pi \epsilon s}} \qquad (4.4.3)$$

Using (4.2.4) and (4.4.2), equation (4.4.1) can be written as

$$\mu_{ns} = \mu_{nb} \left[1 - \frac{r}{g^+ e^{2|u_b|}} \Gamma\left(-|u_b|, |v_s|, r\right) \right] \qquad (4.4.4)$$

The values of μ_s/μ_b for minority carriers in inversion layers under strong inversion as obtained by integrating (4.4.2) numerically, are given in reference 38.

By and large, the quantitative agreement with experimental observation is not particularly good. The observed mobilities are generally greater than that predicted by Schreiffer's theory, although they do fall as the surface potential is increased[39]. By juggling the ratio of the specular to diffuse scattering, the theory can be brought into closer agreement[40].

The discrepancies are not entirely surprising when some of the assumptions underlying the classical approach are considered. In the first place, the inversion layer is normally very narrow, approximately 100Å for (Hg,Cd)Te at 4.2°K, and comparable to the de Broglie wavelengths of a carrier. Consequently, it is doubtful if Boltzmann statistics are appropriate. Secondly, since the electric field within the inversion layer is large (most μ_s measurements employ the field effect), quantization effects in this region may be important. In fact, the

separation of the quantization energies increases as the field becomes larger. Surface transport in the electric quantum limit, in which only the lowest electric sub-band is occupied, has been treated in reference 41.

The temperature dependence of the effective surface mobilities[44,45] in inversion layers of silicon have been measured. For strongly inverted surfaces, the mobilities are constant at low temperatures and decrease as $T^{-\alpha}$ at room temperature where α varies from 1.5 to 2.0. The temperature independence at low temperature is the major characteristic of the effective surface mobilities for large values of the surface potential.

4.5   THE SURFACE-BULK TRANSPORT FORMALISM

The presence of a space charge region at the surface will give rise to a change in the measured transport parameters. The variation in the Hall effect for a sample having space charge layer is due to:

1) the change of the carrier density in the space charge, and
2) the reduction of the carrier mobility by the additional surface scattering.

These two phenomena have been discussed in the foregoing sections. In this section, we will address the influence of the surfaces on the measured transport quantities.

The formulation of the problem starts with the Boltzmann equation, where the distribution function depends on the energy as well as the distance z from the surface. Petritz[42] introduced the effective mobility formalism to transform the Boltzmann distribution integrals into parameters in terms of the z-dependent carrier densities and mobilities. This brings the z-dependent terms into the transport equation. We then eliminate the z-dependence by integrating the equations from the surface into the bulk. Finally, we will apply the effective mobility formalism again to eliminate all the integrals and obtain closed forms for the average conducting Hall coefficient and mobility.

The general expressions for the conductivity and the Hall coefficient with the z-dependence imposed[42] are similar to equations (3.2.1) and (3.2.2):

$$\sigma = \frac{1}{d} \int_0^d \sigma(z)dz; \tag{4.5.1}$$

$$R = \frac{d \int_0^d R(z)\sigma^2(z)dz}{\left[\int_0^d \sigma(z)dz\right]^2} \tag{4.5.2}$$

where d is the sample thickness. From equations (2.1.1) and (2.1.2), we can write the z-dependent transport equations in the x and the y directions formally as

91

$$J_x(z) = |q| \, \Sigma_k n_k(z) <\mu_k(z)> E_x + \Sigma_k q_k n_k(z) <\mu_k^2(z)> E_y B_z; \qquad (4.5.3)$$

$$J_y(z) = |q| \, \Sigma_k n_k(z) <\mu_k(z)> E_y - \Sigma_k q_k n_k(z) <\mu_k^2(z)> E_x B_z, \qquad (4.5.4)$$

where $n_k(z)$ is the density of the kth species (holes or electrons) and $<\mu_k^i(z)>$ are appropriate averages over momentum space for $i = 1$, or 2; q_k is positive for holes, negative for electrons. The total currents are thus given by

$$I_x = W \int_0^d J_x(z) d_z \equiv Wd \, \overline{J}_x \quad ; \qquad (4.5.5)$$

$$I_y = \ell \int_0^d J_y(z) d_z = 0, \qquad (4.5.6)$$

wjere W and ℓ are sample width and length, respectively, and the boundary condition is such that the total current in the y direction vanishes. We can now express σ and R by substituting (4.5.3)-(4.5.6) into their definitions, (2.1.11) and (2.1.13),

$$\sigma \equiv \frac{\overline{J}_x}{E_x} \bigg|_{B_z=0} = \frac{1}{d} \, q \, \Sigma_k \int_0^d n_k(z) <\mu_k(z)> d_z; \qquad (4.5.7)$$

$$R \equiv \frac{E_y}{\overline{J}_x B_z} = \frac{d \, \Sigma_k \int_0^d q_k n_k(z) <\mu_k^2(z)> d_z}{\left[|q| \, \Sigma_k \int_0^d n_k(z) <\mu_k(z)> d_z \right]^2} \qquad (4.5.8)$$

Note that (4.5.7) and (4.5.8) are similar to (4.5.1) and (4.5.2), respectively, if we can write the local conductivity and Hall

coefficient respectively as

$$\sigma(z) = \left|q\right| \sum_k n_k(z) <\mu_k(z)>; \qquad (4.5.9)$$

$$R(z)\sigma^2(z) = \sum_k q_k n_k(z) <\mu_k^2(z)> \qquad (4.5.10)$$

In the bulk, when the surface boundary condition is negligible, we have

$$<\mu_{kb}> = \mu_{kb}; \qquad (4.5.11)$$

and from (2.1.7) and (4.5.11)

$$< \mu_{kb}^2 > = \quad R_b \mu_{kb}^2 \quad = \mu_{Hkb}\mu_{kb} \qquad (4.5.12)$$

As stated in Section 2.1, we let $\gamma_{kb} = 1$ for convenience. In the region near the surface, $<\mu_k^i(z)$ will differ from $<\mu_{kb}^i>$ because of surface scattering. In section 4.4 we discussed essentially $<\mu_k(z)>$ which is the z-dependent effective surface conductivity mobility. Under the presence of the magnetic field, the effective surface mobility will change, just as the bulk mobility.

Zemel[43] has calculated the effective surface Hall mobility and found that it is some 13% less than the effective surface conductivity mobility for large values of the surface potential, that is $\gamma_{ks} \simeq .885$. But again, for convenience, we let $\gamma_{ks}=1$.

We now use the effective mobility formalism again to eliminate the integrations which appear in (4.5.7) and (4.5.2). For simplicity, we begin by considering only the electrons and thus drop unnecessary subscripts. Because of the linearity of (4.5.9) and (4.5.10), the contribution from the holes can be added to the expressions later.   93

The parameters $n(z)$, $<\mu(z)>$ and $<\mu^2(z)>$ in (4.5.7) and (4.5.8) can be written as

$$n(z) = n_b + \Delta n(z); \qquad (4.5.13a)$$

$$<\mu^i(z)> = \mu_b + \Delta<\mu^i(z)>; \qquad (4.5.13b)$$

where $i = 1$ or 2. Ignoring the correlation terms in Ref. 42 which depend on the overlap of two spatial integrals, we can rewrite (4.5.7) and (4.5.8) as follows:

$$\sigma = \frac{|q|}{d} [n_b\mu_b d_b + n_s\mu_s d_s] ; \qquad (4.5.14)$$

$$R = \frac{-|q|}{\sigma^2 d} [n_b\mu_b^2 d_b + n_s\mu_s^2 d_s], \qquad (4.5.15)$$

where

$$d = d_b + d_s; \qquad (4.5.16a)$$

$$n_s = n_b + \Delta n_s; \qquad (4.5.16b)$$

$$\mu_s^i = \mu_b^i + \frac{1}{d_s} \int_0^d \Delta<\mu^i(z)>d_z, \qquad (4.5.16c)$$

and where d_s is defined in (4.2.4), Δn_s is defined in (4.3.4) and, in general, we expect $\mu_s^i \leq \mu_b^i$ for $i = 1$ and 2.

If our concern is the ease that an n-type inversion layer exists on a p-type or intrinsic bulk, then we can ignore the holes in the space change layer. Hence, the apparent conductivity and Hall coefficient are given by:

$$\sigma = \sigma_b \frac{d_b}{d} + \sigma_{ns} \frac{d_s}{d} ; \qquad (4.5.17)$$

$$R = R_b \frac{d_b}{d}\left(\frac{\sigma_b}{\sigma}\right)^2 + R_{ns} \frac{d_s}{d}\left(\frac{\sigma_{ns}}{\sigma}\right)^2 \quad , \tag{4.5.18}$$

where

$$\sigma_b = |q| [n_b \mu_{nb} + p_b \mu_{pb}] \quad ; \tag{4.5.19}$$

$$R_b = \frac{-\mu_b}{\sigma_b} = - \frac{\mu_{nb}^2 n_b - \mu_{pb}^2 p_b}{|q|(\mu_{nb} n_b + \mu_{pb} p_b)^2} \quad ; \tag{4.5.20}$$

$$\sigma_{ns} = |q| \, n_s \mu_{ns} \quad ; \tag{4.5.21}$$

$$R_{ns} = \frac{-\mu_{ns}}{\sigma_s} = \frac{1}{|q| n_s} \quad ; \tag{4.5.22}$$

and where the subscripts are self-explanatory. The apparent mobility is again defined by

$$\mu \equiv R\sigma \quad . \tag{4.5.23}$$

We want to comment on the significance of ignoring the correlation terms which involve integrating over regions where the surface terms overlap the bulk terms. Ignoring these terms is equivalent to decomposing the semiconductor into two independent regions: "surface" ($0 \leq z \leq d_s$) and "bulk" ($d_s \leq z \leq d$) within which the transport properties are thought to be constant. This abrupt separation approximation turns out to be highly admissible because, from exact calculations, the correlation terms always turn out to be negligible compared to the bulk and the surface terms.

95

4.6   BULK CARRIER DENSITY DETERMINATION FROM THE ANOMALOUS
        HALL MEASUREMENTS

If we assume that the anomalous Hall properties are due to a

conducting surface, it is important to know if the anomalous

data can give any information on the bulk properties. This

section will address this issue.

Let us rewrite (4.5.12) in a more transparent form:

$$R = \frac{|q|\mu_{pb}^2(p_b - b^2 n_b) - \mu_{ns}S}{[|q|\mu_{pb}b(p_b + bn_b) + S]^2} \qquad (4.6.1)$$

where

$$b = \mu_{nb}/\mu_{pb},$$

and

$$S = \sigma_s \, d_s/d \, . \qquad (4.6.2)$$

We want to find an expression for p_b when R is a maximum, i.e.,

when $dR/dT = 0$. With some algebraic manipulations, one can

show that for the approximation b>>1, the expression for p_b

when $|R| = |R_{max}|$ is given by (See Appendix)

$$p_b = bn - \frac{1}{b}\left(\frac{\mu_{nb} - 2\mu_{ns}}{|q|\mu_{pb}^2}\right)S \, . \qquad (4.6.3)$$

Substituting (4.6.3) into (4.6.1), one obtains the expression

for $|R_{max}|$ in terms of p or n:

96

$$\left| R_{max} \right| = \frac{P_b}{4\,|q|\,n_i^{2}} \;\; \frac{1 + \left(\dfrac{\mu_{ns}}{\mu_{nb}}\right)^{2}\dfrac{n_s}{n_b}\cdot\dfrac{d_s}{d}\left(1 + \dfrac{\mu_{pb}}{\mu_{ns}}\right)}{\left[1 + \left(\dfrac{\mu_{ns}}{\mu_{nb}}\right)^{2}\dfrac{n_s}{n_b}\dfrac{d_s}{d}\right]^{2}} \qquad (4.6.4)$$

Three approximations can be made.

Case I: when $\mu_{ns} \gg \mu_{pb}$, (5.6.4) becomes

$$\left| R_{max} \right| \simeq \frac{P_b}{4\,|q|\,n_i^{2}} \;\; \frac{1}{\left[1 + \left(\dfrac{\mu_{ns}}{\mu_{nb}}\right)^{2}\dfrac{n_s}{n_b}\dfrac{d_s}{d}\right]^{2}} \qquad (4.6.5)$$

Case II: when $\mu_{nb}^{2}n_b \gg \mu_{ns}^{2}n_s\dfrac{d_s}{d}$, (4.6.4) becomes

$$\left| R_{max} \right| \simeq \frac{P_b}{4\,|q|\,n_i^{2}} \left[1 + \frac{1}{b}\frac{\mu_{ns}}{\mu_{nb}}\frac{n_s}{n_b}\frac{d_s}{d}\right]. \qquad (4.6.6)$$

Case III: when both Case I and Case II are applicable, (4.6.4) becomes

$$\left| R_{max} \right| \simeq \frac{P_b}{4\,|q|\,n_i^{2}} , \qquad (4.6.7)$$

which is identical to the p-type case.

Note that in Case I, $\left|R_{max}\right| \propto d$; in Case II, $\left|R_{max}\right| \propto 1/d$; and in Case III, $\left|R_{max}\right| \neq R(d)$. Experimental data seem to indicate that $\left|R\right|$ is directly proportional to d which makes Case I more favorable. Having solved for p_b from (4.6.5), we obtain from Case I

97

the expression:

$$p_b \simeq N_A = \frac{4 \, \lvert q \rvert \, \lvert R_{max} \rvert \, n_i^2}{1 - 4 \, \lvert q \rvert \, \lvert R_{max} \rvert \left(\dfrac{\mu_{ns}}{\mu_{nb}} \right)^2 n_s \dfrac{d_s}{d}} \, . \qquad (4.6.8)$$

This is the key equation in the determination of the bulk
carrier concentration from the anomalous $R(T)$ curves. It is
valid for both Peak- and DCO samples.

The accuracy of N_A obtained from this equation is limited by
the accuracy in our estimations for μ_{nb}, μ_{ns} and $n_s d_s$. In Sec-
tion 5.7, we will use (4.6.8) to calculate N_A for several
(Hg,Cd)Te ingots, and will discuss in more detail the accuracy
of this equation.

4.7   THE DEPENDENCE OF R ON THE MAGNETIC FIELD

Equation (4.5.18) applies when the magnetic field B is weak.
Now we derive an expression for a magnetic field of arbitrary
strength. We did this for the bulk transport case at the end
of Section 2.1. Equation 2.4.1 is for the bulk; therefore, it
does not take into account the fraction of the total cross
section A of the sample passed by each carrier type (see (3.2.2)).
In general, the dependence of R on magnetic field can be
expressed by

$$R(B) = \frac{D_1}{D_2^2 + B^2 D_1^2} \, , \qquad (4.7.1)$$

where

$$D_1 = \sum_{kj} A_{kj} \sigma_{kj}^2 R_{kj} C_{kj} \quad ;$$

$$D_2 = \sum_{kj} A_{kj} \sigma_{kj} C_{kj} \quad ,$$

where

$$C_{kj} = (1 + \mu_{kj}^2 B^2)^{-1}$$

where the subscript "k" stands for carrier type (n or p) and the subscript "j" indicates the location of the jth carrier (surface or bulk); A_{kj} is the fraction of the total cross section of the sample passed by the carrier "kj". For the case in which we only have an n-type surface on a p-type bulk, (4.7.1) reduces to

$$R(B) = \frac{D_3}{D_4^2 + B^2 D_3^2} \quad , \tag{4.7.2}$$

where

$$D_3 = \sigma_{nb}^2 R_{nb} C_{nb} + \sigma_{pb}^2 R_{pb} C_{pb} + \sigma_{ns}^2 R_{ns} C_{ns} d_s/d;$$

$$D_4 = \sigma_{nb} C_{nb} + \sigma_{pb} C_{pb} + \sigma_{ns} C_{ns} d_s/d.$$

As expected, when B = 0, R(B) returns to its original form (4.5.18).

99

CHAPTER V
EXPERIMENTAL VERIFICATIONS OF THE CONDUCTING-SURFACE MODEL

Having developed the theoretical basis for the conducting-
surface models, we are ready to determine if the theory is
able to explain the previous observations associated with the
anomalous Hall properties of certain (Hg,Cd)Te samples.
Attempts to quantify the model will be made in order that com-
parative studies can be done. Thus, we will compare the results
of four observations with the predictions of the conducting-
surface model. These observations are the doping dependence,
the sample thickness dependence, the electron irradiation and
the magnetic field dependence experiments. Next, we report
the result of our experiment which shows a direct conversion
from a Peak-type to a p-type Hall coefficient by employing a
new sample fabrication technique. We then apply the method
proposed in Section 4.6 to determine N_A for several (Hg,Cd)Te
ingots. Finally, we generalize the conducting-surface model to
allow more flexibility in the physical interpretation of the
anomalies.

5.1   QUANTITATIVE ANALYSIS OF THE MODEL

In the preceding chapter, we defined several quantities which
are essential in the conducting-surface model. Now we calcu-
late these quantities for (Hg,Cd)Te at low temperatures using

the equations we have derived. The first one to consider is the effective Debye length L. For x = 0.2 (Hg,Cd)Te, the permittivity is roughly 20[35]. At $20°K$, the effective Debye length L of a sample having $p_b = 5 \times 10^{15}$ cm^{-3} is, according to (4.2.4), equal to 1.95×10^{-6} cm.

The surface carrier density $\Delta N_s (cm^{-3})$ can be estimated for a given value of $\Delta N_s (cm^{-2})$ and d_s. Experimental results show that $\Delta N_s \sim 10^{12} (cm^{-2})$[23,36]. From this, together with our calculation for L, we obtain at $20°K$,

$$\Delta n_s = \frac{\Delta n_s}{L} = 5.2 \times 10^{17} \ cm^{-3} \quad .$$

From (4.3.4) we know that Δn_s is related to p_b by g^+. Given that $p_b = 5 \times 10^{15} \ cm^{-3}$, equation (4.3.4) implies that

$$g^+ = \frac{\Delta n_s}{p_b} \simeq 10^2 \quad .$$

With the help of Ref. 34, we find that the condition for $g^+ = 10^2$ is

$$\left| \nu_s \right| - 2 \left| u_b \right| \simeq 8.5, \quad for \quad 0.5 < \left| u_b \right| < 50.$$

Now we want to know the value for μ_{ns} when $\left| \nu_s \right| - 2 \left| u_b \right| \simeq 8.5$. In order to do this, we have to evaluate u_b and r in (4.4.4). u_b is defined in (4.2.2)

$$u_b = \ln \frac{p_b}{n_i} \simeq 20 \quad ,$$

where $n_i(T=20°K) \approx 5 \times 10^8$ [27]. r is the ratio of the mean free path of electrons λ to the effective Debye length L.

The mean free path for electrons is

$$\lambda = \frac{\mu_{nb}}{q} \sqrt{\frac{KT \, m_e^*}{2\pi}} \approx 2.8 \times 10^{-6} \text{ cm}$$

where we have used μ_{nb} (4.2°K) = 1×10^5 cm^2/V-sec [29] and $m_e^* = .005 \, m_o^3$ for x = .2 (Hg,Cd)Te materials. Hence, r can be evaluated:

$$r = \frac{\lambda}{L} \cong 1.4 \quad .$$

Now we are ready to get a feel for the value of the ratio μ_{ns}/μ_{nb}. Given that r = 1.4 and $\left|\nu_s\right| -2\left|u_b\right| \approx 8.5$, a value for μ_{ns}/μ_{nb} estimated from Ref. 38 is roughly

$$\frac{\mu_{ns}}{\mu_{nb}} \approx .05,$$

which is almost independent of $\left|u_b\right|$. μ_{nb} at low temperature has been measured on n-type samples to be from 1 to 8×10^5 cm^2/ v-sec.

Thus, the limits estimated for μ_{ns} lie within:

$$5 \times 10^3 < \mu_{ns}(cm^2/\text{v-sec}) < 4 \times 10^4 \quad .$$

These values are in good agreement with experimental results. The measured mobilities at low temperatures for samples which exhibit "Peak" Hall behavior usually lie within 10^3 to 4×10^4

cm^2/v-sec. According to our assumption that the surface com-
ponent appearing in (4.5.17) and (4.5.18) predominates at low
temperatures, the measured mobilities must be the surface
effective mobilities. This shows the consistency between the
theoretical calculations and experimental observations. To
understand the effects of doping on μ_{ns} and we turn to equa-
tion (4.4.3) and (4.2.4) together with Figure 4.3.2. Increasing
the doping (p_b) would result in a larger r, a smaller μ_{ns},
and a narrower L.

Having calculated these values, we are ready to compare quan-
tiatively the surface terms and the bulk terms in equations
(4.5.17) and (4.5.18). From Figure 2.3.1 in Chapter II, we
know that at 20°K, $\mu_{pb} \simeq 300$ cm^2/v-sec. Hence

$$\sigma_b = q p_b \mu_{pb} = .24 \ (1/\Omega\text{-cm}).$$

The surface contribution to conductivity for a sample of 20μ
thick is

$$\sigma_s \frac{d_s}{d} = q n_s \mu_{ns} \frac{d_s}{d} \simeq 3.24 \ (1/\Omega\text{-cm}).$$

where we use $\mu_{ns} = 2 \times 10^4$ and $d_s = 2L$. These two terms will
be comparable when a thicker sample is used. But p_b at 20°K
is usually much less than $5 \times 10^{15} \ cm^{-3}$ due to the freeze-out
effect and the surface conduction will be further enhanced.
The overall conductivity is the sum of the two,

$$\sigma = \sigma_b + \sigma_s \frac{d_s}{d} = 3.48 \ (1/\Omega\text{-cm}),$$

103

which corresponds to a resistivity ρ given by

$$\rho = \frac{1}{\sigma} \cong .287 \ (\ \Omega\text{-cm}),$$

which is consistent with measurements. The surface and bulk

components of the Hall coefficient equation (4.5.18) can also

be calculated as follows,

$$R_b \cong \frac{d_b}{d} \left(\frac{\sigma_b}{\sigma} \right)^2 \sim \frac{-1}{qp_b} \left(\frac{\sigma_b}{\sigma} \right)^2 \sim 5.95 \ \text{cm}^3/\text{coul} \ ,$$

where we let $d_b = d$, and

$$R_s \cong \frac{d_s}{d} \left(\frac{\sigma_s}{\sigma} \right)^2 \sim \frac{-1}{qn_s} \frac{d_s}{d} \left(\frac{\sigma_s}{\sigma} \right)^2 = 4.5 \times 10^4 \ \text{cm}^3/\text{coul}$$

Therefore, we have shown quantitatively that at low temperature,

the calculated surface terms predominate and have values close

to the experimental results. The calculations are very impor-

tant in two regards. First, they verify the assumption that at

low temperatures the contribution from the inverted surface to

the total conduction is larger than that from the p-type bulk;

secondly, they show excellent consistency between theory and

data which makes the conducting surface model very appealing.

Before closing this section, we want to make the following

assumptions which enable us to do variable temperature calcula-

tions for the surface-bulk system. The first assumption is

that $\mu_{ns}(T)$ is constant at low temperatures until it reaches

the intrinsic region, and falls off exactly the same way as

$\mu_{nb}(T)$ at high temperatures. The second assumption is that n_s is independent of temperature. These two assumptions are supported by experimental results in which both $\mu(T)$ and R(T) are rather temperature insensitive at low temperatures and by our analysis which proved quantitatively that μ and R measured at low temperatures represent their surface components. At higher temperatures, however, the bulk terms will be dominant and any error introduced by our oversimplified assumptions about the surface quantities will not be significant.

Our assumption of $\mu_{ns}(T)$ gains further support from research done on the inverted Si surface because $\mu_{ns}(T)$ of Si shows exactly the same temperature dependence[44,45] as we assumed.

5.2   THE IMPURITY DENSITY DEPENDENCE OF R(T)

Dixon[15] had found that a definite correlation existed between acceptor concentration and the behavior of the anomalous Hall coefficient in InAs. As in (Hg,Cd)Te, the Hall coefficient of heavily doped InAs ($N_A > 2 \times 10^{17}$ cm^{-3}) showed p-type behavior. At a carrier concentration of 1.5×10^{17} cm^{-3}, the Hall coefficient was further decreased the DCO behavior was replaced by a Peak behavior.

As we pointed out in Chapter III, both InAs and (Hg,Cd)Te were reported to show anomalies in a very similar fashion which may in part be due to the fact that both semiconductors have very

high electron to hole mobility ratios (both are greater than one hundred).

In Figure 5.2.1 we show the calculated R(T) as a function of N_A by means of (4.5.18) with the assumed parameters shown in the figure. The heavily doped ($N_A > 2 \times 10^{17}$ cm^{-3}) material shows p-type behavior. At a carrier concentration between 5×10^{16} cm^{-3} and 2×10^{17} cm^{-3}, R(T) shows a DCO and further decrease in N_A ($N_A < 10^{16}$ cm^{-3}), R(T) reduces to a peak.

The anomalies can be understood in the light of the conducting-surface model as follows. At low temperatures conduction via n-type surface predominates due to either one or a combination of these reasons: high surface electron to bulk hole mobility ratio, weakly doped p-type bulk, or freezing out the acceptors in the bulk. If the acceptor density is so low that conduction via the valence band is still incomparable even at exhaustion temperatures, then R will remain negative throughout. Since a low acceptor density corresponds to a large $\left|R_{max}\right|^{26}$, as the temperature reaches T_{max}, R which is the sum of $\left|R_s\right|$ and $\left|R_{max}\right|$ will give rise to a peak.

For more heavily doped p-type materials, the conduction via the valence band may at some temperatures prevail the conduction via the n-type surface due to either the rising hole mobility or the diminishing freeze-out effect with increasing temperatures.

$N_A = 10^{15} cm^{-3}$

5×10^{15}

10^{16}

5×10^{16}

10^{17}

$|R|$ $(cm^3/Coul)$

ASSUMED PARAMETERS

$N_D = 10^{13} cm^{-3}$

$E_A = .003 eV$

$d = 8 \times 10^{-2} cm$

$n_s = 2 \times 10^{18} cm^{-3}$

$\mu_{ns}(4\,^\circ K) = 2 \times 10^4 cm^2/V\text{-sec}$

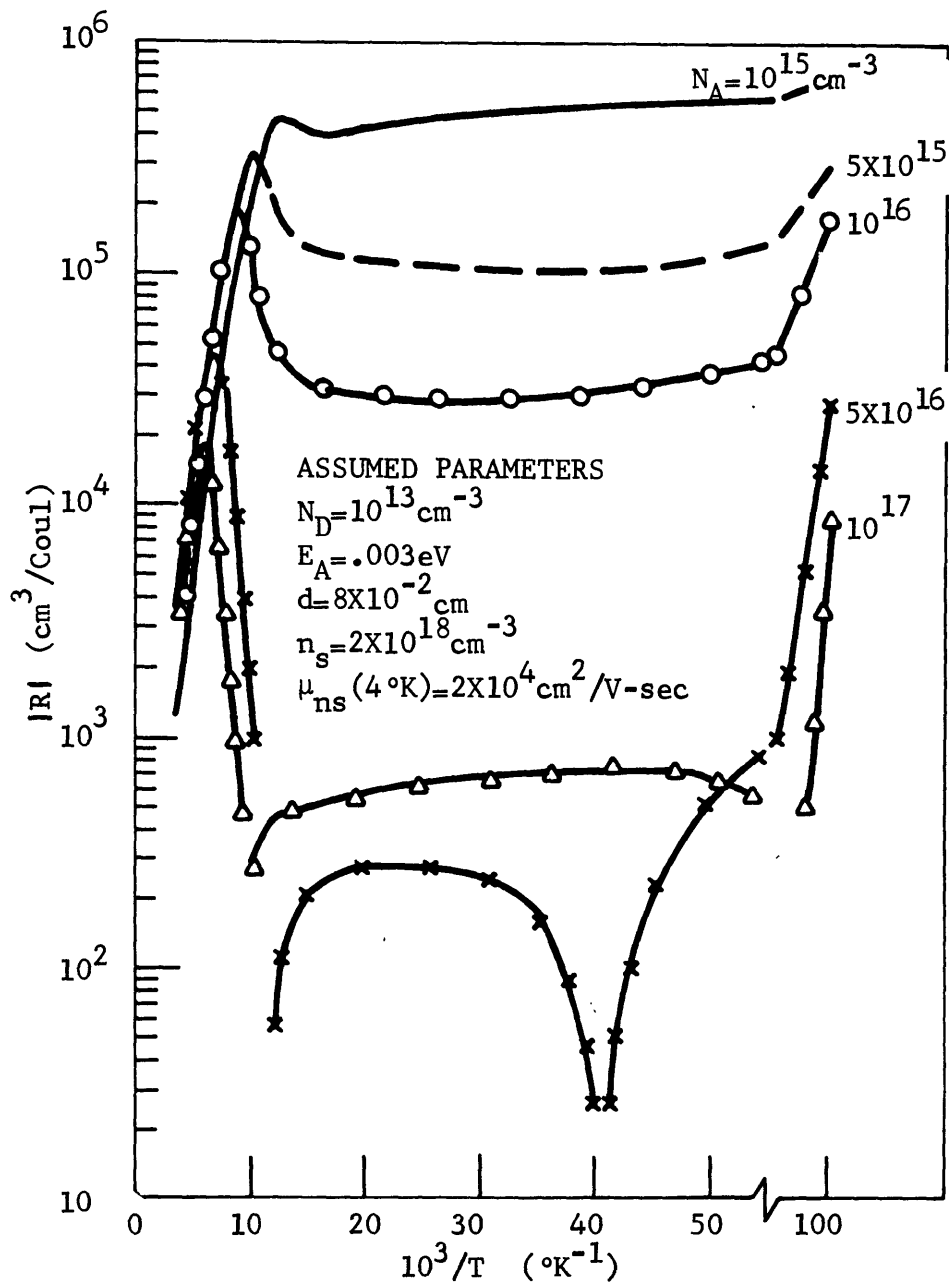$10^3/T$ $(\,^\circ K^{-1})$

FIG. 5.2.1 THE CALCULATED ANOMALOUS R(T) AS A
FUNCTION OF N_A.

107

This results in a change of sign (from negative to positive) for R. When the intrinsic temperature is reached, R will eventually change back to negative because the higher electron mobility will dominate. As a result a DCO is observed.

Caution must be noted on the transition from one type to another. The condition for type-changing depends on the surface excess density, surface mobility, compensation, freeze-out as well as acceptor concentration. Therefore, the situation described by Figure 5.2.1 is an idealized one in which we assume N_A is the only independent parameter while the rest of the quantities remain constants. In general, we can make the following statement:

On the basis of the conducting-surface model, the temperature dependent Hall coefficient of a p-type sample having an inverted surface will show

(i) Classical p-type if

$$p_b > n_s \left(\frac{\mu_{ns}}{\mu_{pb}} \right)^2 \frac{d_s}{d} \quad , \quad \text{for all temperatures;} \quad (5.2.1)$$

(ii) DCO if

$$p_b < n_b \left(\frac{\mu_{nb}}{\mu_{pb}} \right)^2 + n_s \left(\frac{\mu_{ns}}{\mu_{pb}} \right)^2 \frac{d_s}{d} \quad \text{at low temperatures,}$$

and

$$p_b > n_s \left(\frac{\mu_{ns}}{\mu_{pb}} \right)^2 \frac{d_s}{d} \quad \text{at medium temperatures;}$$

$$\left. \right\} \quad (5.2.2)$$

108

(iii) Peak if

$$P_b < n_b \left(\frac{\mu_{nb}}{\mu_{pb}} \right)^2 + n_s \left(\frac{\nu_{ns}}{\mu_{pb}} \right)^2 \frac{d_s}{d} \text{, for all temperatures}$$

and

$$n_b > n_s \left(\frac{\mu_{ns}}{\mu_{nb}} \right)^2 \frac{d_s}{d} \text{, at high temperatures} \qquad (5.2.3)$$

5.3 THE SAMPLE THICKNESS DEPENDENCE OF R AND σ

We have shown in Section 5.1 that at low temperatures, the sur-
face terms predominate. Applying this condition in equations
(4.5.17) and (4.5.18), we obtain

$$\sigma(T_L) \simeq \sigma_s \frac{d_s}{d} \; ; \qquad (5.3.1)$$

$$R(T_L) \simeq R_s \frac{d_s}{d} \left[\frac{\sigma_s}{\sigma(T_L)} \right]^2 \sim R_s \frac{d}{d_s} \; ; \qquad (5.3.2)$$

and

$$\mu(T_L) \equiv \frac{R(T_L)}{\sigma(T_L)} \sim \frac{R_s}{\sigma_s} \; , \qquad (5.3.3)$$

where T_L stands for low temperature. From the above equations,
it is clear that both $R(T_L)$ and $\sigma(T_L)$ are dependent on d while
$\mu(T_L)$ is not. Thus, an investigation was made on the existing
low temperature Hall data at Honeywell to see whether such
correlations exist.

We carefully examined R, σ and μ at 4.2°K of fourteen samples
with an average x value equal to 0.2 and ten samples with an
average x value equal to 0.3. All of these samples showed

109

Peak-type behavior in the R(T) curves. They are listed in Table 5.3.1 and R, σ and μ for these samples are plotted versus sample thickness in Figure 5. 3.1-3.The thickness dependence of R and σ are apparent for the two values of x. The scattered diagram of $\mu = \mu(d)$ shows no apparent correlation.

Figure 5.3.4 shows the temperature dependent Hall coefficients and resistivities for two Peak-type samples from adjacent slabs of the same ingot; one is thick (d = 8.75 X 10^{-2} cm) and one is thin (d = 4 X 10^{-4} cm). The thickness dependence of both R and ρ appears in a wide range of temperatures. This indicates that the surface does play an important role even at about 100°K.

In Figure 5.3.5 we calculate R and ρ for various thicknesses on the basis of the conducting-surface model from (4.5.18). The thickness dependence is apparent and similar to the experiment results.

The thickness dependence of a DCO-type sample is expected to be more drastic since thinning the sample down may enhance the surface in such a way that it prevails over the bulk holes throughout the temperature range. We picked a DCO-type sample and lapped it down to 4 microns and then remeasured R as a function of T.

SAMPLE	LABLE	x	$\sigma(1/\Omega\text{-cm})$	$R(cm^3/coul)$	$\mu\ (cm^2/V\text{-}s)$	$d(cm)$
D59-149-F4	1	.196	3.57	5.0×10^3	2×10^4	1.8×10^{-3}
D82-80-E1	2	.199	7.14	2.0×10^3	1.5×10^4	4.0×10^{-4}
D82-81-F3	3	.191	0.33	7.0×10^4	2.0×10^4	8.8×10^{-2}
D9-141-F3	4	.204	0.45	2.0×10^4	9.0×10^3	7.7×10^{-2}
1008-150-P4	5	.213	0.40	3.0×10^4	1.0×10^4	7.8×10^{-2}
D63-121-F3	6	.196	0.67	1.6×10^4	1.0×10^4	8.1×10^{-2}
D63-161-F4	7	.202	0.40	2.0×10^4	8.0×10^3	9.9×10^{-2}
D77-216-F2	8	.199	1.30	1.9×10^4	2.5×10^4	8.7×10^{-2}
D82-120-F5	9	.206	1.25	1.8×10^3	2.0×10^3	2.8×10^{-3}
D87-138-E2	10	.197	7.14	1.4×10^3	1.0×10^4	2.0×10^{-3}
D85-120-F3	11	.208	0.10	$>.0 \times 10^4$	2.0×10^3	1.1×10^{-1}
D85-142-F3	12	.204	0.14	2.6×10^4	3.6×10^3	8.1×10^{-2}
D82-121-F2	13	.206	0.15	8.0×10^4	1.2×10^4	8.5×10^{-2}
D82-121-F4	14	.214	0.25	6.0×10^4	1.5×10^4	8.6×10^{-2}
05-180-F3	1	.311	0.22	4.0×10^3	1.0×10^3	2.8×10^{-3}
05-230-001	2	.315	0.24	4.9×10^3	1.2×10^3	1.0×10^{-3}
10-132-F2	3	.313	0.03	1.0×10^5	2.2×10^3	9.2×10^{-2}
05-180-F4	4	.309	0.83	1.3×10^3	1.1×10^3	1.4×10^{-3}
05-203-2-1-2	5	.308	0.91	3.8×10^3	3.0×10^3	9.5×10^{-4}
05-203-2-1-4	6	.306	0.10	7.0×10^3	7.0×10^3	2.0×10^{-3}
05-203-2-1-5	7	.310	0.59	8.5×10^3	5.0×10^3	2.7×10^{-3}
05-196-F3-5	8	.309	0.77	2.4×10^3	2.0×10^3	1.0×10^{-3}
08-167-F2	9	.313	0.03	1.3×10^5	3.5×10^3	1.1×10^{-1}
08-167-F3	10	.313	0.02	9.0×10^4	2.0×10^3	1.1×10^{-1}

Table 5.3.1 R, σ, AND μ AT 4.2 °K OF SAMPLES WITH VARIOUS THICKNESSES
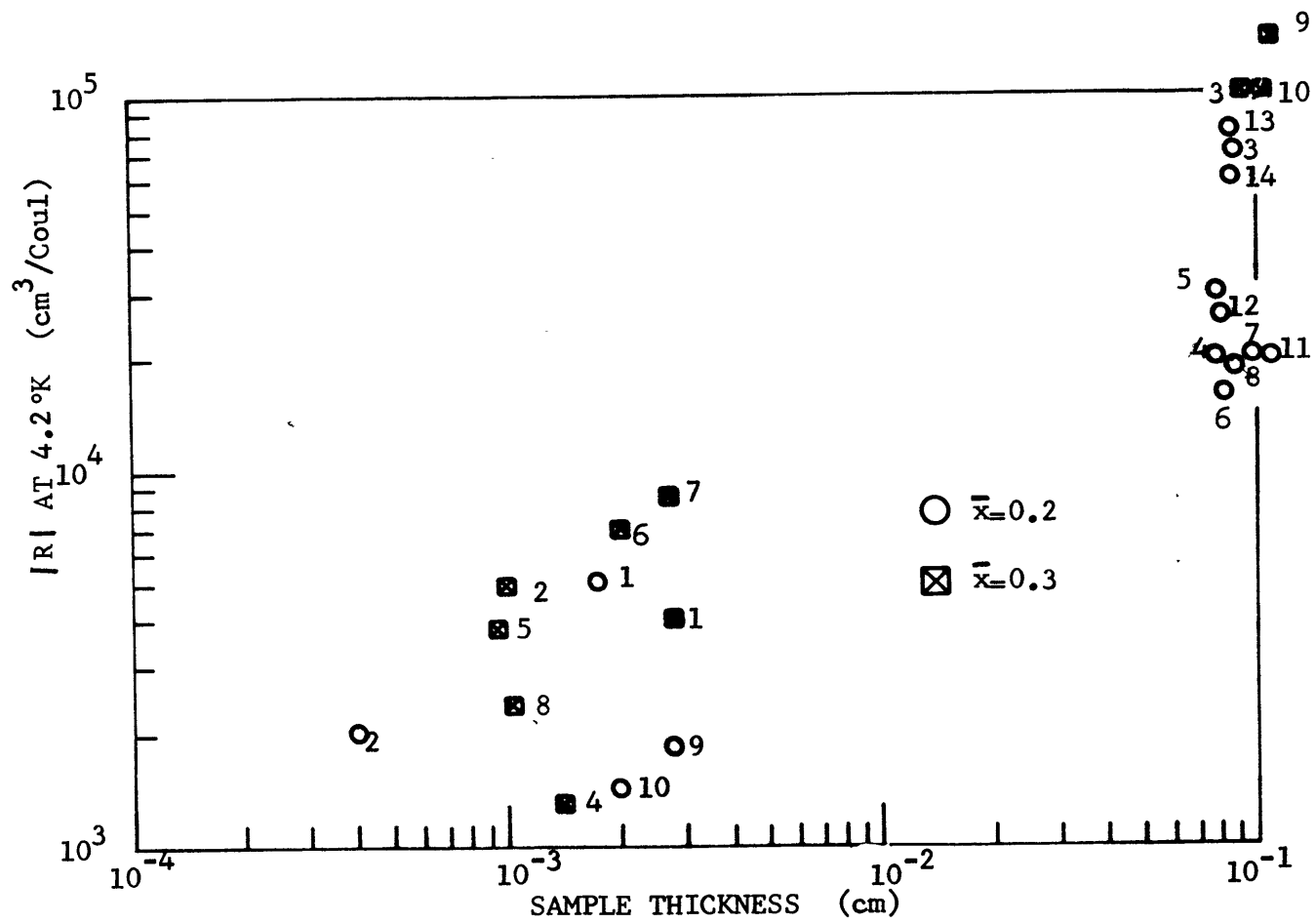
FIG. 5.3.1 MEASURED R AT 4.2 °K VS SAMPLE THICKNESS.

112

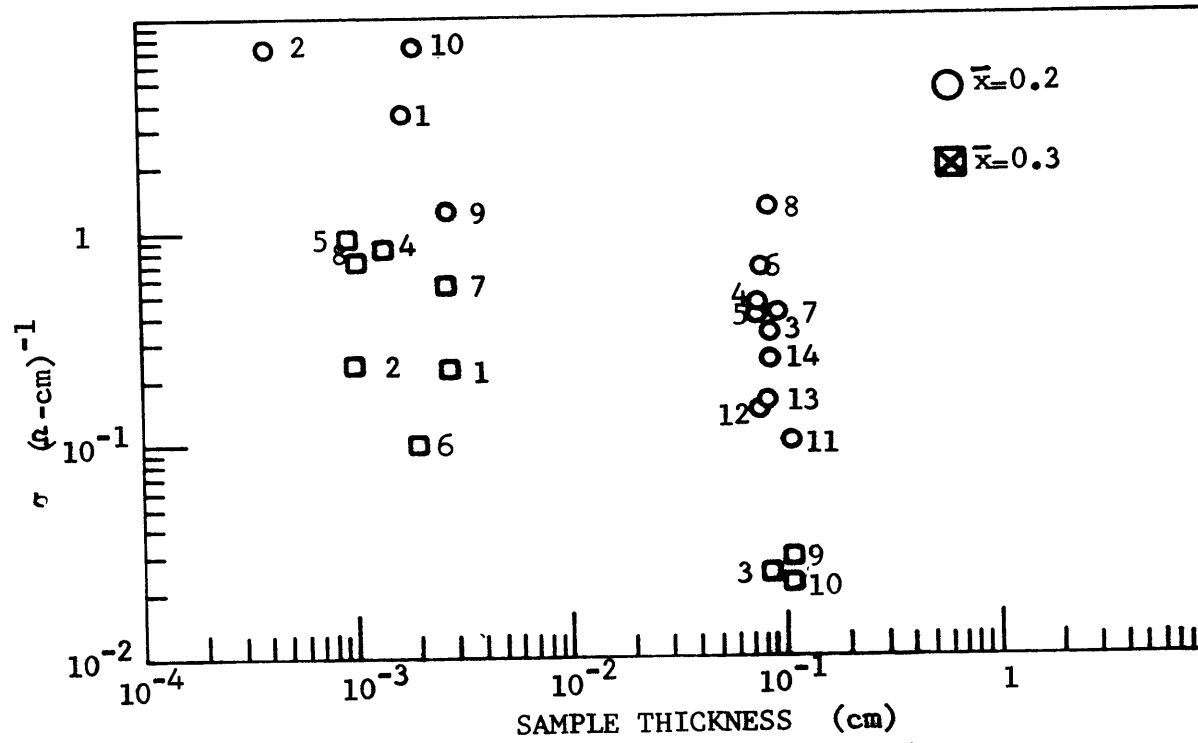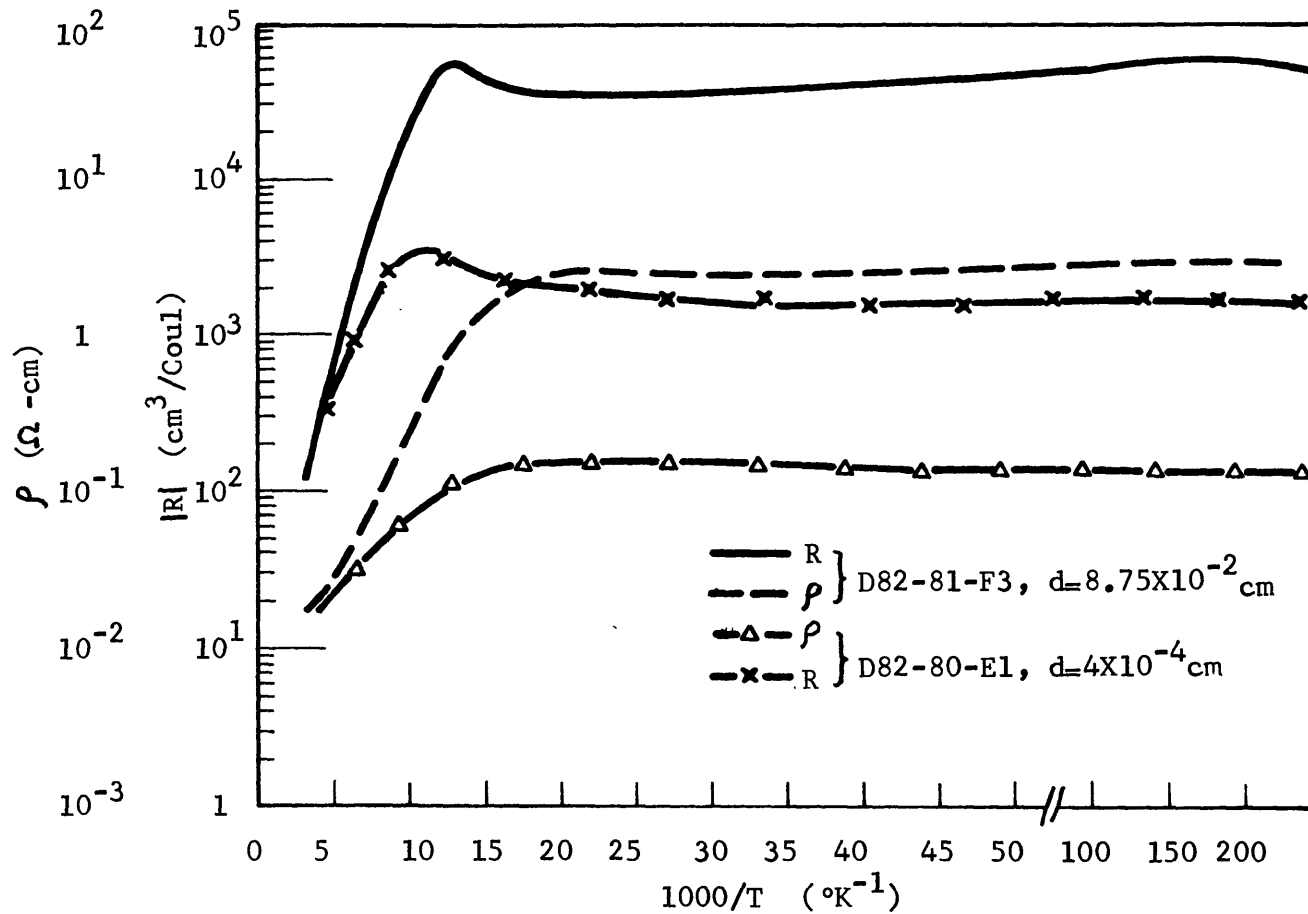FIG. 5.3.2   MEASURED σ AT 4.2°K VS SAMPLE THICKNESS

113

FIG. 5.3.3 MEASURED μ AT 4.2°K VS SAMPLE THICKNESS.

FIG. 5.3.4 MEARSURED R(T) AND ρ(T) OF TWO PEAK-TYPE SAMPLES
WITH DIFFERENT THICKNESSES.

FIG. 5.3.5 CALCULATED R(T) AND ρ(T) AS FUNCTIONS OF THICKNESS.

The axes and labels:

ρ (-cm)

$|R|$ (cm^3/Coul)

$10^3/T(°K^{-1})10^{-2}$
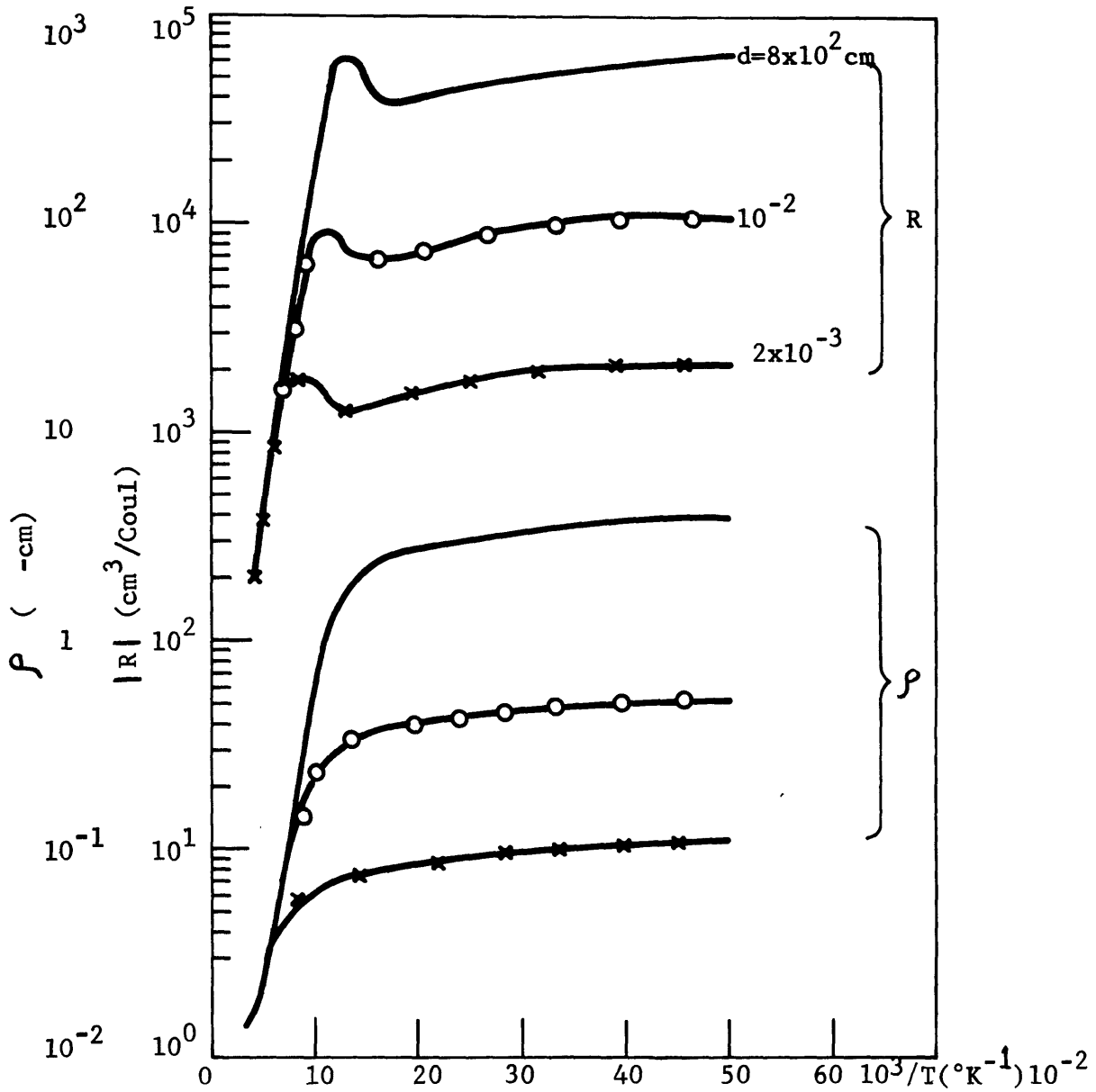
Assumed Parameters

$N_A = 5 \times 10^{15}$ cm^{-3}

$E_A = .0003$ eV

$N_D = 4 \times 10^{14}$ cm^{-3}

$n_s = 2 \times 10^{18}$ cm^{-3}

$\mu_{ns}(4.2°K) = 1 \times 10^4$ cm^2/V-sec

d=8x10^{2}cm

10^{-2}

2x10^{-3}

R

ρ

Figure 5.3.6 shows that the previously DCO-type sample 100 ses
all its crossovers as it is thinned down. In the same figure, we
show that the calculations based on our model predict the losing of
both crossover points for a thin DCO-type sample.

No attempt was made to fit the calculated curves to the data
points. The calculations were intended to show the qualitative
features of the anomalous thickness dependence as compared to
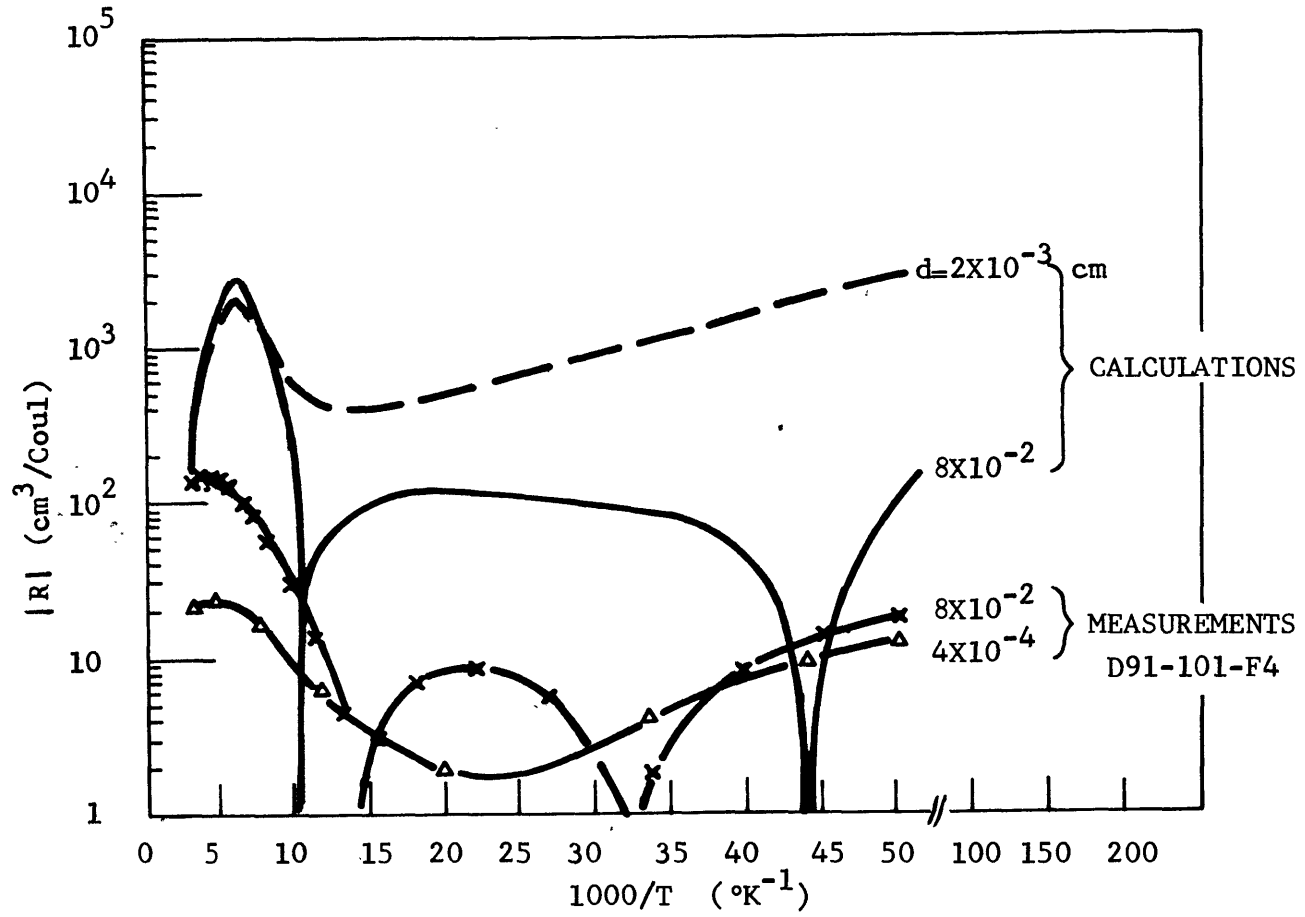experimented observations.

FIG. 5.3.6 COMPARISIONS BETWEEN CALCULATIONS AND MEASUREMENTS FOR A DCO-TYPE SAMPLE WITH DIFFERENT THICKNESSES.

118

The thickness dependence is one of the strongest supports for the conducting-surface model. Of the models reviewed in Section 3.2, none of them except the conducting-surface model give rise to the dependence of R and σ on sample thickness.

5.4   THE ELECTRON IRRADIATION EXPERIMENT

A series of experiments employing high energy electrons incident on (Hg,Cd)Te Hall-samples have been done since 1972[30,46]. The Hall measurements were made as a function of temperature from about 80° to 300°K both before and after irradiation by 4.5 to 5.0 MeV electrons up to a fluence of 8.5 X 10^{14} e/cm^2. Since measurements were performed at temperatures higher than 80°K, it is not clear from the R(T) curves done whether the sample was classical or anomalous. But with the help from the ρ(T) and μ(T) curves, the sample type can still be identified.

The pre-irradiation electrical properties of two samples used in the experiment are shown in Figure 5.4.1 and Figure 5.4.2. Sample QM13-9 was clearly n-type since μ at 80°K was high and ρ(T) revealed the presence of a "dip". On the other hand, sample 217 (3.5-4.2)H was what we call Peak-type since μ showed a peak at 100°K (compare it with curve (c) in Figure 1.2.3).

The experimental set-up allowed the electrical properties of these two samples to be measured at various intervals during the irradiation of electrons. The measured carrier densities

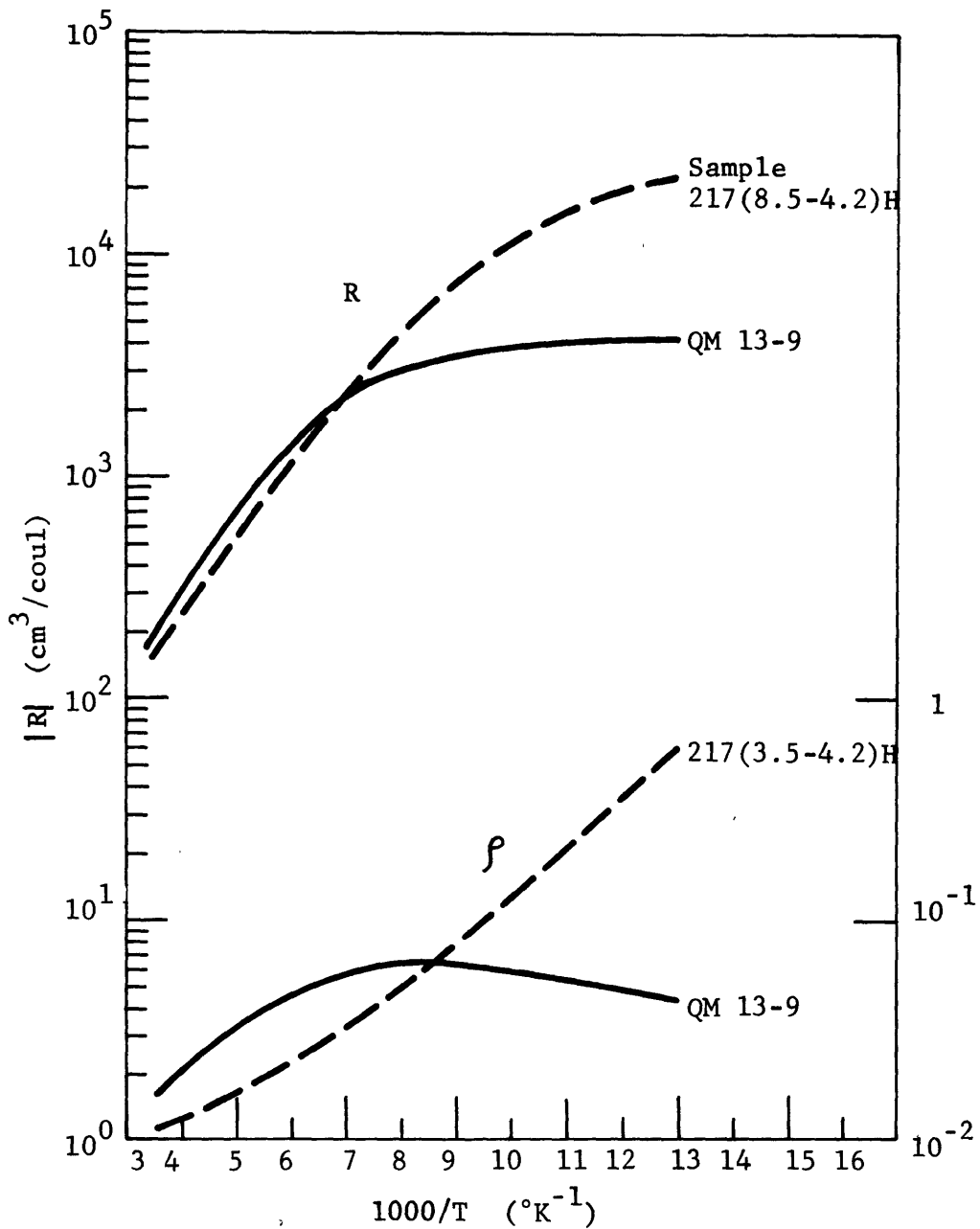Figure 5.4.1 R(T) AND ρ(T) OF TWO HALL SAMPLES BEFORE
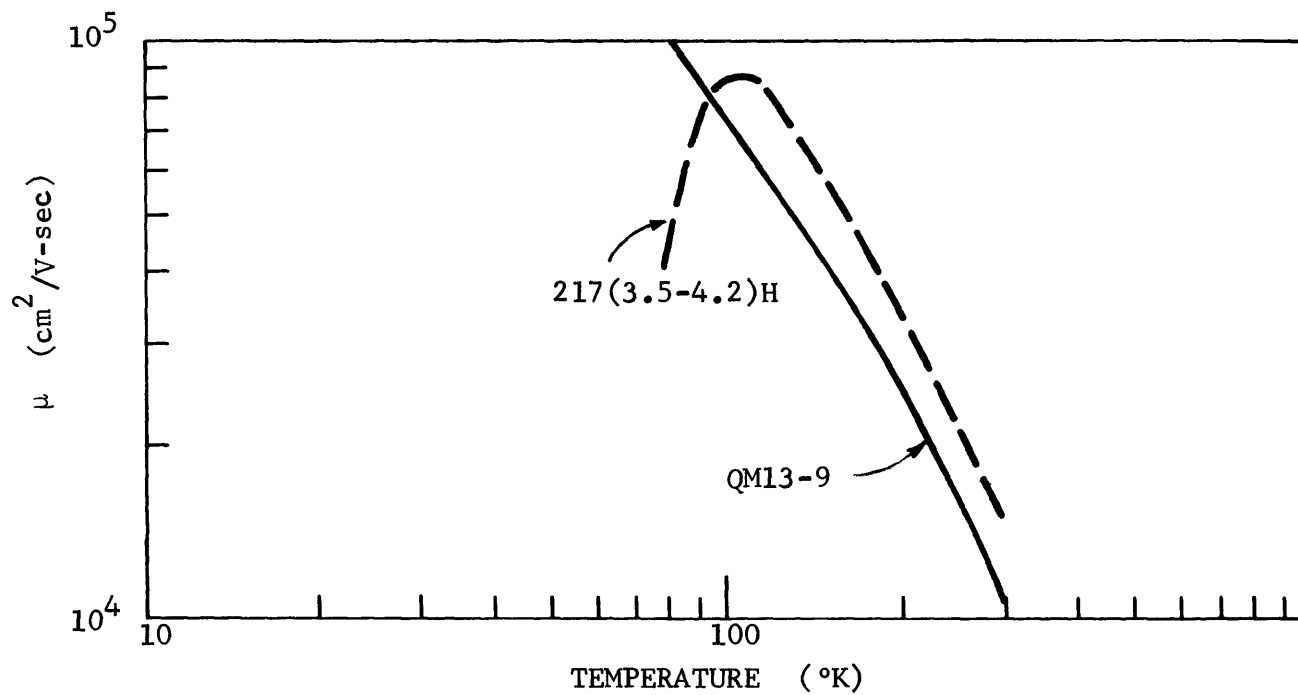ELECTRON IRRADIATION (Ref 46)

FIG. 5.4.2 $\mu(T)$ OF TWO HALL SAMPLES BEFORE ELECTRON IRRADIATION (REF. 46).
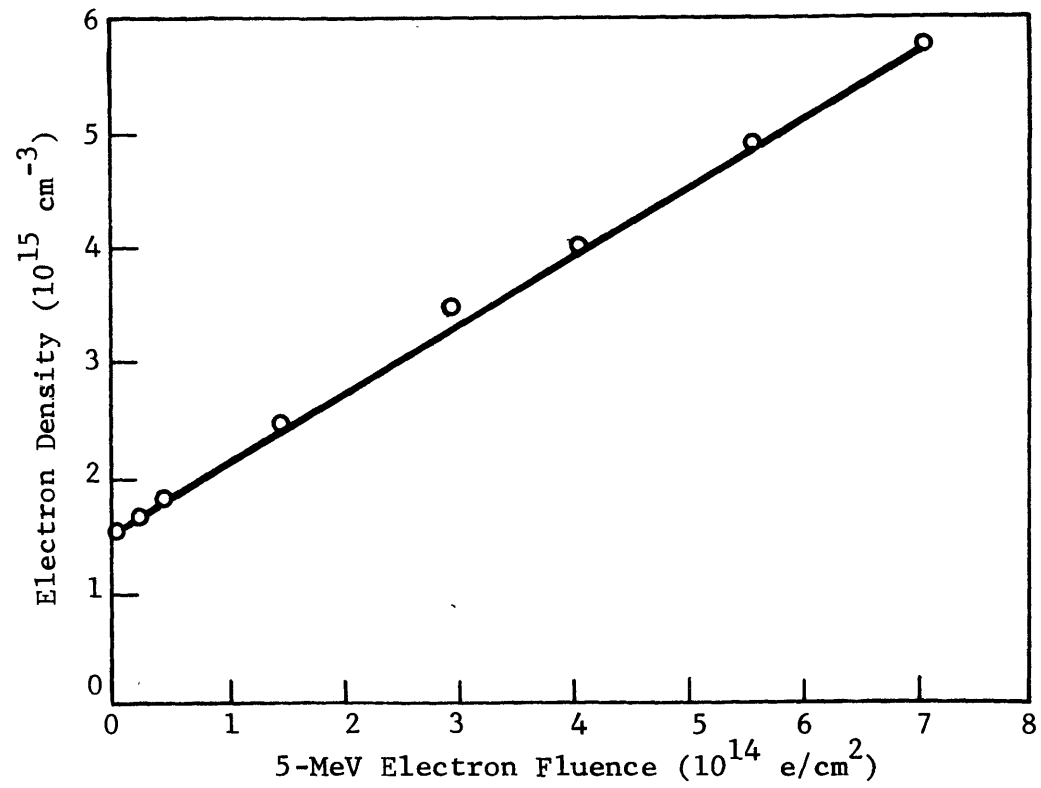
Figure 5.4.3 CARRIER CONCENTRATION VERSUS 5-MeV ELECTRON FLUENCE
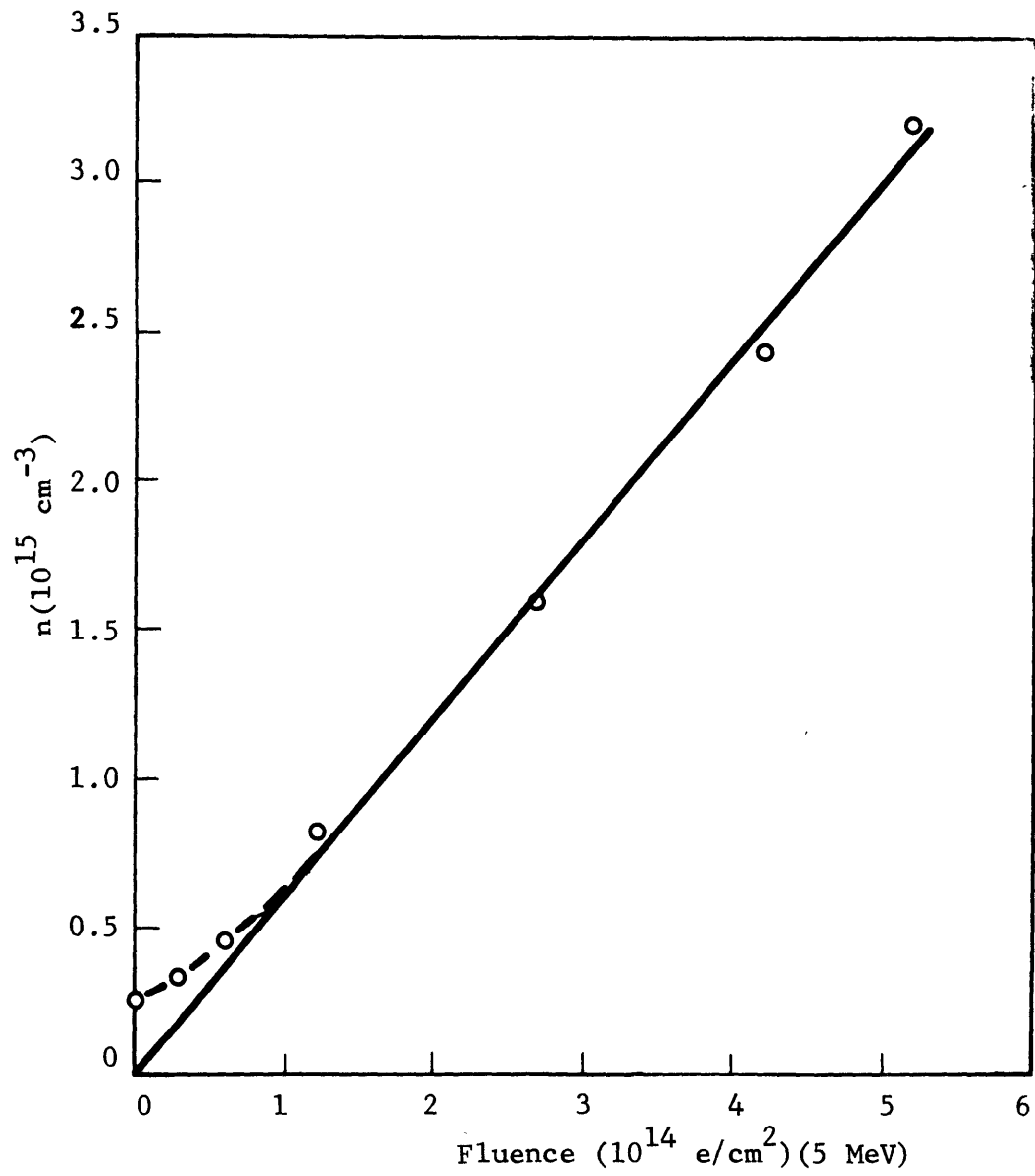FOR SAMPLE QM 13-9; IRRADIATION AT 80 °K (Ref 46).

Figure 5.4.4   CARRIER CONCENTRATION VERSUS 5-MeV ELECTRON
FLUENCE FOR SAMPLE 217(3.5-4.2)H; IRRADIATION
AT 80 °K (Ref 46).

123

(electrons) as a function of the irradiation fluence are plotted in Figure 5.4.3 and Figure 5.4.4. The electron irradiation resulted in an increase in donor density. The range of 5 MeV electrons in (Hg,Cd)Te is estimated to be deeper than the thickness of the samples[49], hence these created donors are expected to be uniform in the bulk.

Comparing Figure 5.4.3 with Figure 5.4.4, one notes that for the n-type sample (QM13-9), the slope of the plot is constant throughout and intersects the ordinate axis at a value equal to the pre-irradiation electron comcentration. For the Peak-type sample (217(3.5-4.2)H), however, the slope can be extrapolated to approach the origin and at low fluence values the curve bends upward to approach the pre-irradiation carrier concentration. Consequently, the electron radiation results show that for a Peak-type sample, the conduction mechanisms before and after the irradiation are not quite the same as indicated by the nonlinearity of the slope in the electron density versus fluence plot.

The results of the electron radiation experiment can well be understood by the conducting-surface model which postulates that a Peak-type sample is essentially a p-type sample with an n-type skin. Hence, the model actually predicts a zero electron density in the bulk before electron irradiation as illustrated by

extrapolating the slope in Figure 5.4.4 which approaches the origin. According to the model, the upward bending of the curve at low fluence can be understood as due to the prevailing shielding effects of the surface. In this region, new donors created by the fluence merely serve to compensate the holes in the bulk. Until these added donors exceed the number of acceptors in the bulk and predominate the electrons at the surface, the curve in Figure 5.4.4 starts to have a constant slope.

5.5   THE MAGNETIC FIELD DEPENDENCE OF R

At the end of Section 4.5, we derived an expression for the B-field dependent Hall coefficient on the basis of the conducting-surface model.

Equation 4.7.2 is the crucial equation in the magnetic field dependence calculations. For (Hg,Cd)Te, $(\mu'_{ns}B)^2$ and $(\mu_{pb}B)^2$ are much less than $(\mu_{nb}B)^2$, therefore, we can ignore the first two as compared to unity but keep the term $1 + \mu_{nb}^2 B^2$.

Let us apply these approximations to (4.7.2) and analyze it at the region where the surface terms predominate, in other words, at low temperatures. We consider the two asymptotic forms of R at the limits of high and low magnetic field.

Case I: If $1 >> (\mu_{nb}B)^2 \geq (\mu_{ns}B)^2 \geq (\mu_{pb}B)^2$, then

$$\left| R(B) \right| \to \left| R_s \right| d/d_s, \text{ at low B} \tag{5.5.1}$$

Case II: If $(\mu_{nb}B)^2 >> 1 >> (\mu_{pb}B)^2$, then

$$R(B) \rightarrow R_s \frac{d}{d_s} \frac{1}{\mu_{nb}^2 B^2} , \quad \text{at high B-field} \qquad (5.5.2)$$

In fact, the Hall coefficient of a Peak-type (Hg,Cd)Te sample measured at low temperatures was reported to decrease with increasing B-field and the results are shown in Figure 5.5.1[25].

It had been reported also that a sufficiently high magnetic field could actually cause the Hall coefficient of a Peak-type sample to show DCO[47] (see Figure 5.5.2). A computation is made based on equation 5.5.1 with the magnetic field as a parameter and is shown in Figure 5.5.3.

One can see that calculations are qualitatively in agreement with measurements. The appearance of the DCO at higher B field can be explained by the fact that both bulk and surface electron mobilities are higher than hole mobility which makes the electron terms in (4.7.2) diminishing at higher field, as a result the p-type bulk terms prevail.

Note that there are discrepancies between the theoretical predictions and experimental results. Equation 5.5.2 predicts that R is proportional to B^{-2} but Figure 5.5.1 shows that R is proportional to $B^{-1/2}$. Equation 4.7.2 predicts that as B is further increased, eventually R will change from DCO to p-type. But Figure 5.5.2 shows that R is p-type at a medium magnetic field and becomes DCO at a higher field. The reason for these discrepancies is not obvious.
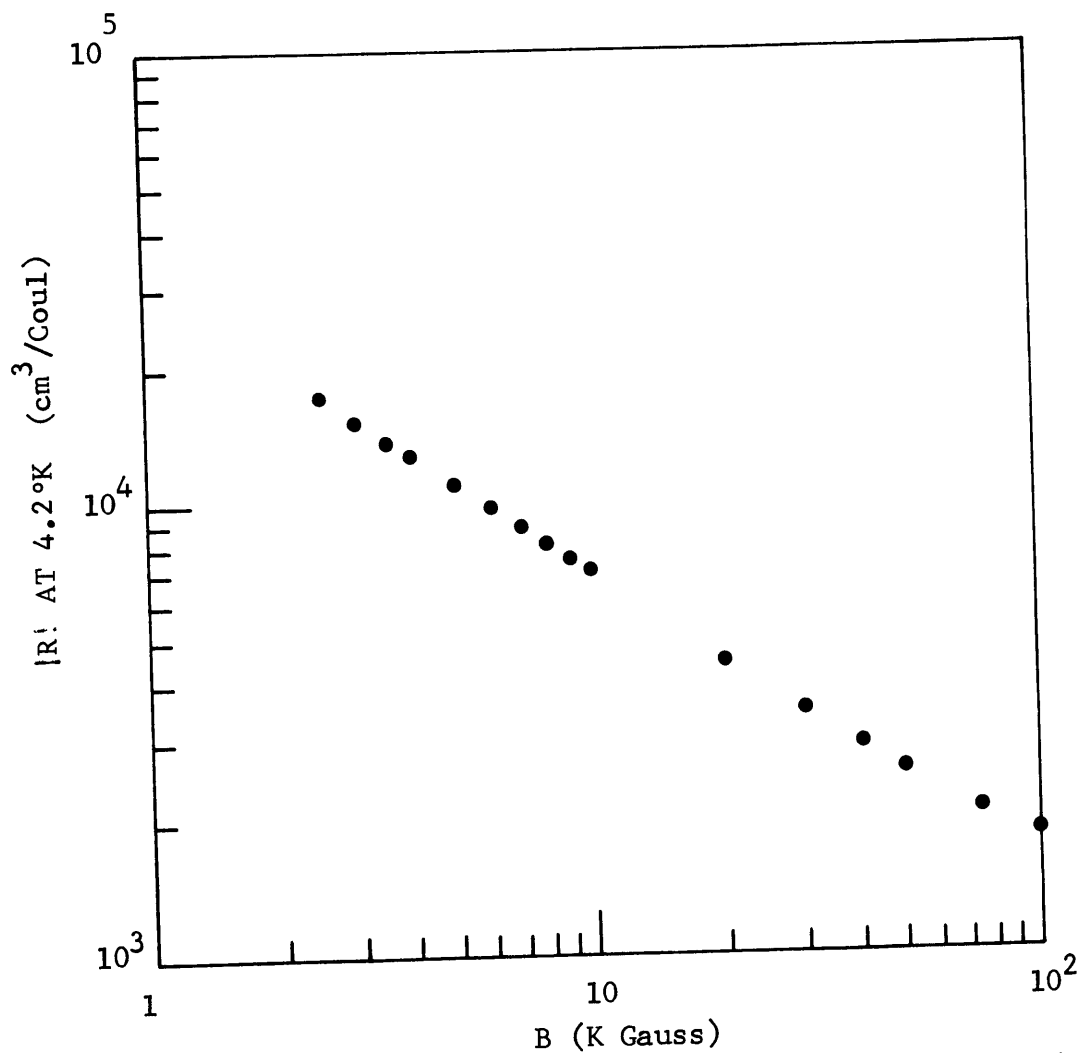
FIG. 5.5.1 MEASURED |R| AT 4.2°K VS MAGNETIC FIELD B (REF. 25).
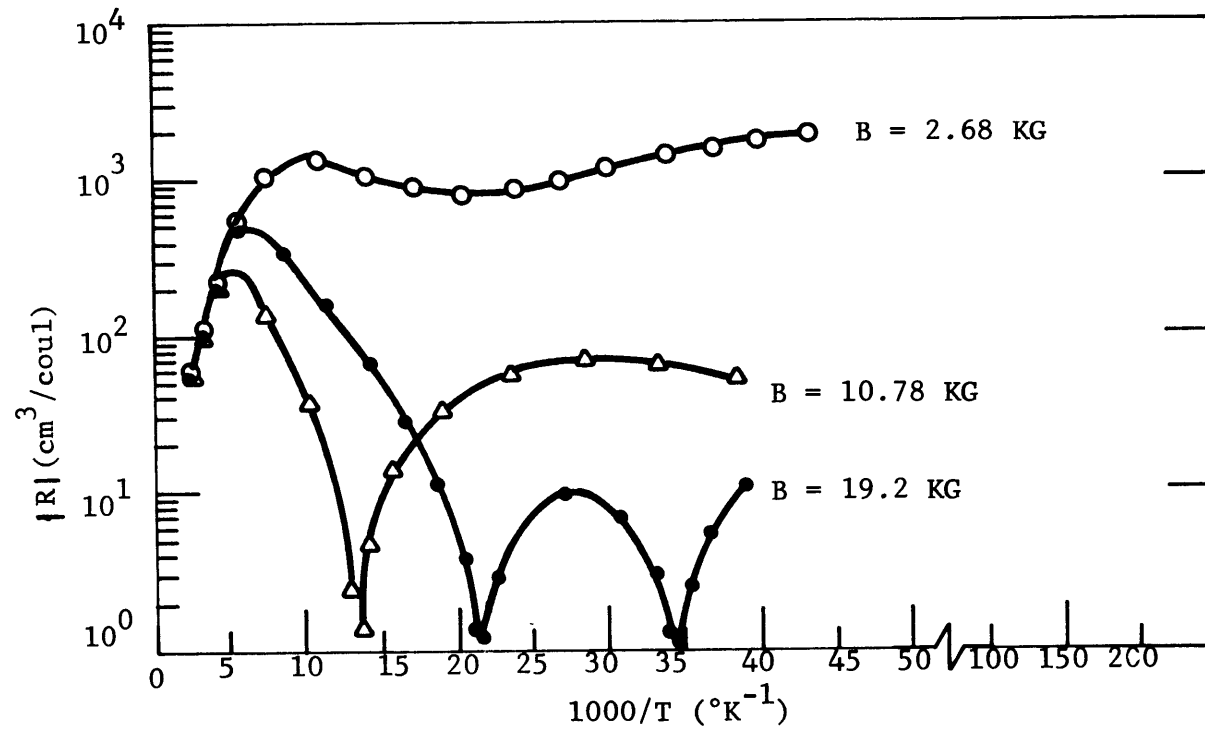
Figure 5.5.2   MEASURED MAGNETIC FIELD DEPENDENCE OF R(T) ON SAMPLE
ZPU-4-32 (Ref 47)
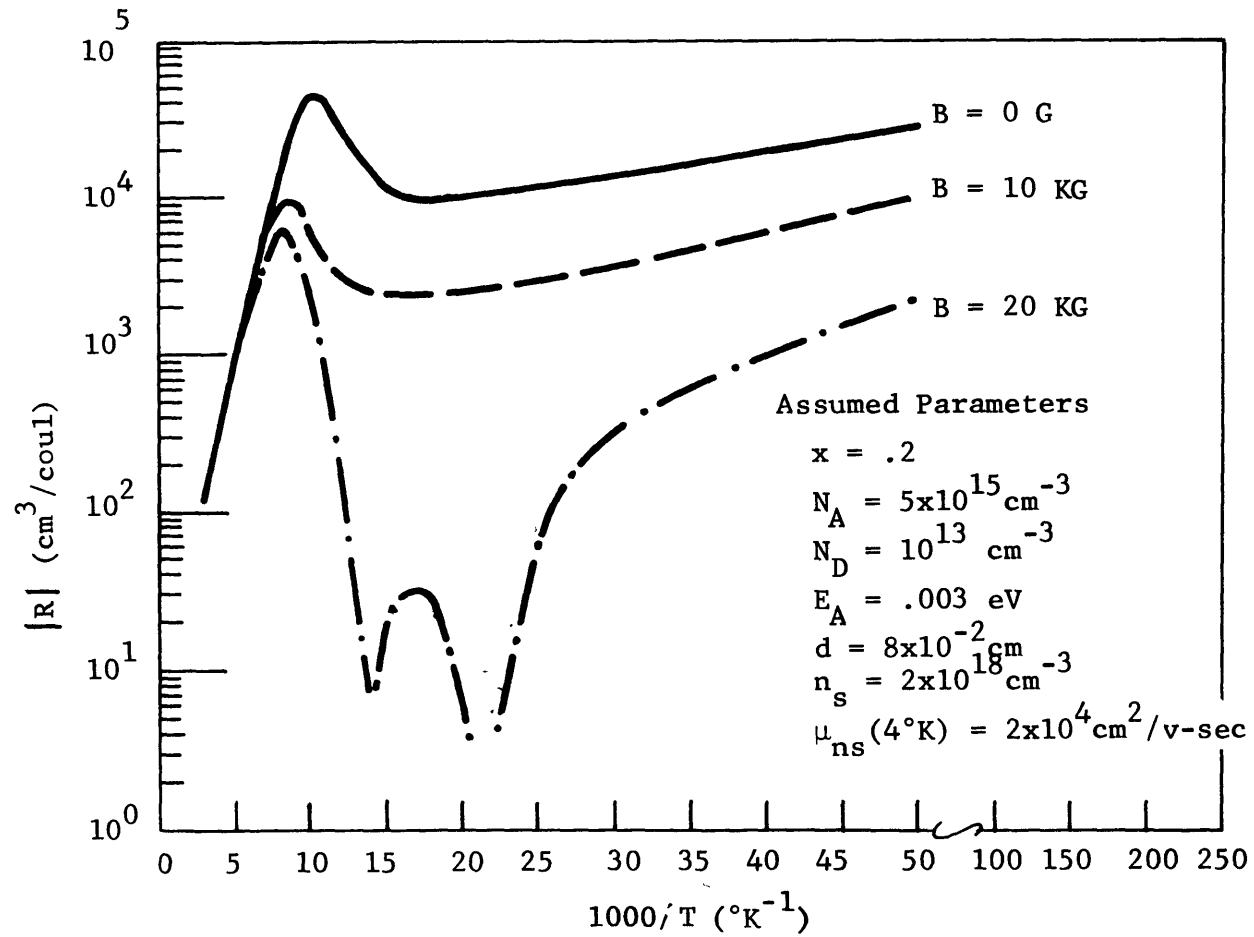
Figure 5.5.3   CALCULATED R(T) AS A FUNCTION OF THE MAGNETIC FIELD B.

The plot shows $|R|$ $(cm^3/coul)$ on the vertical axis versus $1000/T$ $(°K^{-1})$ on the horizontal axis, with three curves:

- B = 0 G
- B = 10 KG
- B = 20 KG

Assumed Parameters

$x = .2$

$N_A = 5 \times 10^{15} cm^{-3}$

$N_D = 10^{13} cm^{-3}$

$E_A = .003$ eV

$d = 8 \times 10^{-2} cm$

$n_s = 2 \times 10^{18} cm^{-3}$

$\mu_{ns}(4°K) = 2 \times 10^4 cm^2/v\text{-}sec$

129

The virtue of the conducting-surface model, however, is that it is able to account for the two anomalous phenomena associated with the magnetic field: first, it shows that R decreases with increasing magnetic field at low temperatures; secondly, it predicts that DCO will appear for a Peak-type sample under the influence of high magnetic field.

5.6   OBSERVATION OF PEAK- TO p-TYPE CONVERSION

We have developed a way to restore the p-type Hall characteristic from the Peak-type (Hg,Cd)Te samples. We applied this new sample fabrication technique to prepare several Hall samples. The results showed good reproducibility.

We outline the experimental procedure as follows:

(1) A sample with a parallelioipiped shape was polished and etched in bromine methane solution.

(2) Six Cu leads were bonded to the sample by In soldering (Figure 5.6.1).

(3) Hall effect measurements were made from $4.2°K$ up to $300°K$, results are shown in Figures 5.6.3 and 4.

(4) If the results showed a peak in R(T), then the leads were removed from the sample and the sample was patterned with teflon tapes as shown in Figure 5.6.2(a) for air-brading.

(5) Pattern the Hall sample again with teflon tapes as shown in Figure 5.6.2(b) for In evaporation.
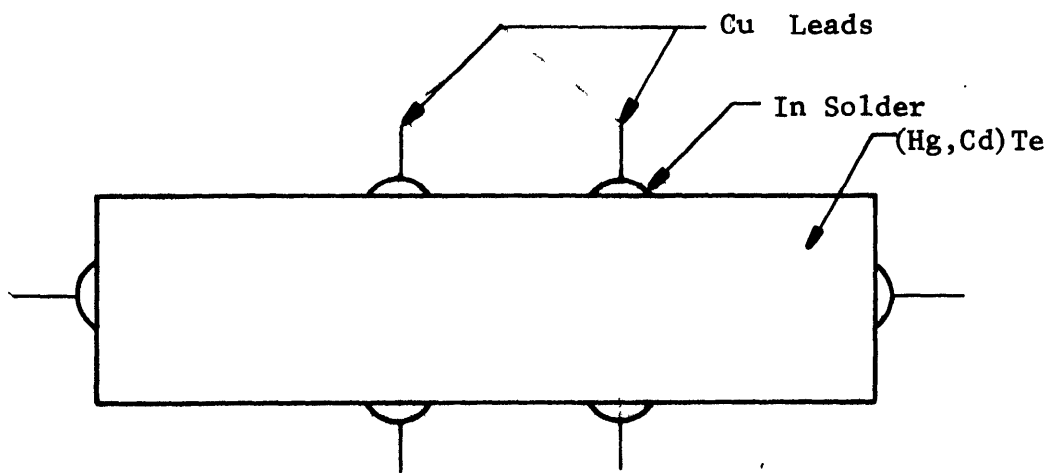
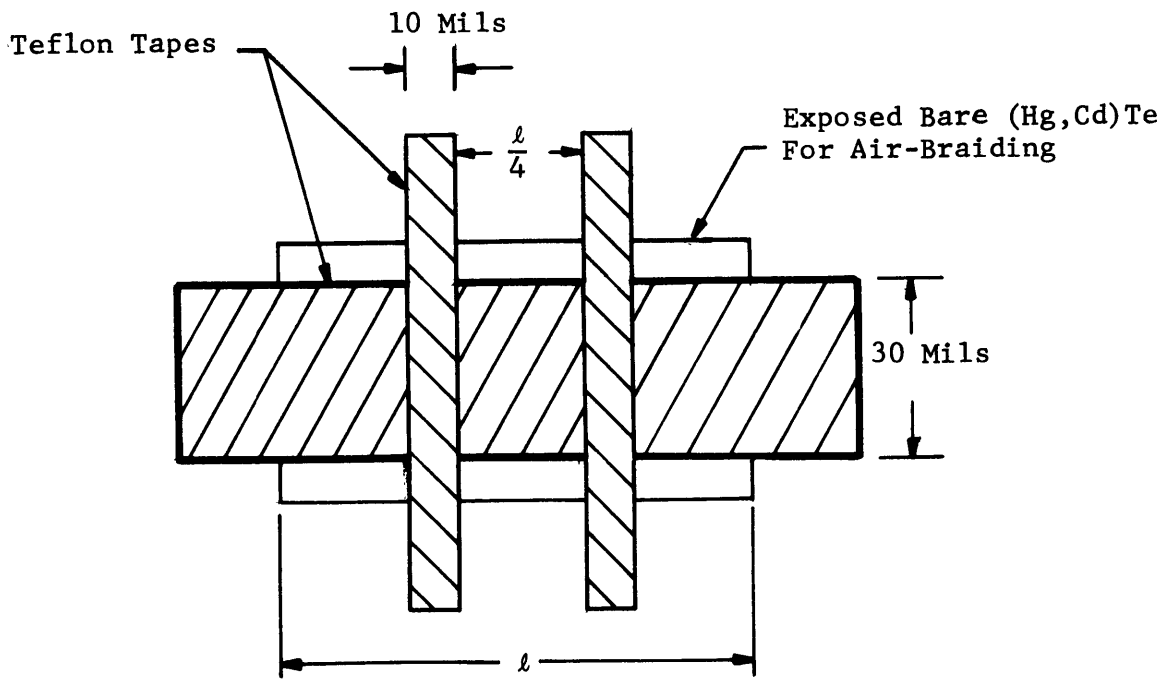Figure 5.6.1   HALL SAMPLE WITH IN SOLDERED CONTACTS.

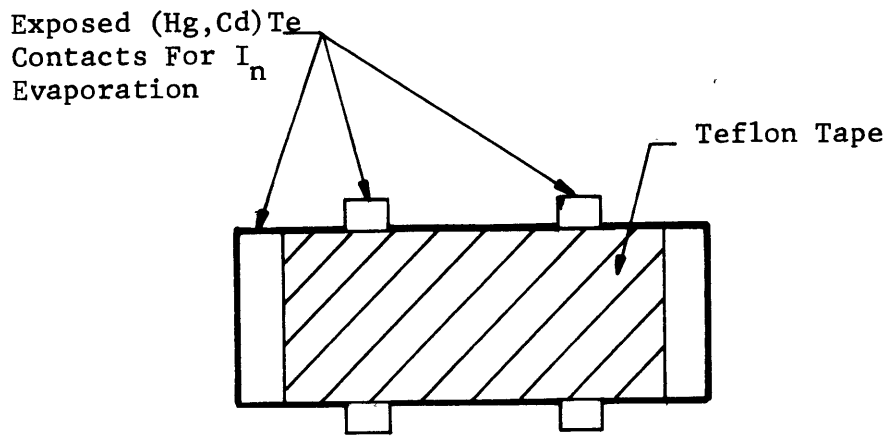Figure 5.6.2(a)   HALL SAMPLE CONFIGURATION
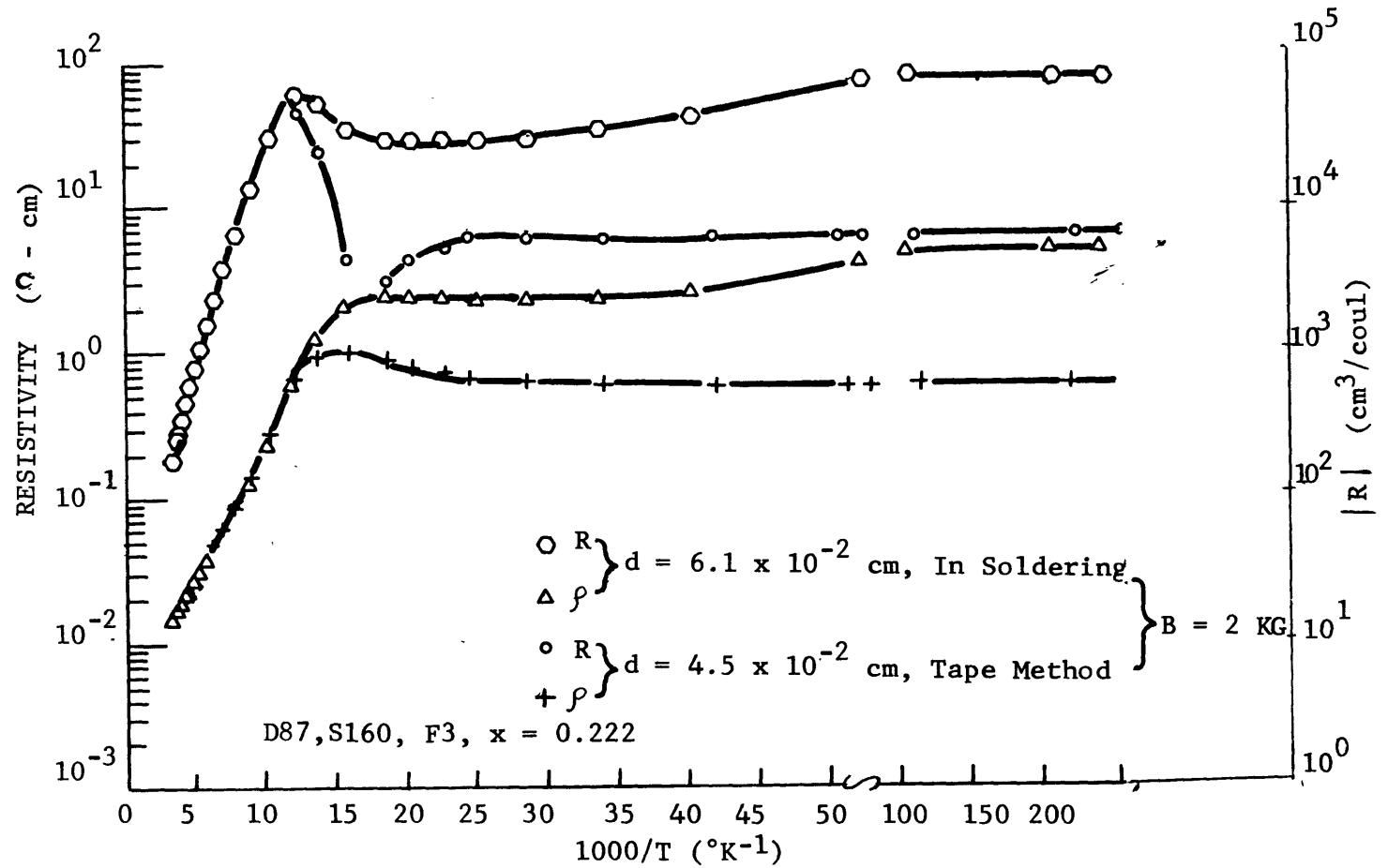

Figure 5.6.2(b)   HALL CONTACTS EVAPORATION

Figure 5.6.3   TEMPERATURE DEPENDENT R AND ρ FOR A SAMPLE WITH TWO DIFFERENT
FABRICATION TECHNIQUES (see Text).
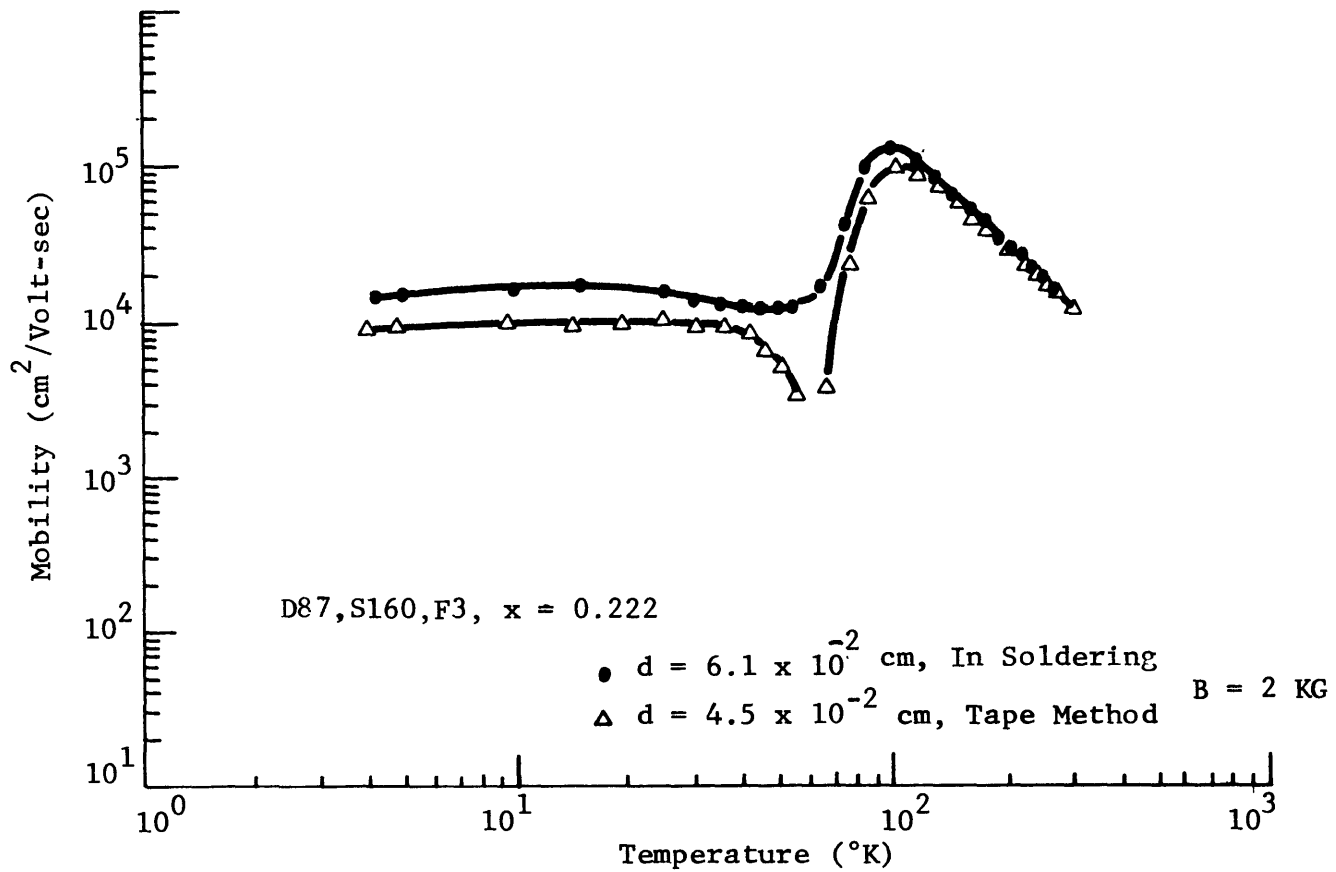
Figure 5.6.4   TEMPERATURE DEPENDENT μ FOR A SAMPLE WITH TWO DIFFERENT FABRICATION
TECHNIQUES (see text).

(6) Au leads were bonded to the In contacts by thermal compression.

(7) Remeasured the variable temperature Hall properties. Results are shown in Figure 5.6.3 and 4.

The results of this experiment show that the anomalous Hall properties are very sensitive to the sample fabrication procedures. It also gives us some important insight in the understanding of the anomalous data. It demonstrates experimentally that the peak in the Peak-type R(T) is closely related to R_{max} if the same sample becomes p-type. This proves the validity of using the peak values in determining N_A as suggested in Section 4.6.

The question arising from the results of this experiment is: What are the major factors involved in our new fabrication procedure that cause the conversion? If our research leads to the belief that anomalies are due to an inverted surface, then we know that these factors somehow reduce or eliminate the effects of the inverted surface. In order to answer the above question, more experiments have to be done to isolate these factors so that each of them can be identified. All we know now is that samples with either soldered In or evaporated In (through photo mask) contacts do show anomalies. This is the rule rather than the exception.

5.7 CALCULATING N_A FROM THE ANOMALOUS DATA

In section 4.6, we have derived an expression for the acceptor density in terms of the measured anomalous Hall quantities (see 4.6.8) The accuracy of this expression can be estimated by examining the validity of the assumptions we made in our derivation.

The first assumption we made was that the bulk electron to hole mobility rates is temperature independent. This is not so as shown in Figure 2.3.1. However, at the temperatures where the peak occurs, the changes of carrier concentrations with temperature are much larger than that of the mobility ratio. Hence this assumption is still valid.

The second assumption we made was the the magnetic field B is small compared to the reciprocal of the bulk electron mobility in order that the weak magnetic field limit can be applied, i.e.

$$(\mu_{nb}B)^2 \ll 1 \quad .$$

This assumption is clearly questionable where the magnetic field is as high as 2KG at which the data were taken. In order to show the dependence of R on B for a peak-type sample, we show the calculated

Hall coefficients by means of (4.5.18) in Figure 5.7.1 for two different values of B. We can see the effects of the 2KG magnetic field on R(T). At low temperatures the effects are minor, but those at temperatures near the peak cannot be neglected because the N_A calculations depend on the value of R_{max}.

In order to understand the effects of the magnetic field on the acceptor density calculations, we compare the values of the calculated N_A with those of the assumed N_A. The calculated N_A is determined by means of (4.6.8) in which the Hall quantities are taken from the theoretical R = R(T) curve which a 2KG magnetic field is assumed. The assumed N_A is the input parameter for calculating the theoretical R = R(T) curve. The comparison are shown in Table 5.7.1. The results indicate that the calculated and the assumed values of N_A are within a factor of 2 over the range from $N_A = 10^{14} cm^{-3}$ to $2 \times 10^{16} cm^{-3}$. It leads us to believe that (4.6.8) can still be used to estimate N_A from the anomalous Hall measurements taken at a magnetic field of 2KG.

Let us now proceed to calculate the values of N_A for several peak-type samples. Several assumptions have to be made which are similar to the ones we made in all our theoretical calculations.
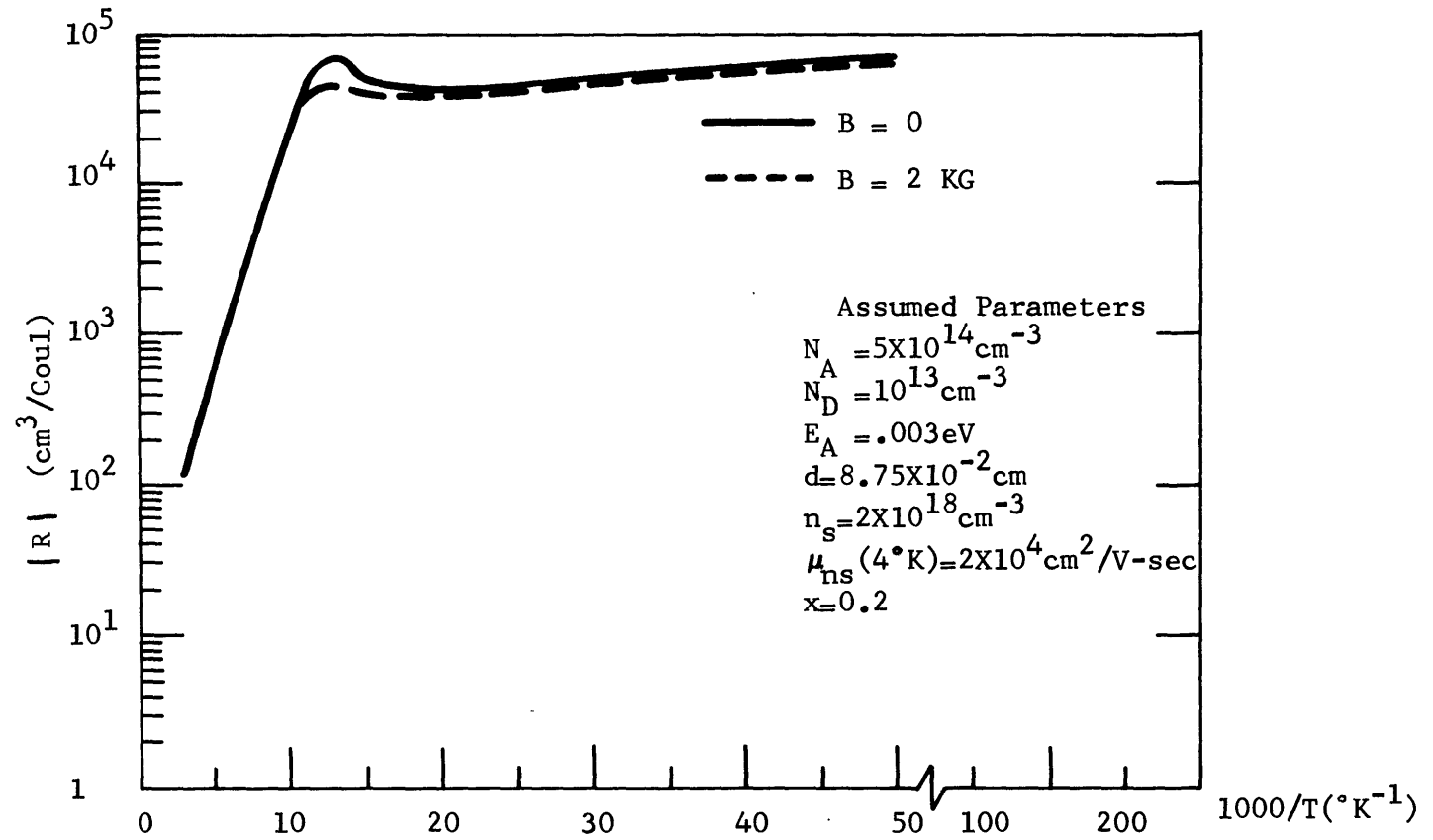
Fig. 5.7.1   THE CALCULATED HALL COEFFIIENTS FOR TWO DIFFERENT
MAGNETIC FIELDS B.

First, we assume that μ_{ns} is constant from 4.2°K up to the intrinsic region and then it falls off as $T^{-2.27}$ at higher temperatures. Seconndly, $\mu_{nb}(T)$ is assumed to be given by curve (C) in Figure 1.2.3 which is a typical n-type mobility curve. Thirdly, $n_s d_s$ is assumed to be temperature independent and its value is given by:

$$n_s d_s = d/(\; q \; R(4.2°K \;)$$

with all three assumptions in mind, we rewrite (4.6.8) as follows

$$N_A = 4 \; q \; R_M \; n_i^2(T_M)/D(T_M) \, ,$$

where

$$D(T_M) = 1-4(\; R_M \; / \; R(4.2°K) \;)(\mu_{ns}(T_M)/\mu_{nb}(T_M))^2$$

where T_M is the temperature at which R is at a maximum R_M, and $n_i(T_M)$ can be evaluated by means of (2.3.1). Using these two equations, we calculate N_A for seven peak-type samples. The results are listed in Table 5.7.2. Note that five out of seven are taken from the same ingot D82.

To conclude, we may remark that the conducting surface model has for the first time enabled estimates for the bulk acceptor density for anomalous samples. The results show that peak-type $Hg_{0.8}Cd_{0.2}Te$ samples are generally weakly doped p-type with $N_A \leq 10^{15} cm^{-3}$.

ASSUMED N_A (cm^{-3})	CALCULATED N_A (cm^{-3})
1.0×10^{14}	1.22×10^{14}
5.0×10^{14}	6.70×10^{14}
1.0×10^{15}	1.39×10^{15}
5.0×10^{15}	3.59×10^{15}
2.0×10^{16}	3.61×10^{16}

Table 5.7.1   THE COMPARISON BETWEEN THE CALCULATED AND THE ASSUMED N_A; OTHER ASSUMED PARAMETERS ARE $x = .2$, $d = 8 \times 10^{-2}$ cm, $n_s \simeq 2 \times 10^{18}$ cm^{-3}, μ_{ns} (4 °K) $= 2 \times 10^4$ cm^2/V-s, $B = 2 \times 10^3$ G.

SAMPLE	CALCULATED N_A (cm^{-3})
D9-141-F3	4.8×10^{13}
D59-149-F4-3	6.9×10^{14}
D82-80-E1	2.0×10^{14}
D82-81-120F3	3.8×10^{15}
D82-120-F2	5.1×10^{14}
D82-120-F4	1.0×10^{15}
D82-120-F5	1.1×10^{15}

Table 5.7.2   THE CALCULATED N_A OF SEVERAL PEAK-TYPE ($Hg_{0.8}Cd_{0.2}$)Te SAMPLES

5.8 THE GENERALIZATION OF THE MODEL AND OTHER REMARKS

In all our calculations we have assumed the surface layer thickness d_s to be equal to the effective debye length which is a function of temperature and the free carrier density in the bulk. Because of this assumption, the calculated R(T) always shows a finite slope at low temperatures since R is proportional to $T^{-1/2}$. However, this constraint on d_s can be removed without affecting our conducting surface model; in fact, in doing so, we generalize it. We will now address these points.

Recall that the effective Debye length was defined by the Poisson equation. We later introduced the quantity called "surface excess carrier density" which is the product of surface density and surface layer thickness; namely, $n_s d_s$. From then on, n_s and d_s always appeared together in all equations we derived, including the magnetic field dependent ones. Therefore, it does not matter if d_s is the effective Debye length as long as $n_s d_s$ had the appropriate values. By removing the constraints on d_s, we are free from having the $T^{-1/2}$ dependence on R(T) and from giving account for the presence of $10^{18} cm^{-3}$ n_s.

We now generalize the conducting surface model to the four parallel conductor model. Figure 5.8.1 shows how the semiconductor slab is
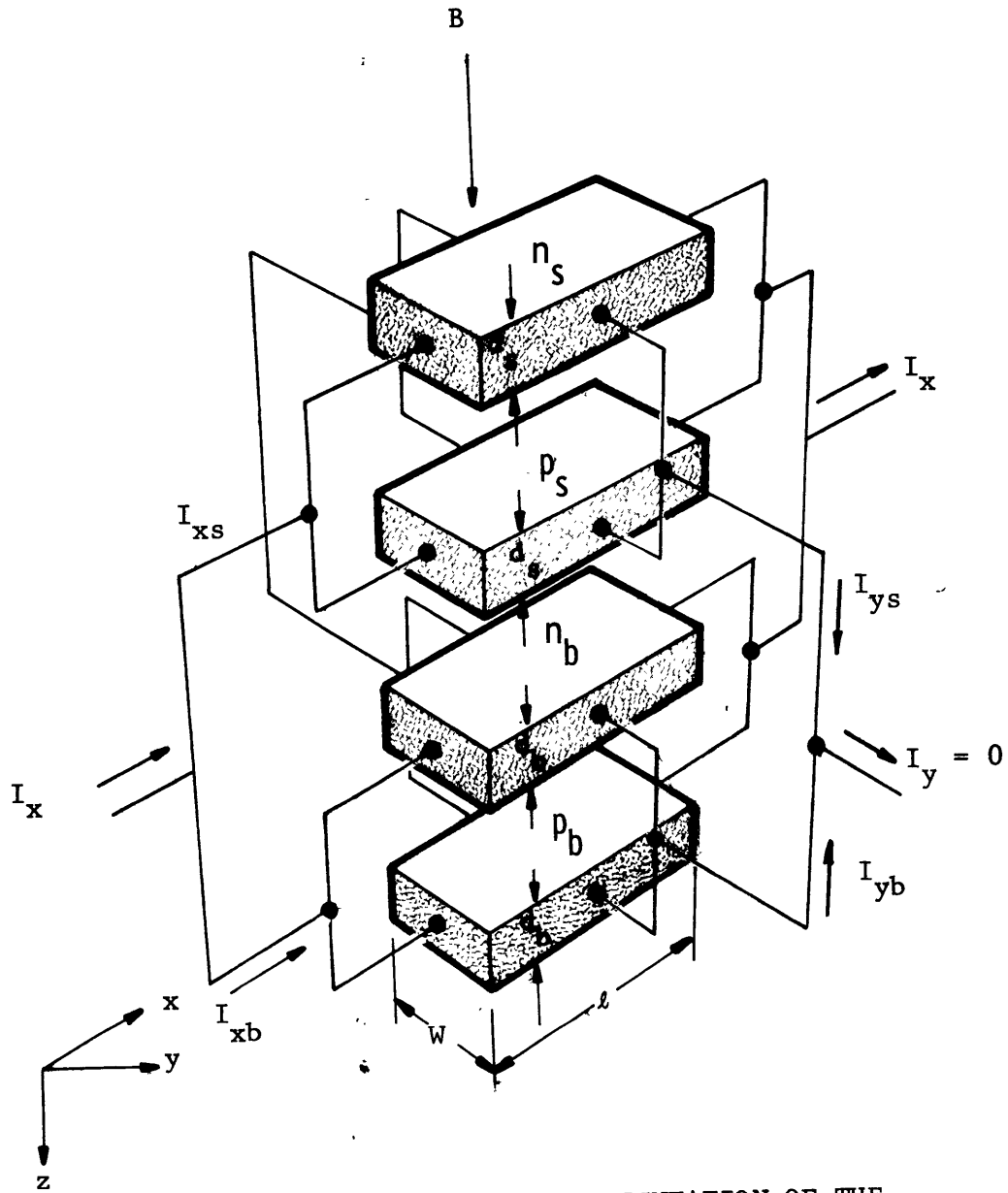
Figure 5.8.1   SCHEMATIC REPRESENTATION OF THE
FOUR-CONDUCTOR MODEL

142

separated into a bulk (with thickness d_b) and a surface (with thickness d_s) region and each of which is separated into single-band conductors n and p. These four slabs are considered to be homogenious and they are electrically connected in parallel in both the x and y-directions. Two boundary conditions are given: (1) the thickness of the sample $d = d_b + d_s$; (2) $I_y = I_{ys} + I_{yb} = 0$. The magnetic field is in the z-direction. This model automatically satisfies all our equations if the contribution from slab "ps" is small compared to the rest which means that the surface holes are less conductive. It allows us more degrees of freedom in the interpretations of the anomalies. It no longer requires the concept of outer surface inner bulk as described by the Poisson equation. As long as the four conductors are connected in parallel, they will give rise to anomalous Hall properties.

We next comment on the influence of the p-n junctions on the anomalies which was neglected in all our calculations (see Section 3.2e). As one may expect, if an n-type layer (or p-type) exist on the yz-plane, covering the whole lateral surfaces of a sample. Then the effects of the p-n junctions on the Hall voltage have to be considered. According to Madeling[24], there is always a "floating potential" V_m set up at each of the surface p-n junction parallel to the direction of the magnetic field because of the Hall current of the minority

carriers. This additional potential is always negative. This means that for a p-type sample, the positive R_{pb} due to holes has one more negative opponent in addition to the negative R_{nb} and R_{ns}. The presence of the Madelung potential results in shifting the second crossover to a higher temperature in a DCO-type sample.

We will now calculate how high in temperature this second crossover point will drift to due to this additional negative component in the overall Hall coefficient. m can be estimated if we assume the diffusion length L_p to be $\sim 4 \times 10^{-3} cm$[48] at 77°K. From (3.2.4) V_m is given by $V_m = - (\mu_n + \mu_p) E_x B_z L_p \cong - 4 \times 10^2 E_x B_z$. Compare it to the value of V_p due to holes in the bulk given by

$$V_p = \mu_p d_b E_x B_z \cong 50 E_x B_z.$$

These calculations show that the measured R being dominated by negative terms will be negative throughout regardless of the dopant concentration N_A. As a result, including the Madelung voltage will eliminate the DCO behavior in R = R(T). The reason for the absence of the Madelung voltage in the measured Hall coefficient is that the boundary between the n-type inversion layer and the p-type bulk cannot be considered as a p-n junction because the thickness of this layer is much smaller than a diffusion length on which the Madelung voltage is based. For a layer thickness on the order of a few hundred anstrongs, the carriers can actually tunnel through without experiencing any resistance. 144

We also remark that in all our calculations x = .2 was assumed.
This is because this material is better understood and has more
data available, both classical and anomalous. But similar anomalies
have been reported in samples having various compositions and the
conducting-surface model is certainly valid in them as well.

To conclude this chapter, we want to illustrate the perfection of
the conducting surface model by comparing the calculated R, p and μ
to their corresponding measured quantities. The electrical properties
of a $Hg_{0.8}Cd_{0.2}Te$ sample of 8.75 x 10^{-2}cm thick was measured under
2KG B-field and the measurements are given in Figure 5.8.2 and 3
by discrete points. We calculated $n_s d_s$ from Hall coefficient measured
at 20°K from (5.3.3) and assumed it to be independent of temperature.
Then we obtained μ_{ns} from the measured μ at 20°K. Substituting
these values in (5.5.1) (4.5.17) and (4.5.23) with p_b as an
adjustable parameter for curve fitting, we calculated. R, p and μ
as shown in Figure 5.8.2 and 3 by lines. The agreement between
calculations and measurements is more than satisfactory for such
a simplifying model we employed.

10^2

10^1

10^0

10^{-1}

10^{-2}

10^{-3}

Resistivity (ohm-cm)

10^5

10^4

10^3

10^2

10^1

10^0

$|R|$ (cm^3/coul)

|R|

ρ

Sample   D82,S81,F3
Lines = Calculations
Points = Measurements
Assumed Parameters
x = .2
N_A = $6x10^{14}$ cm^{-3}
N_D = 0
E_a = 0
d = 8.15 cm
$n_s d_s$ = $9x10^{12}$
μ_{ns}(20 °K) = 2.2 x $10^4 cm^2$/v-sec
B = 2 KG

0   5   10   15   20   25   30   35   40   45   50   100   150   200
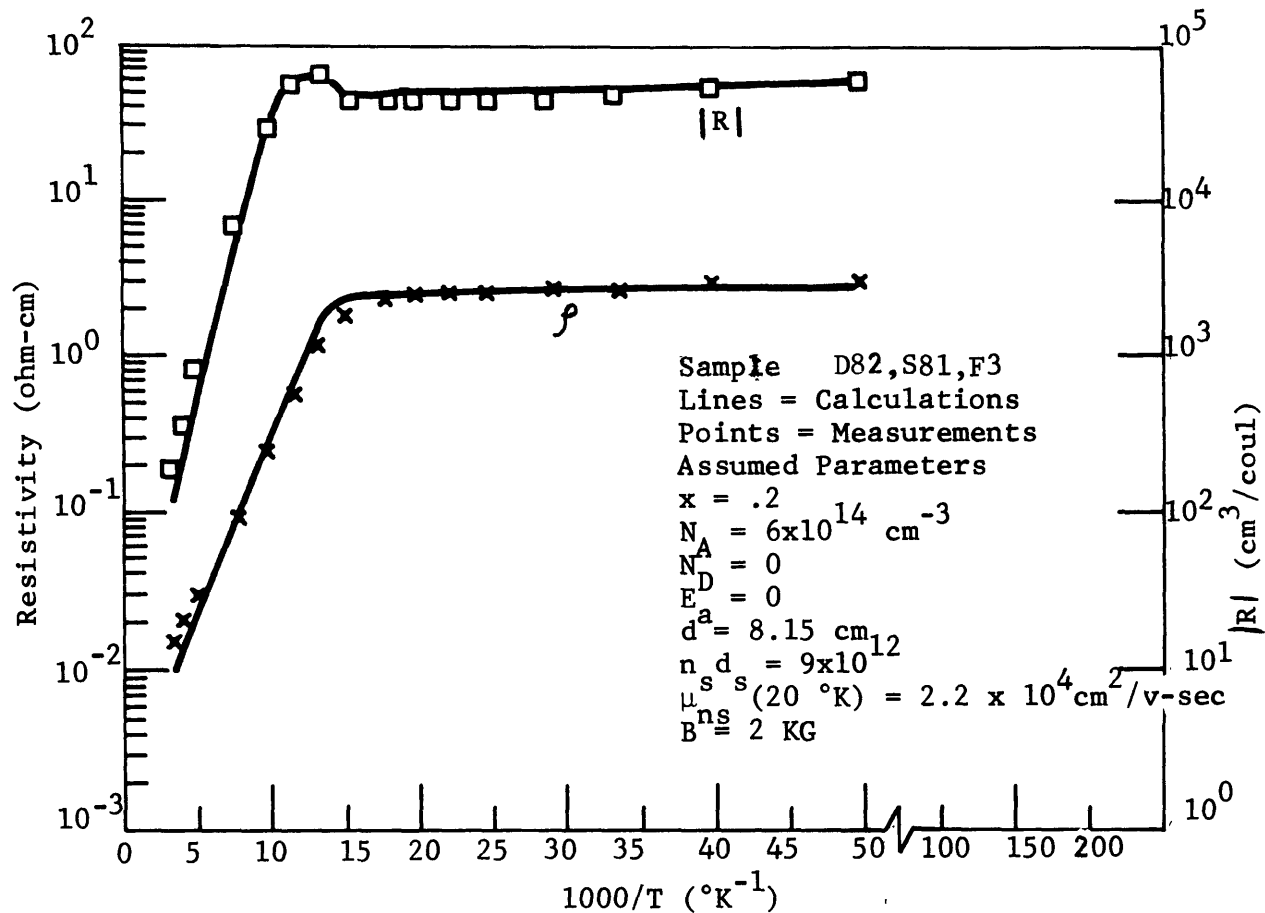
$1000/T$ ($°K^{-1}$)

Figure 5.8.2   COMPARISONS BETWEEN CALCULATIONS AND MEASUREMENTS
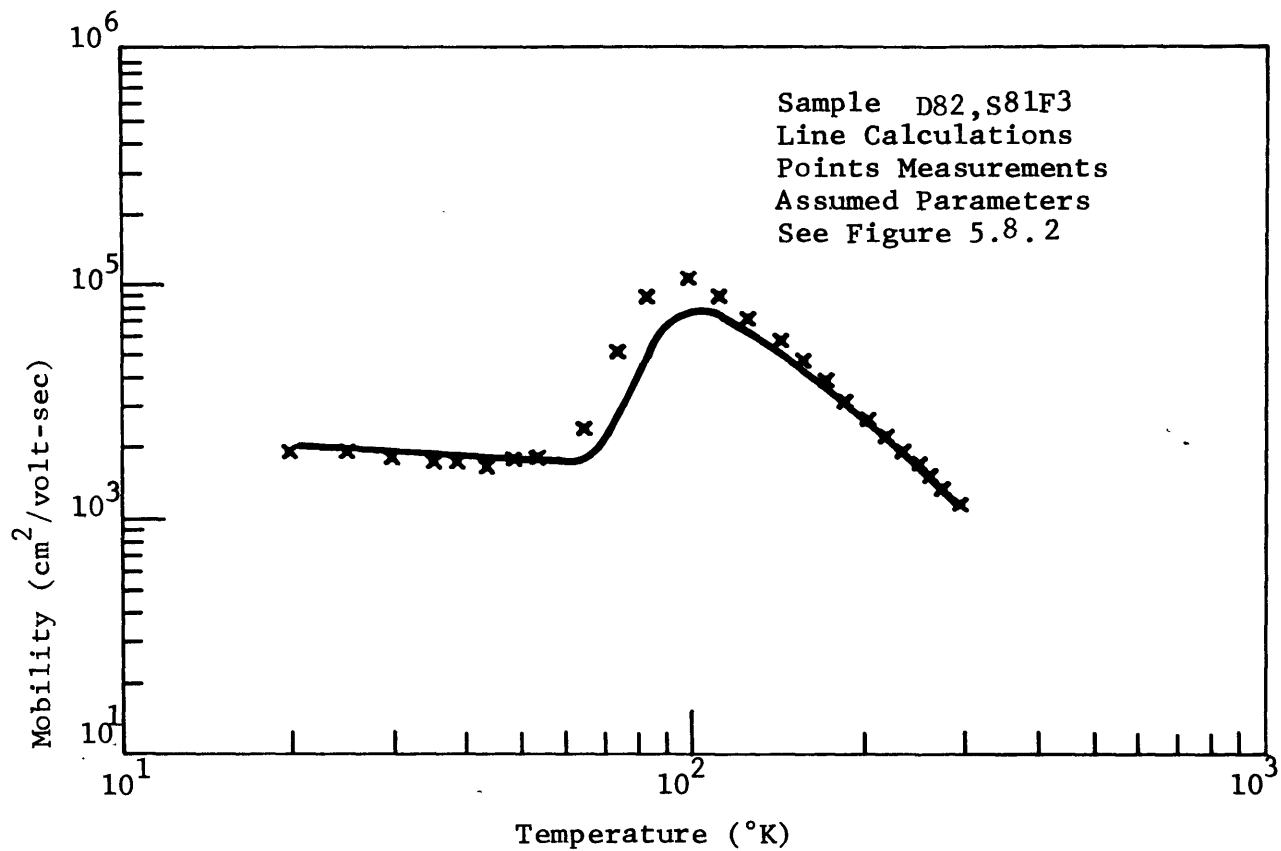OF R(T) AND ρ(T).

146

Figure 5.8.3 COMPARISON BETWEEN CALCULATIONS AND MEASUREMENTS OF $\mu(T)$

CHAPTER VI

CONCLUSIONS

Surveying the results described in this thesis, we may draw the
following conclusions and point out certain areas for further
investigation.

The peak and DCO-type variable temperature Hall coefficients in
(Hg,Cd)Te are classified as anomalous because they cannot be
interpreted in terms of semiconduction via the conduction band or/and
the valence band in a homogenious material. Scott et al[23] first
postulated that these anomalies were attributable to the presence
of an n-type layer on a p-type (Hg,Cd)Te sample. In chapter IV
we derived expressions for the apparent Hall coefficient, conductivity
and mobility on the basis of the conducting surface model. The
numerical calculations based on these expressions with appropriate
values for material parameters showed satisfactory agreement with
the experimental results.

The anomalies can be understood in the light of the conducting
surface model as follows. At low temperatures conduction via n-type
surface predominates due to either one or a combination of these
reasons : high surface electron to bulk hole mobility ratio, weakly
doped p-type bulk, or freezing out the acceptors in the bulk. If

If the acceptor density is so low that conduction via the
valence band is still incomparable even at exhaustion temperatures,
then R will remain negative throughout. Since a low accepter
density corresponds to a larger $|R_{max}|$ [26], as the temperature
reaches T_{max}, $|R|$ which is the sum of $|R_s|$ and $|R_{max}|$ will give rise
to a peak.

For more heavily doped p-type materials, the conduction via the
valence band may at some temperature prevail the conduction via
the n-type layer due to either the rising hole mobility or the
diminishing freeze-out effect with increasing temperatures.
This results in a change of sign (from negative to positive)
for R. When the intrinsic temperature is reached, R will
eventually change back to negative because the sample is p-type.
As a result a DCO is observed.

This hypothesis is supported by five observations presented in
Chapter V. First, anomalies in InAs[15] as well as (Hg,Cd)Te
showed that values of N_A for DCO type samples were always
greater than those for peak type. Secondly, a definite correlation
existed between the low temperature R, ρ and the thickness of
the anomalous type samples. Thirdly, the results of the electron
radiation experiment[30/46] showed that the preirradiation electron
density of a peak-type sample was actually zero. Forthly, the
anomalies were shown to be highly sensitive to the magnetic

field[47]. A peak-type might convert to have a DCO under an appreciable magnetic field strength. Finally, peak-type sample fabricated with the "taped" method could show p-type characteristic. All these experimental observations are in qualitative agreement with the conducting surface model of Chapter IV.

At the end of Chapter V, we expanded the conducting surface model to a more general parallel-conductors model. The difference is that the n-type layer now is not directly bonded to the surface but can be present via intermediate layers. This generalized model gains more flexibility in the physical interpretation of the anomalies. The conducting surface model thus becomes a special case, although there is a clear correlation between the surface treatments and the anomalies as reported by Scott et al.[23]

The conducting surface model (or the parallel-conductors model) has for the first time enabled estimates of the bulk acceptor density for anomalous samples. The values of N_A calculated from the Hall properties of several peak-type $Hg_{0.8}Cd_{0.2}Te$ samples vary from 5×10^{13} to $1 \times 10^{15} cm^{-3}$.

The consequences of this research give us more insight on interpreting 77°K Hall data. For x = 0.2 peak-type $Hg_{1-x}Cd_xTe$ at 77°K is in the multi-conduction region where all three conductions,

the bulk electrons, the bulk holes and the surface electron

conduction, are comparable. For $x \geq 0.3$ peak-type materials,

77°K Hall data are still surface conduction limited due to the

wider band gaps. Thus the 77°K Hall data can be used to

investigate the surface properties for $x \geq 0.3$ materials.

If an n-type surface is shown to exist on a p-type sample, it

is possible that this n-type surface may exist on an n-type

sample as well. But because of the fact that μ_{ns} is always

smaller than μ_{nb} by an order of magnitude, the surface

conductivity is negligible compared to the bulk.

There are at least two areas in which further investigation is

needed. The first is the cause for the n-type layer. The

results of the present research have demonstrated that fabrication

techniques do play an important role for the existence of this

n-type layer. In order to explain the existence of the n-type

layer, a comparative study of various fabrication techniques

has to be done.

The second area recommended for future research will be based

on the results of the first. It concerns the ability to create

or eliminate the existence of the n-type layer or even to control

the measure of the n-type layer in order that we can operate the device in peak-, DCO- or p-type mode by design.

In conclusion, we feel that the conducting surface model (or parallel-conductors model) is a satisfactory explanation for the anomalous Hall properties of (Hg,Cd)Te and this model predicts some of the quantitative features of the experimental observations presented in Chapter V.

APPENDIX

DERIVATION OF AN EXPRESSION FOR THE "PEAK" IN THE ANOMALOUS R(T)

From equation (4.6.1), we have

$$R = \frac{|q|\,\mu_{pb}^2(p_b - b^2 n_b) - \mu_{ns}S}{\{|q|\,\mu_{pb}b(p_b + bn_b) + S\}^2} \quad , \qquad (4.6.1)$$

where

$$S = \sigma_s \frac{d_s}{d} \; .$$

We want to find the condition at which R is a maximum. By taking the derivative of R with respect to T, we have

$$\frac{\partial R}{\partial T} = \frac{|q|\,\mu_{pb}^2}{(\sigma_b + S)^2}\frac{\partial}{\partial T}(p_b - b^2 n_b) - \frac{2\{|q|\mu_{pb}^2(p_b - b^2 n_b) - \mu_{ns}S\}}{(\sigma_b + S)^3}\frac{\partial \sigma_b}{\partial T} \; . \quad (A.1)$$

The maximum of $|R(T)|$ always appears near the intrinsic region and as a result all impurities should be completely ionized at this temperature region. Thus we have

$$n = p - N_A \; ,$$

or

$$\frac{\partial n}{\partial T} = \frac{\partial p}{\partial T} \; ; \qquad (A.2)$$

and

$$\frac{\partial \sigma_b}{\partial T} = |q|\,\mu_{pb}(1+b)\frac{\partial p}{\partial T} \; . \qquad (A.3)$$

Substituting (A.2) and (A.3) into (A.1), and setting $\dfrac{\partial R}{\partial T} = 0$, we have

$$|q|\mu_{pb}^2(b+2)P_b - |q|\mu_{pb}^2 b^2 n_b + (\mu_{nb} - 2\mu_{ns})\, S = 0. \qquad (A.4)$$

For the case where $b \gg 1$, (A.4) becomes

$$P_b = bn_b - \frac{(\mu_{nb} - 2\,\mu_{ns})\, S}{|q|^b \mu_{pb}^2} \,. \qquad (A.5)$$

REFERENCES

1. D. Long and J. L. Schmit, Semiconductors and Semimetals, (Edited by Willardson and Bean), Vol. 5, (Academic Press, New York 1970).

2. C. S. Hung and J. R. Gliessman, Phys. Rev. 79, 726 (1950).

3. C. S. Hung, Phys. Rev. 79, 727 (1950).

4. C. S. Hung and J. R. Gliessman, Phys. Rev. 96,1226 (1954).

5. H. Fritzche, Phys, Rev. 99, 406 (1955).

6. Z. Oda, K. Sugiyama, H. Arata, A. Kobayashi, Proc. International on Semiconductor Phys., (Academic Press, New York 1966).

7. H. Yonemites, H. Macda, and H. Miyazawa, J. Phys. Soc. Japan 15, 1717 (1960).

8. H. Fritzsche and K. Lark-Horovitz, Phys. Rev. 99, 400 (1955).

9. E.H. Putley, Proc. Phys. Soc. (London) 73, 1 (1959).

10. K. I. Vinogradova, D. N. Nasledov, Yu S. Smetannikova, and V. R. Felitsiaut, Sov. Phys. Semicond. 3,592 (1969).

11. O. V. Emelyanenko, T. S. Lagnnova, D. N. Nasledov, and G. N. Talalakin, Sov. Phys. Solid State, 7 1063 (1965).

12. O. G. Folberth and H. Weiss, Z. Naturforsch 100, 615 (1956).

13. J. M. Whelan and G. H. Wheatley, J. Phys. Chem. Solids, 6, 169 (1958)

14. H. P. R. Fredericke, W. R. Hosler, and R. E. Roberts, Phys. Rev. 103,67 (1956).

15. J. R. Dixon, Phys Rev. 30,1412 (1959).

16. O. G. Folberth and H. Weiss, Z. Naturforsch 11a, 510 (1956).

17. V. H. Rupprecht, Z. Natruforsch 13a, 1094 (1958).

18. V. H. Rupprecht and H. Weiss, Z. Naturforsch 14a, 531 (1959).

19. F. P. Kesamanly, T. S. Lagunova, D. N. Nasledov, L. A. Nikolaeva, and M. N. Pivovavov, Sov. Phys. Semicond. 2,46 (1968).

20. R. C. Chamber, Proc. Phys. Soc. A 65, 903 (1952).

21. F. A. Kroger, H. J. Vink, and J. Volger, Philips Res. Rep. 10,39 (1955)

22. V. V. Voronkov, E. V. Soloveva, M. I. Iglitsyu, and M. N. Pivovarov, Sov. Phys. Semicond. 2,1499 (1969).

23. W. Scott, and R.J. Hager, J. Appl. Phys. 42,803 (1971).

24. V. O. Madelung, Z. Naturfovschg 14a,951 (1959).

25. C. T. Elliott and I. L. Spain, Solid State Commun 8, 2063 (1970).

26. E. H. Putley, The Hall Effect and Related Phenomena, (Butterworths, London, 1960).

27. J. Schmit, J. Appl. Phys. 41, 2876 (1970).

28. J.L. Schmit and E. L. Stelzer, J.Appl. Phys. 40, 4865 (1969).

29a. W. Scott, J. Appl. Phys. 43,1055 (1972).

29b. D. Chattopadhyay, B. R. Nag, J. Appl. Phys. 45,1463 (1974).

30. J. F. Colwell et al., AFCRL-TR-73-0134, Scientific Report No. 1,30 November 1972.

31. J. Tamm, Physik. Z. Sowjetunion, 1,733 (1932).

32. W. Shockley, Phys. Rev. 56,317 (1939).

33. H. Flietner, Ann. Phys. 3,396 (1959).

34. A. Many, Y. Goldstein, and N. B. Grover, Semiconductor Surfaces (North Holland Pub. Co., Amsterdam, 1965).

35. D. L. Carter, M. A. Kinch, and D. D. Buss, The Phys. of Semi-metals and Narrow Gap Semicond, (Pergamon Press New York 1970)

36. G. A. Anticliffe, R. T. Bile and R. A. Reynolds, <u>The Phys.</u> <u>of Semimetals & Narrow Gap Semicond.</u> (Pergamon Press New York 1970).

37. I. R. Schrieffer, Phys. Rev. <u>97</u>,641 (1955).

38. N. B. Grover, Y. Goldstein and A. Many, J. Appl. Phys. <u>32</u>, 2538 (1961).

39. O. Leisleko, A. S. Grove and C. T. Soh, IEEE Trans. <u>ED-12</u>, 248 (1965).

40. F. Fang, and S. Triebwasser, IBM J. Res. DCV <u>8</u>,410 (1964).

41. F. Stern and W. E. Howard, Phys. Rev. <u>163</u>,816 (1967).

42. R. L. Petritz, Phys. Rev. <u>110</u>, 1254 (1958).

43. J. N. Zemel, Phys. Rev. <u>112</u>,762 (1956).

44. F. F. Fang and A. B. Fowler, Phys. Rev. <u>169</u>,619 (1968).

45. C. A. Riberro and J. C. Pfister, Solid State Commun <u>10</u>, 63 (1972).

46a. J. F. Colwell et al AFCRL-TR-73-0761, Scientific Report No. 2, 3 December 1973.

46b. C. E. Mallon et al IEEE Trans. NS-20 No. 6,December (1973),

47. V. V. Ptashinskii and P. S. Kireev, Sov. Phys. Semicond. <u>6</u>, 1398 (1970).

48. M. A. Kinch, M. J. Brau, and A. Simmons J. Appl. Phys. <u>44</u>, 1649 (1973)

49. J. Melngailis, J. L. Ryan, and T. C. Harman, J. Appl. Phys. <u>44</u>, 2647 (1973).

50. J. S. Blakemore, <u>Semiconductor Statistics</u> (Pergamon Press, New York 1962).